MARTIN MARIETTA ENERGY SYSTEMS LIBRARIES

3 4456 0064798 6

ORNL/TM-10031
CESAR-86/05

OAK RIDGE NATIONAL LABORATORY

MARTIN MARIETTA

Modelling Early Stages of Human Vision

C. C. Jorgensen
R. Gawronski
F. Holly

OAK RIDGE NATIONAL LABORATORY
CENTRAL RESEARCH LIBRARY
CIRCULATION SECTION
4500N ROOM 175
LIBRARY LOAN COPY
DO NOT TRANSFER TO ANOTHER PERSON
If you want someone else to see this report, send in name with report and the library will arrange a loan.

OPERATED BY
MARTIN MARIETTA ENERGY SYSTEMS, INC.
FOR THE UNITED STATES
DEPARTMENT OF ENERGY

Printed in the United States of America. Available from
National Technical Information Service
U.S. Department of Commerce
5285 Port Royal Road, Springfield, Virginia 22161
NTIS price codes—Printed Copy: A07 Microfiche A01

This report was prepared as an account of work sponsored by an agency of the United States Government. Neither the United States Government nor any agency thereof, nor any of their employees, makes any warranty, express or implied, or assumes any legal liability or responsibility for the accuracy, completeness, or usefulness of any information, apparatus, product, or process disclosed, or represents that its use would not infringe privately owned rights. Reference herein to any specific commercial product, process, or service by trade name, trademark, manufacturer, or otherwise, does not necessarily constitute or imply its endorsement, recommendation, or favoring by the United States Government or any agency thereof. The views and opinions of authors expressed herein do not necessarily state or reflect those of the United States Government or any agency thereof.

ORNL/TM-10031
CESAR-86/05

MODELLING EARLY STAGES OF HUMAN VISION

C. C. Jorgensen
R. Gawronski*

Oak Ridge National Laboratory
Oak Ridge, TN 37831

and

F. Holly

U.S. Army Human Engineering Laboratory
Aberdeen Proving Grounds, MD

*Research performed while a visiting Professor at ORNL from the University of West Florida.

Research sponsored by
Human Engineering Laboratory
U.S. Army
through the
Office of Basic Energy Sciences
U.S. Department of Energy

Date Published - August 1986

MARTIN MARIETTA ENERGY SYSTEMS LIBRARIES
3 4456 0064798 6

Prepared by the
Oak Ridge National Laboratory
Oak Ridge, Tennessee 37831
operated by
Martin Marietta Energy Systems, Inc.
for the
U.S. DEPARTMENT OF ENERGY
under Contract No. DE-AC05-84OR21400

FOREWORD

Major strategic initiatives within the United States such as SDI have highlighted a growing inadequacy of traditional Von Neuman serial processors to deal with real time computing requirements anticipated in the battlefields of the 1990's. Paralleling a growth in numeric processing is an enhanced need for real time image acquisition and processing. Although advancing at a rapid pace, existing image processing methods may soon face the same type of serial bottleneck that has confronted computer technology. Anticipating requirements for new approaches to increase image processing speed, the U.S. Army Human Engineering Laboratory has initiated a basic research effort with Oak Ridge National Laboratory to examine the feasibility of using biological image processing as a design basis for advanced robot vision sensors.

Although near term generation of biologically based sensors is still beyond the state of the art, the development of hybrid systems having highly parallel neuron-like processors at the front end and serial pattern recognition technologies at higher levels may be feasible. Such hybrids could provide definite advantages over existing systems in both speed and adaptive feature recognition characteristics.

The present effort is designed to produce a mathematical description of what occurs in the first stages of human visual processing. Emphasis is placed on selection of appropriate neural mechanisms and precise description of their information processing characteristics. The goal for 1985 was to develop mathematical equations that describe human retinal function. These equations were evaluated by comparing predicted patterns

to effects perceived by human subjects when exposed to a series of optical illusions. In the longer term, the project seeks to describe higher image processing functions and to represent selected visual mechanisms in specially fabricated hardware architectures. This report details the progress made during 1985.

TABLE OF CONTENTS

	Page
FOREWORD	iii
LIST OF TABLES	vii
LIST OF FIGURES	viii
LIST OF PICTURES	x
ABSTRACT	xi
ACKNOWLEDGMENTS	xii
1.0. EXECUTIVE SUMMARY	1
2.0. CHARACTERISTICS OF HUMAN RETINAL VISION	7
2.1. Stages in a Generic Visual System	7
2.2. Early Pattern Recognition Efforts	9
2.3. The Fundamental Human Visual Properties	10
2.4. Assumptions and Justification	12
3.0. MATHEMATICAL REPRESENTATION OF NEURON CONSTRUCTS	21
3.1. Individual Neuron Characteristics	21
3.2. Neuron Interconnections in the Retina	33
3.3. The Static Linear Model	39
3.4. The Gawronski Model	46
4.0. PSYCHOPHYSICAL EXPERIMENT	81
4.1. Background	81
4.2. Approach	86
4.3. Illusion Administration Procedure	88
4.4. Subjects	91
4.5. Apparatus	91
4.6. Experimental Results	93

TABLE OF CONTENTS (cont'd)

	Page
5.0. CONCLUSIONS AND FUTURE DIRECTIONS	113
6.0. REFERENCES	117
APPENDIX A: FORTRAN code for the Fourier solution of the Linear Matrix Model	A.1
APPENDIX B: Graphics Program Description	B.1
APPENDIX C: FORTH Code for the Psychophysical Experiments	C.1

LIST OF TABLES

Page

Table 1. Summary Statistics and Surface Plot for the Herman Grid Illusion 94

Table 2. Analysis of Variance and 95% Confidence Intervals for the Herman Grid Illusion 95

Table 3. Summary Statistics and Surface Plot for the Mach Band Illusion 96

Table 4. Analysis of Variance and 95% Confidence Intervals for the Mach and Illusion 97

Table 5. Summary Statistics and Surface Plot for the Star Illusion 99

LIST OF FIGURES

		Page
Fig. 1.	Levels of Descriptive Complexity	3
Fig. 2.	Steps in Psychological Data Collection for the Static Linear Model	4
Fig. 3.	Functional Organization of the Visual System	11
Fig. 4.	Typical Response of a Neuron to a Square Wave Input Signal	19
Fig. 5.	Dynamic Range of Vision for Human Rods	24
Fig. 6.	Simplified Model of the Neuron	26
Fig. 7.	Equivalent Circuit Modelling Input Dynamic Processes in a Neuron	27
Fig. 8.	Simplified Model of Analog Properties of the Neuron	29
Fig. 9.	Simplified Model of a Non-Adaptive Ganglion Neuron	31
Fig. 10.	Simplified Diagram of the Most Important Connections in the Human Retina	35
Fig. 11.	Organization of Receptive Fields with Circular Symmetry	36
Fig. 12.	Photoreceptor Influences	40
Fig. 13.	Lateral Inhibition in the Eye of Limucus	41
Fig. 14.	One-Dimensional Layer Nets	47
Fig. 15.	Two-Dimensional, Two-Layer Organization of Parallel Data Processing	50
Fig. 16.	Two-Dimensional Net with Local Feedback	62
Fig. 17.	Algorithm for Modelling Static Data Processing in the Retina	67
Fig. 18.	Algorithm for Modelling Dynamic Data Processing in the Retina	69
Fig. 19.	Two Wave Fronts Passing Through Three Retinal Layers	71

LIST OF FIGURES (cont'd)

Page

Fig. 20. Edge Detection by a Net with Lateral Inhibition 73

Fig. 21. Some Examples of the Detection of Local Features 78

Fig. 22. Herman Grid Illusion 83

Fig. 23. Mach Bands Illusion 84

Fig. 24. Star Grid Illusion 85

LIST OF PICTURES

		Page
Picture 1.	Capturing Illusions	87
Picture 2.	The Herman Grid with Gray Scale Window	89
Picture 3.	Modified Mach Bands	90
Picture 4.	"Star" Illusion	92
Picture 5.	Plot of a 2-D Photo in 3-D	102
Picture 6.	Mach Band Illusion in 3-D	103
Picture 7.	One Quarter of the Star Illusion in 3-D	104
Picture 8.	Herman Grid Before and After Visual Operator Application	106
Picture 9.	3-D Plot of an Estimated Illusory Dot in the Herman Grid	107
Picture 10.	Original Picture of a Tank and its 3-D Plot	108
Picture 11.	Plot of a 3-D Tank Picture After Application of the Matrix Operator	109

ABSTRACT

This report presents the first results of an effort to model vision processes operating in the early layers of the human retina. The ultimate goal of this research is to develop a robot vision system based on computational principles of human vision. These include massive parallelism, dynamic feedback, and multilayer pattern recognition. Two neural models were developed. The first represented early vision in terms of static two-dimensional linear equations using a linear matrix and limited feedback. The second considered dynamic two-dimensional nonlinear processes and used matrices of nonlinear differential equations. The first set of equations was parameterized using psychophysical data from subjective intensity judgements for visual illusions. Illusions were quantified by creating a digitized image representing the subjective effect of human perception when exposed to input patterns. A Fourier transform was made of the input and output patterns and used to solve for the coefficients of the retinal operator equations. The equations were then applied to new illusions and compared with human subjective results through three dimensional plots of output pixel intensities. The second model with dynamic equations was studied using a computer simulation developed to operate on varying input wave forms and variable neural connection topologies.

ACKNOWLEDGMENTS

A team effort of individuals contributed to the success of this research. Special thanks are due to the ORNL staff scientists whose technical suggestions, programming assistance and creative insights helped mold the final result. I would first like to thank Dr. Chuck Weisbin for his continuing help in obtaining key personnel and program resources. His insightful reviews and technical suggestions were most helpful in guiding the direction of the program. Dr. Len Grey provided the insight and expertise necessary to solve the static linear equations using the psychophysical illusion data. Mike Bjerke developed the graphic plot procedure in Appendix 2 and generated 3-D plots of the retinal equation outputs. Dr. Ed Oblow's expertise in differential equations provided early insight into the nonlinear characteristics of the retinal grid, Steve Killough's programming assistance was responsible for decoding the IRI vision system frame grabber into a form that could be processed on external computers. Curtis Roland built the light chamber used for the vision experiments, and Jim Lucius helped coordinate data exchange between computer systems at the X-10 and Y-12 facilities. Anita Weil and Ruth Lawson took on the formidable task of typing the report and the numerous drafts, which consisted of large numbers of equations present in the early versions. Dr. Ralph Einstein provided considerable time and effort in the selection of computer and image processing hardware. Finally, special thanks are due to Dr. Oscar Manley of the DOE Office of Basic Energy Sciences who initiated the machine intelligence program at Oak Ridge, and who has encouraged us to interact with R&D facilities such as the present effort with the U.S. Army Human Engineering Laboratory.

1.0. EXECUTIVE SUMMARY

The research in this report had five phases. The first was the identification of retinal features most likely to cause superior pattern recognition performance. This phase included examination of neurophysiological literature, assessment of its worth, and summary conclusions. The output was a specification of three generic stages in human vision (image transduction, feature selection, and recognition described in Chapter 2.1), a consideration of deficiencies in prior pattern recognition research (Chapter 2.2), and an enumeration of six important retinal properties (Chapter 2.3). The properties were: parallel processing and data transfer, hierarchical organization of recognition, mixed continuous and discrete signal handling, plasticity of neural interconnections, spatial and temporal transformations, and intra- and inter-layer feedback.

The second phase selected features to include in math models. These features were: the number of neurons to be modeled (<1.25 times 10^8 rods and the omission of cones), an assumption of a homogeneous distribution of photoreceptor cells, the initial use of monocular vision processes, the inclusion of limited dynamics in neural feedback loops, the analysis of still photographs only, and the omission of tremor, drift, and saccadic movement in the eye assembly (Section 2.4 details this information).

The third phase involved the generation of two retinal models. The first model consisted of a set of two-dimensional linear equations contained in a linear matrix with limited neural feedback distances. This model was based on a modified version of the lateral inhibitory model proposed by Hartline and Ratliff (1957). Figure 1 shows a hierarchy of model

representation formats based on increasing complexity and sophistication of neural description. Level one is the easiest to emulate in hardware but is probably too simple to provide the necessary power required. Level eight is the most powerful descriptively but may be too complex to solve with existing technology. Details for the selection of a modified Hartline and Ratliff model can be found in Chapter 3 Sections 3.1 through 3.3. A unique feature was that this model was parameterized by psychophysical experiments which provided numeric values for equation variables.

A second nonlinear dynamic model was also developed. Due to its complexity, this model was only simulated. It emphasized computation requirements and time behaviors. It is discussed in Section 3.4. The purpose was to explore a retinal model at a high level of detail and determine whether a more complete description of neural dynamics and symmetries would lead ultimately to simpler and more efficient processing.

The fourth phase was an experiment on human performance with visual illusions. The results were used to compare the output of the modified Hartline and Ratliff model with human psychological judgements. Figure 2 outlines the procedure. Pictorial information was captured from illusion drawings using a frame grabber and was digitized as a matrix of gray scale picture elements (pixels). This matrix was used as an argument for the matrix of linear operators. The application of the linear operator matrix resulted in a transformed picture matrix which was then displayed as a three-dimensional plot (the third dimension was the intensity level of a pixel). The human psychological judgments of illusion effects were measured by a specially constructed experimental apparatus. A picture representing these judgments was produced using the same three-dimensional

Equation Complexity

Levels {1-4 Equations without feedback, 5-8 Equations coupled with feedback}

LOW

1. One-dimensional linear operators with static processes.
2. Two-dimensional linear operators with static processes.
3. Two-dimensional non-linear static operators with matrix based on non-linear operators.
4. Two-dimensional non-linear dynamic models with a matrix operator of both non-linear functions and convolution integrals.
5. One-dimensional static linear equations with feedback.

*6. Two-dimensional static linear equations with a linear matrix and limited feedback.

7. Two-dimensional non-linear static equations with a matrix of non-linear operators and feedback.

**8. Two-dimensional non-linear dynamic models with matrices of non-linear differential equations.

HIGH

*The Hartline and Ratliff Equations
**The Gawronski Equations of a nonlinear dynamic retina

Fig. 1. Levels of Descriptive Complexity

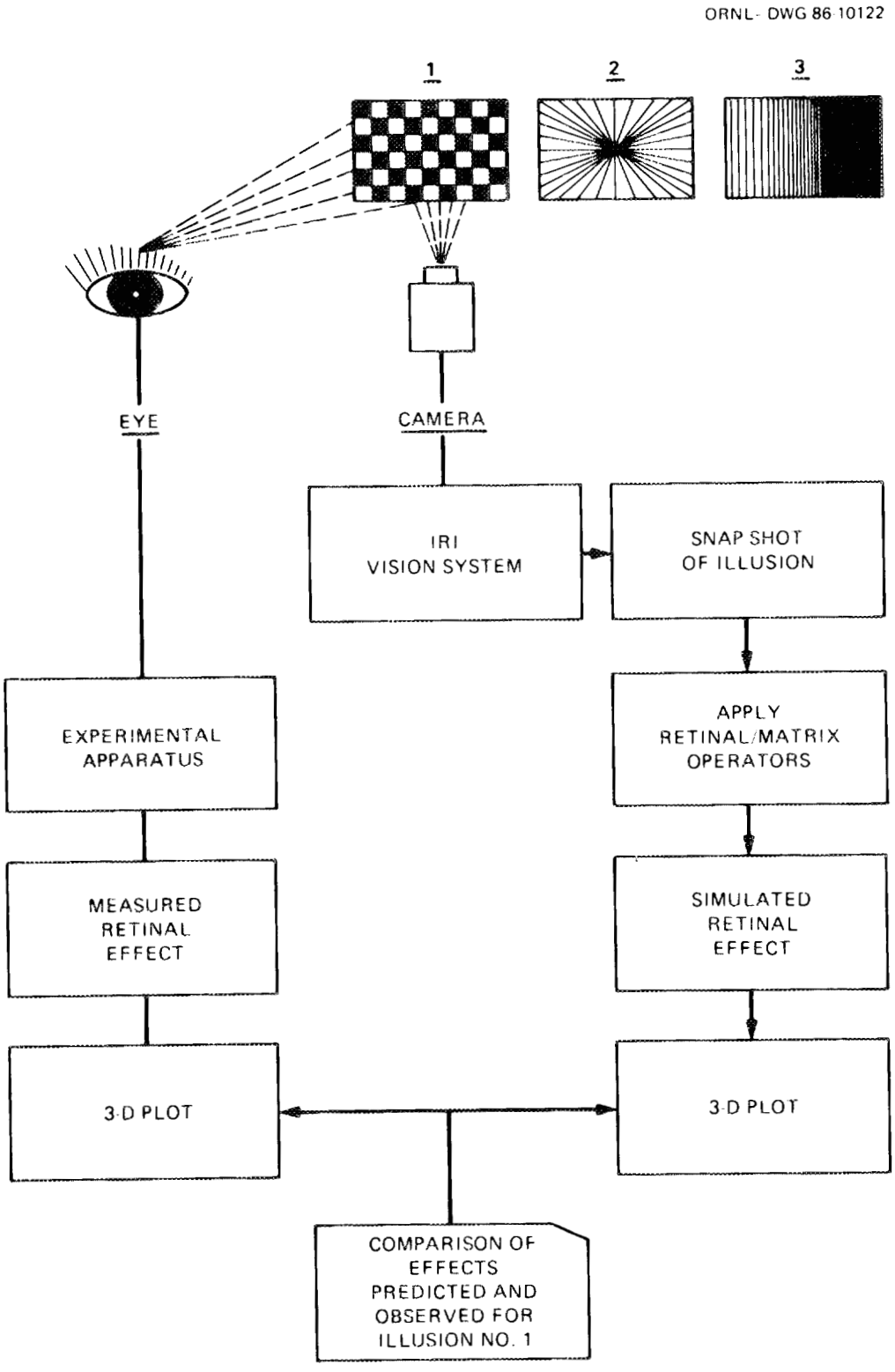

Fig. 2. Steps in Psychological Data Collection for the Static Linear Model.

plotting routines. Human output and model output were then compared. The experimental method is presented in Chapter 4.

Finally, preliminary conclusions were drawn regarding future research. The conclusions were that a transition from static to dynamic models was necessary because powerful human image processing effects operate in the time domain. Second, a strategy needs to be selected to compare existing pattern recognition technology to the potential inherent in biologial simulation approaches. Finally, more detail is required to connect early perceptual processing and the higher order neural mechanisms of adaptive pattern learning and cognitive control. Overall, the effort made more progress than anticipated and met or exceeded programmatic goals for the initial exploratory period (this information is detailed in Chapter 5).

2.0. CHARACTERISTICS OF HUMAN RETINAL VISION

2.1. Stages in a Generic Visual System

In the last decade, there has been a growing interest in the practical application of information extracted from visual images.

Character recognition, detection of objects in aerial photographs, selection of damaged assembly line parts, or robot motion control, are all examples of potential applications for more sophisticated vision processing systems. This report considers one approach to visual processing, specifically, the application of biological principles.

We specify three main stages in a generic biological vision system:

1. Image Transduction
2. Data Selection, and
3. Recognition.

Image Transduction

The first stage requires an appropriate sensory architecture to map light signals from the environment into an optic storage medium. To represent movement, the time of this storage must be very short and in animals the mapping is performed by the lens of the eye and the first layer of the retina (the photoreceptors including the rods and cones).

Current TV technology, and Computer Vision input devices may enable an emulation of the mapping process with quality close to human vision (excluding sensitivity). Such a level of resolution is sufficient for most technical applications but further decreases in size, weight, and cost of the sensing cameras will be crucial for many applications, especially robotics.

Selection

Visual images are characterized by an enormous amount of data and high speed of data transfer. When an image captures some motion, more than 10^9 bits/sec must be transferred to memory. Therefore the next stage of a visual system involves the selection of information,* necessary for classification or recognition. The extraction of information and rejection of all but useful data is a very complex task. There are two main problems:

a. To find the appropriate rules for data processing.

b. To deal with high speed data processing requirements.

The solution to the first problem may be found in the study of the visual system of animals; for the second, parallel processing and a hierarchy of data processing activities is needed. We believe that parallel processing may also require some learning procedures.

Recognition Labelling

The last part of a visual system involves utilization of information extracted from visual data. For example, in pattern recognition every object needs an appropriate label designating a class to which the picture belongs. It may be a letter of the alphabet, name of an object in a photograph, or assignment of a qualitative property. It is in the labelling

*We will distinguish "data" represented by intentionally introduced signals - stored in the system independent of final application - and "information" as it is understood in modern information theory. Information in this context is data which may be used for process functions. Therefore, we speak about "information extraction" from existing data.

stage that learning occurs, and there is a great need for new ideas and algorithms to improve that decision process.

2.2. Early Pattern Recognition Efforts

Initial attempts to build a visual recognition system (e.g., Rosenblatt, 1958) resulted in the construction of the Perceptron. The Perceptron used the idea of stochastic learning with reinforcement, but lacked preliminary data processing. Limited numbers of input pixels in the Perceptron raised difficulties for the recognition of more complex images. Sufficient results were obtained only with simple geometric figures such as triangles or rectangles. Application of stochastic methods in pattern recognition (G. Sebastyan, 1962, K. S. Fu, 1968 and many others) though very successful in applications like medical diagnosis, have had little influence on the present structure of commercial recognition systems.

Major progress in pattern recognition was achieved only after the utilization of several key research findings on the physiology of the visual systems in animals. H. K. Hartline (1938) first described so called receptive fields in the visual system of vertebrates. It was a step toward explaining how mutual interactions between parallel channels may be used for practical data processing. These investigations continued and a second important step was performed by J. T. Lettvin, et al. (1959), and later K. Kupfmuller and F. Janik (1961). They explained the role of lateral inhibition in feature extraction, and found concrete feature detectors in the retina of the frog. Some progress was also made in the description and analysis of parallel neuron models (Gawronski 1971). At the same time new information came from neurophysiological investigations

that showed the early models needed to be considerably improved. Later it was determined that the organization of the visual system is much more complex, and more specific experiments were necessary to understand the working principles.

2.3. The Fundamental Human Visual Properties

Parallel Processing

As mentioned above, parallel processing and parallel channels of data transfer are one of the basic concepts in the organization of an animal's visual system. The first stage of image processing is performed by a surface of photoreceptors (see Fig. 3) which transforms a two-dimensional distribution of light intensity: $i(\xi,\eta,t)$ into an electrical or electrochemical) set of signals $e(\xi,\eta,t)$. This surface may be treated as a plane.

The next step in data processing involves spatial operations performed on each signal $e(\xi,\eta,t)$ in parallel and transferred to the following stage. Some efforts to model these operations using standard computer algorithms have been performed for simple images and slow data processing. Slow data processing becomes one of the most important constraints in the investigation of visual systems when using only sequential algorithms and classical computer architectures.

Hierarchical Organization

Hierarchical organization of visual data processing and recognition is the second key concept in the human vision system. Theoretically it is possible to assume the existence of a specific mechanism performing classification in only one stage but such systems would of necessity be

ORNL-DWG 86-10128

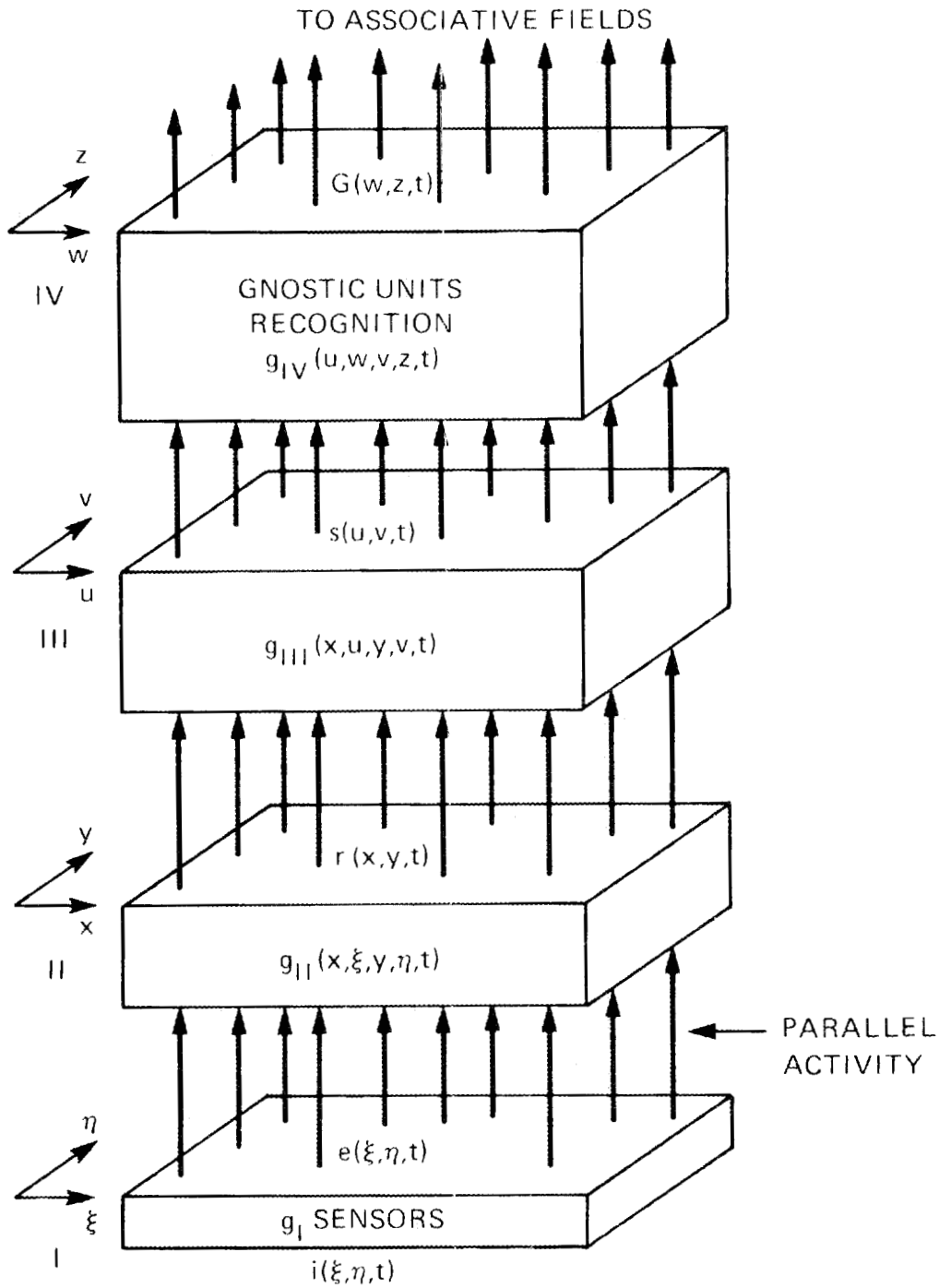

Fig. 3. Functional Organization of the Visual System.

limited to very specific applications [for example the linear classification of separable subsets (N. Nilsson, 1965)]. A more universal system always seems to involve hierarchical organization.

2.4. Assumptions and Justification

To simplify formulas in this section we have temporarily assumed a continuous signal distribution over a planar surface. Later we will include discrete signals, corresponding to the discrete elements that form the visual tract. The four main stages of data processing are illustrated in Fig. 3.

Stage I. A photoreceptor layer transforming an intensity distribution of incident light $i(\xi,\eta,t)$ on electrical signal distribution $e(\xi,\eta,t)$

Stage II. The spatio-temporal transformation of signals:

$$r\ (x,y,t) = \iint_R g_{II}(x,\xi,y,\eta,t)\cdot e(\xi,\eta,t)\cdot d\xi\cdot d\eta \qquad (1)$$

where:

ξ,η - cartesian coordinates in the first stage.

x,y - coordinates in the second stage.

$g_{II}(\cdot)$ - kernel of the transformation of stage II.

R - region of the integration (over the whole retinal surface)

$r(x,y,t)$ - an output signal from the second stage.

Regarding Eq. (1), if there exists a kernel $G_{II}\ (\cdot)$ for the inverse operation with a unique solution so that:

$$e(\xi,\eta,t) = \iint_R G_{II}\ (x,\xi,y,\eta,t)\cdot r(x,y,t)\ dx\cdot dy \qquad (2)$$

then data processing can be performed without any loss of information.

There is much evidence that an inverse operation, Eq. (2) and appropriate kernel $G_{II}(\cdot)$ exists in the retina of higher animals. We also assume that no essential loss of information exists in this second stage of the visual system. It was proved (Rodieck 1973) that the accuracy of spatial discrimination in the retina has the same order as the acuity of the optical lens of the eyeball.

Stage III. Another Transformation Stage:

$$s(u,v,t) = \iint_S g_{III}\,(x,u,r(x,y,t),\ y,v,t)\cdot r(x,y,t)\cdot dx\cdot dy \tag{3}$$

where:

u,v = new coordinates corresponding to the next stage of signal processing,

$s(u,v,t)$ = the distribution of signals after third stage of signal processing.

But in this stage an inverse operation:

$$r(x,y,t) = \psi\,\{s\,(u,v,t)\,\} \tag{4}$$

and a corresponding unique kernel does not exist. That means that some data will be lost, and we must select information. The main problem centers on an appropriate selector [defined by $g_{III}(\cdot)$] which rejects all unnecessary data but preserves information necessary for making a final decision. There is strong evidence (Konorski, 1967) that learning processes are very important at this stage. In living organisms the final shape of Eq. (3) is established by a learning procedure.

Stage IV. A Classification and Recognition Layer G(w,z,t)

According to many neurologists (Hebb 1957, Konorski 1967), the act of recognition in an animal's brain is described by the excitation of a group of cells (called a "gnostic unit" that responds to all pictures belonging to the same class. "By definition, each unit of a generic area represents a complex sensory pattern obtained by convergence of receptive units at lower levels (representing its elements). A perception which gives rise to the activation of a gnostic unit is called a unitary perception ..." (Konorski, 1967).

Excitation of a gnostic unit, or set of units, corresponds to a higher level category of defined sub-classes, and is a typical decision process. A logical, or threshold, element, is excited only if the image at the input $(i(\xi,\eta,t))$ belongs to a class represented by this unit. Such excitation is performed in a nonlinear operation:

$$G(w,z,t) = \iint_G g_{IV}\,(u,w,v,s(u,v,t),z,t)\cdot s(u,v,t)\cdot du\cdot dv \qquad (5)$$

where:

$s(u,v,t)$ is now a variable in g_{IV}

w,z = position of the gnostic unit and

$G(w,z,t)$ = state of the excitation (usually 0 or 1).

of the gnostic unit with coordinates w,z.

Note that a gnostic unit may be connected with many other associative units by means of recognition operators.

Learning plays a crucial role in the final shape of kernel $g_{IV}(\cdot)$ which is "adaptable" and gradually "improved" during the life of an animal.

Because of changes in gnostic units, we see that the decision process existing in higher stages of the human visual system requires some nonlinear features in the operators. In reality, almost all neural processes show

some nonlinear properties. In most cases we assume that some processes in an artificial vision system will also be essentially nonlinear. As long as we consider only a one-to-one mapping of data from stage to stage, we may try to solve vision model equations using a linear transformation, as we will attempt later in this paper, but caution is in order because the selection of information is a typical nonlinear process.

From everyday experience it is also evident that for recognition of images it is necessary to take into account both local and global information. Spots, line crossings, or sharp bends in figures are examples of local features. On the other hand, dimensional proportions and relative positions of picture parts, are examples of global features. For example, we can describe an operator selecting local features using formula (3) for $s(u,v,t)$. If kernel g_{III} selects local features:

then: $g_{III}(x,u,y,v,t) \leq \varepsilon$;

if: $|x-\mu|$ or $|y-v| > \eta$;

where: $\varepsilon <<< g_{III}(x,x,y,y,0)$;

and η = range of the influence;

i.e., operator (3) is a local operator with a range smaller than n and accuracy ε.

All neural processes are actually represented by signals varying in time. Even the recognition of static images will usually be proceeded by many <u>dynamic processes</u>. Therefore if we want to compare a hardware model with neurophysiological results, we have to consider modeling some dynamic processes. Any attempt to extend vision research and recognize moving pictures requires introduction of dynamic processes at all stages of the

visual system. We know that even for static images, data processing raises essential computational problems, and for dynamic, multilevel systems the computational burden is enormous. We must somehow achieve substantial relaxation by using symmetries and equal time constants for many of the processes considered. Some assumptions must also be made about the spatial distributions of neurons.

One issue is how to select the number of receptor elements on the eye surface. If we want our system to approximate the capabilities of human vision, we must select approximately 10^6 (or even more). Though the number of photoreceptors in the retina is much greater, ($\sim 10^8$, or $125*10^6$rods and 6.4 - 10^6 cones) space summation and neglecting peripheral vision (if possible) may decrease this number.

A second issue is the selection of a density distribution for photoreceptors. Applications almost always assume a uniform distribution. But in biology we observe very nonuniform distributions with the greatest density in the central part of the retina. Such a distribution permits taking advantage of the tremendous acuity of central vision with a broad angular range of perception. In this year's retinal models, we will also assume a uniform distribution of photoreceptors because we must develop and verify lower order mechanisms for visual data processing. Next year we may also consider nonuniform distributions and their advantages.

Third, perception and recognition of three-dimensional objects (3D) is an important goal for many visual applications, especially robotics. In principle we can use binocular vision, or a method to shift the optical

axis, and use parallax for three-dimensional perception. We will however model only two-dimensional vision as a necessary step towards 3-D.

Fourth, most existing vision systems are black and white with gradations of grayness. For recognition of images containing shadows and different surface textures, it is necessary to introduce as many steps of grayness as possible for a high level of resolution. We will assume 64 to 128 steps of gradation of light intensity or about a 1% change in differentiation at maximum illumination. Closely related to gray scale resolution is the problem of dynamic range. The visual systems of higher animals have an extremely wide range under average illumination. Some methods to increase range will be presented later. Where color vision has been studied, two main problems need clear explanation:

1. The mechanism of utilizing different percentages of light wavelengths from photoreceptors. (It is known that three kinds of photoreceptors exist, corresponding to three colors, but the mechanism permitting such high sensitivity and discrimination is not clear.)

2. The mechanism for using color coded neural signals to recognize objects that depend on other context information.

In color TV cameras the first problem has already been solved in a analogous way but the construction of a "biosensory" method would be an interesting achievement. A solution to the second problem is important for several applications. An example is texture recognition which uses colors, minute picture details, and selection of objects from a complex background.

The last issue is the characterization of dynamic processes in the visual tract. This problem may be divided into two parts:

1. How dynamic neural processes are involved in the recognition of both static and moving scenes, and
2. how recognition of the objects that move with respect to the perceptual system is achieved, i.e., "dynamic scene analysis."

Most pattern recognition systems assume static images and static representations. But, it is also necessary to consider continuous processing of time and space dependent signals. It has been suggested that for static images it is reasonable to use static representations of visual signals for one image. However, in all stages of the visual tract of higher animals, a different situation is actually observed.

A positive front (sharp increase) of the signal produces a strong response (called the ON-response) which decays with a time constant τ_{on}. After decay, only a small static signal remains. As the signal is switched off we again observe a strong response, but of opposite sign that decays with time constant τ_{off} (called an OFF-response). Notice that the dynamic part of a neuron's response is much stronger and evidently plays an important role in visual signal processing.

Images in living systems also have a dynamic character because of eye movements. Several kinds of these movements have been observed in humans. Some are voluntary and connected with the perception of complex forms as the optical axis is shifted among attention points. There also exist involuntary movements having random character. Three broad categories of movement have been distinguished (Tulunay-Kessey 1978):

ORNL–DWG 86-10130

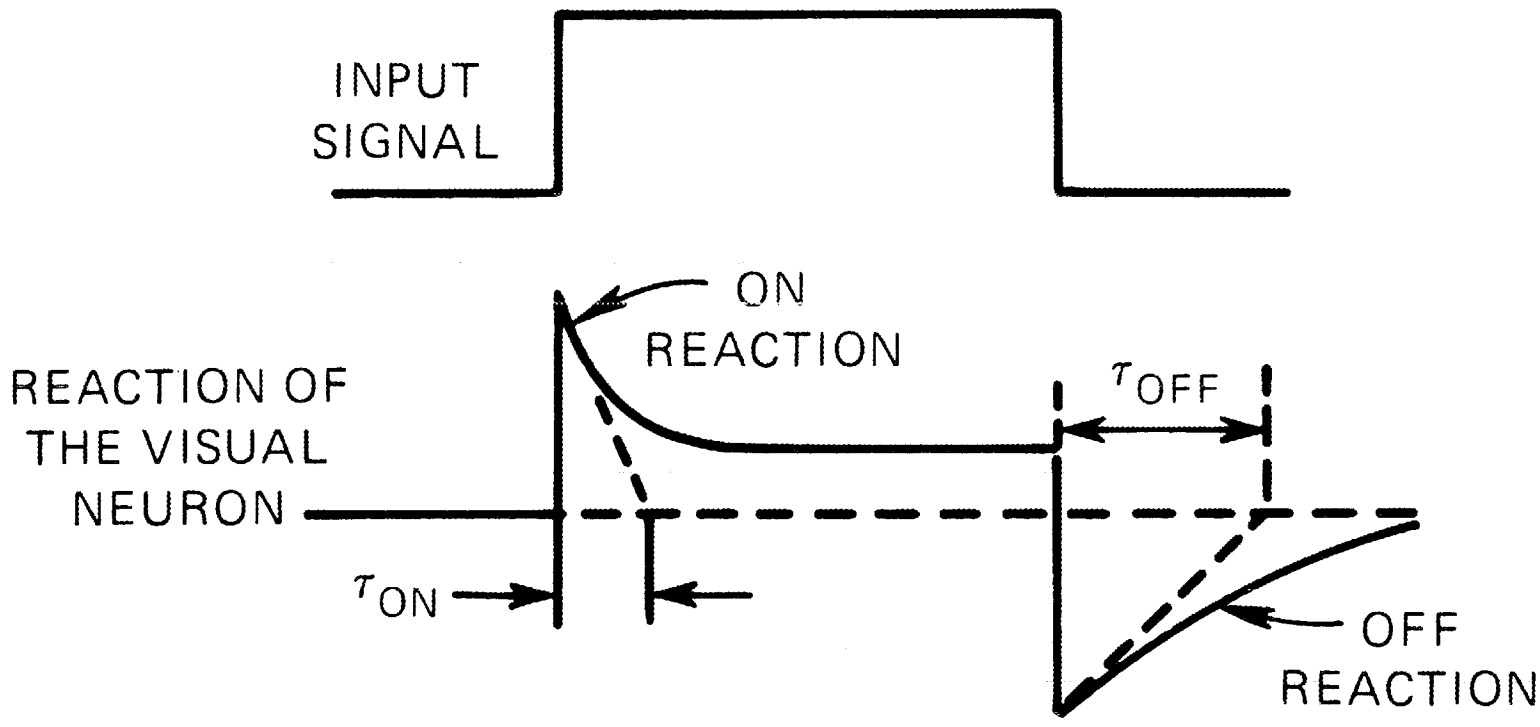

Fig. 4. Typical Response of a Neuron to a Square Wave Input Signal.

1. Tremor - very small, rarely exceeding 20 sec of arc in amplitude, but quite fast with a frequency of between 30 and 70 Hz.

2. Drifts - a gradual shift in the direction of the gaze; with mean amplitude about 5 min of arc and rate of occurrence between 1 to 5 times per sec.

3. Saccades - an irregular rapid jerky movement; with mean amplitude of 5 min of arc and occasionally a movement of 20 min of arc, duration $\leqslant$ 200 msec.

Results for many studies of eye movement in human perception have been published. It has been verified that image motion has an important role in regulating contrast sensitivity. The mechanism by which contrast sensitivity regulation occurs is not clear (Tulunay-Kessey 1978, S. M. Ebenholtz 1984) but it is evident that eyeball movements are closely related to the dynamic properties of the retina and play an important role in visual data processing.

Thus, there are three important reasons to include research on dynamic processes in the retina:

1. To enable the quantitative comparison of a retinal model with the results of electrophysiological and neuropsychological experiments which always contain some dynamic components.

2. To apply the results of dynamic modelling to more advanced systems that include dynamic scene analysis.

3. To decrease the influence of initial value instabilities (because dynamic systems are less dependent on slow steady state variations).

3.0. MATHEMATICAL REPRESENTATION OF NEURON CONSTRUCTS

3.1. Individual Neuron Characteristics

We now consider the modelled neuron properties. These properties were chosen because of some difficulties that must be resolved.

First, should we use analog models or select a digital representation of the neuron. Because of a large number of parallel elements (10^6 to 10^8) in each layer, and a computation time problem we must select the most parsimonious elements possible. There are two main choices:

1) Select slower elements that work in parallel, or
2) Select faster elements that repeat the same function simulating many adjacent elements.

We would like to use simple analog devices with properties close to the properties of well understood neurons. The second possibility, however, would be easier to implement using electronic chips and calculating the final results by digital algorithms.

Digital components may be easier initially because many nonexpensive components are available and some procedures may be adapted from existing computer vision software. Also digital components do not raise problems concerning the stability of parameters and reference values.

An increase in the speed of data processing may also be achieved by the application of parallel processing. That is the application of a great number of very simple elements with mutual connections. One advantage of the lower levels of the human visual system is that these connections have a great degree of symmetry.

Second, neurons forming the retina are similar to other neurons in the brain, but they have some unique features as well. We considered three special types:

1. Photoreceptors. For black and white images, photoreceptors may be treated as a series connection of two process elements. The first process is a nonlinear illumination transducer:

$$e = f(i) \tag{7}$$

where i = intensity of the incident light on a receptor

e = output signal from the transducer.

The second process may be represented by a simple RC inertial circuit.

For color vision we must ultimately consider different properties of cones, but for the purposes of this project we will assume average properties of the transducer independent of light wavelength.

Relation (7) may be specified for an illumination transducer using the following formula, (Baylor and Fuortes 1970, or Hagins et al. 1970):

$$\frac{\Delta e}{\Delta e_m} = i + i_0 \quad . \tag{8}$$

Where:

Δe - the change of output voltage

Δe_m - the maximum observed change

i - the intensity of the light flash

i_0 - a constant equal to the intensity of the light flash

When $i \ll i_0$ the response is linear (proportional to the light intensity)

When $i \approx i_0$ the relation is approximately logarithmic

When $i > i_0$ the response saturates to a peak value Δe_m.

The resultant sensitivity diagram is presented in Fig. 5 (Roedieck 1973).

Standard electronic photoreceptors do not have this wide dynamic range of stability and for long term application it will be necessary to introduce:

1. An automatic diaphragm reacting to average intensity of visual field illumination, similar to the pupil in the human eye.

2. Some nonlinear feedback existing between first and second layers (horizontal cells) of the retina.*

3. Automatic gain control for every photoreceptor, which expands the dynamic range of the transducer.**

For the purpose of computer modelling we will assume that for every photoreceptor having the coordinates (ξ, η) the output is given by (9) where k_i is a constant

$$e = k_i \cdot i \tag{9}$$

[other notations are the same as for Eq. (8)]. In later development it would be interesting to model the nonlinear dependence shown in Fig. 6 because nonlinearities plus adaptation properties of the later stages can considerably improve image contrast.

---

*This feedback locally changes the sensitivity of the photosurface. It may be very useful for images with great contrast of illumination.

**The absolute psychophysiological threshold for human vision is about 10 absorped photons for a 1/2° spot (or 1 photon per 500 rods). It is very difficult to achieve the same sensitivity and the same dynamic range in non-biological systems. This problem should be solved separately by specialists in solid state electronics. The time constants of the processes in photoreceptors are in general small (2 to 5 msec) in comparison with the processes in later layers. Therefore we may neglect them if the hardware device doesn't exceed these values.

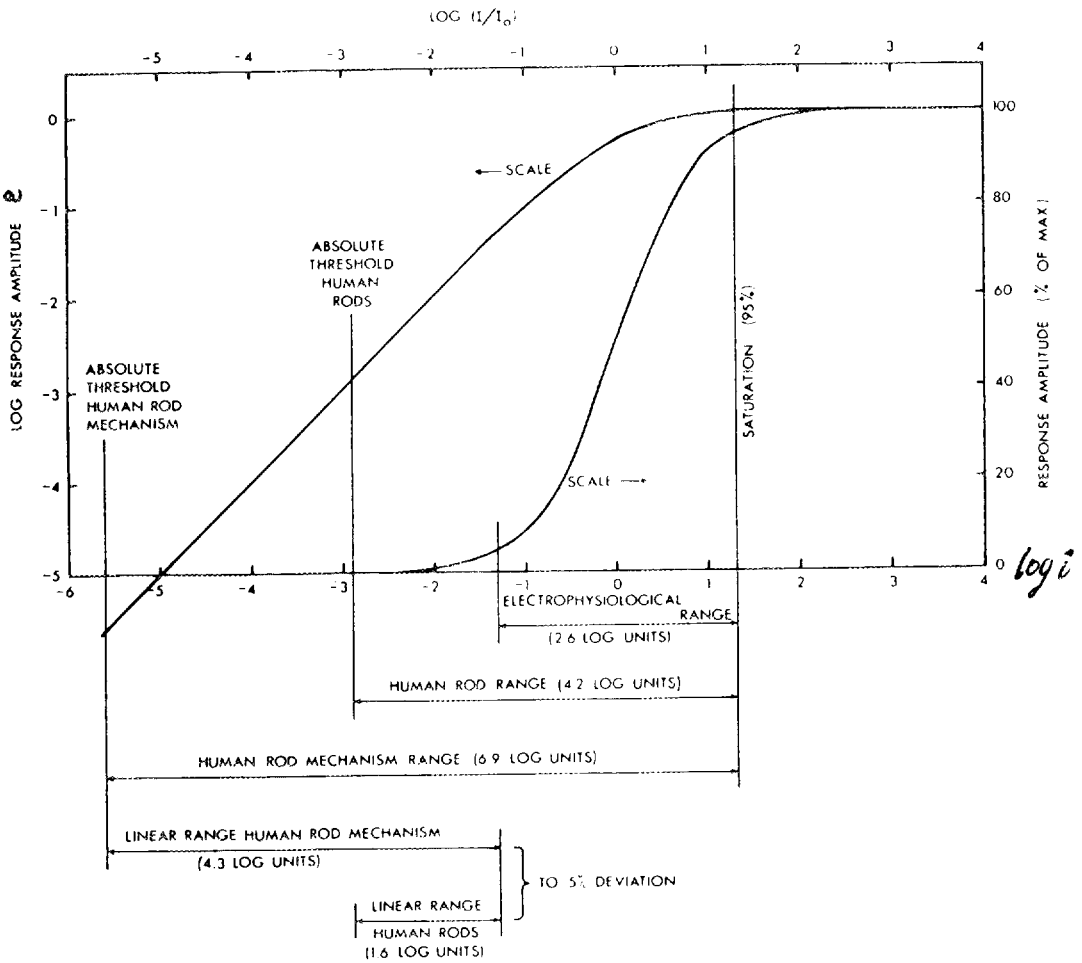

Fig. 5. Dynamic Range of Vision for Human Rods.

Assumptions Regarding Neurons After the Transduction Layers

Four kinds of neurons exist in the retina besides photoreceptors. Three of them: bipolar cells, horizontal cells and amacrine cells are characterized generally by low level analog outputs. This is a rare feature in nerve cells. The last layer of the retina is composed of ganglion cells generating sequences of pulses. These pulses are then transmitted to the lateral geniculate nucleus in the thalamus.*

Basic properties of a neuron may be found in any modern neurophysiological textbook and we will not consider them here. Also many mathematical and technical models of neurons have been previously reported starting with the famous threshold model of McCulloch and Pitts 1943. For a survey, see R. R. Gawronski 1971, 1975.

It is well known that retinal neurons have constant properties. No changes (long-term modifications) connected with learning have been found. But this is not the case for the higher levels of the visual tract where we must take learning into account and adaptive plastic properties of neurons.

The most important properties of the neuron which we consider in the present effort are presented in Figs. 6 and 7.

Every neuron has many (sometimes hundreds or thousands) of inputs through synaptic connections. Every input signal $e_k(t)$ is transmitted through a linear dynamic element characterized by a pulse response $g_k(t)$. Usually these elements may be approximated by a second order circuit (Fig. 7) having the response previously presented in Fig. 4. Input

*Other destination areas include the superior colliculus, accessory optic nucleus, and ventral lateral geniculate nucleus.

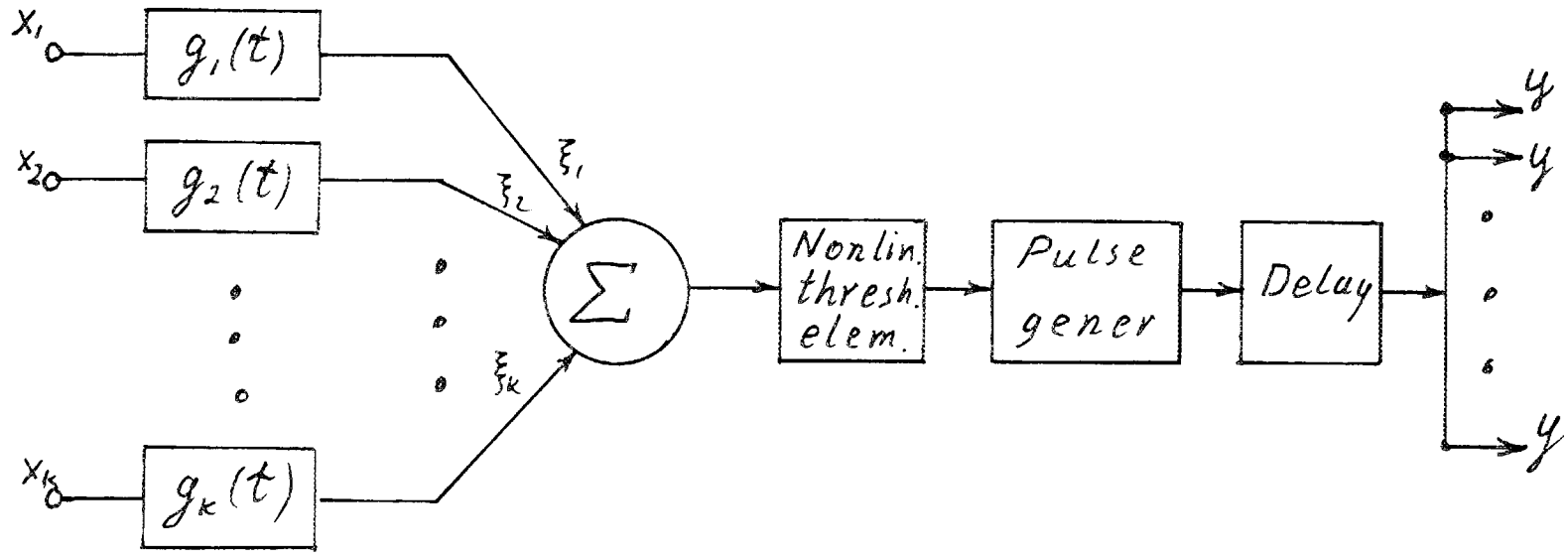

Fig. 6. Simplified Model of the Neuron.

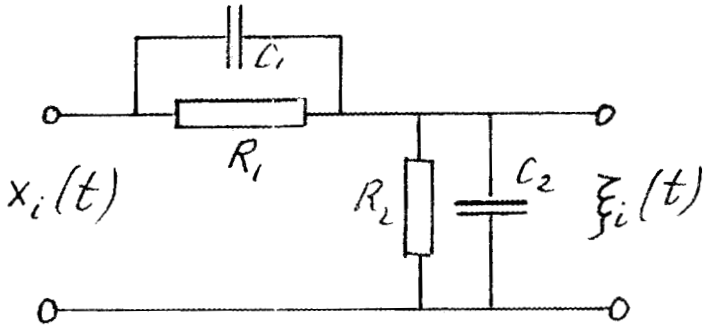

Fig. 7. Equivalent Circuit Modelling Input Dynamic Processes in a Neuron.

signals $e_k(t)$ may be positive: $e_{e_k}(t) > 0$ - which represents excitation or negative: $e_{i_k}(t) < 0$ which represents inhibition. The next element of the neuron is approximated by a linear summing element. The resulting signal X may then be described by a formula:

$$X(t) = \sum_{k=1}^{K} e_k(t) * g_k(t) \tag{9}$$

where: K = number of independent inputs.

and the star "*" represents a convolution operation.

$$e_k(t) * g_k(t) = e_k(0) \cdot g_k(t) + \int_0^{\tau} e_k(\tau) \cdot g_k(t-\tau)\, d\tau \tag{10}$$

On the basis of voluminous literature (see Roedieck 1973) we may simplify further. It is known that time constants for positive signals (excitation) are approximately the same for all inputs 1, ..., K_e. For negative signals (inhibition) we can assume another time constant for inputs 1,..., K_i. Therefore we can replace all inertial elements by two equivalent circuits, one for excitation, the second one for inhibition.

For horizontal, bipolar and amacrine cells we can neglect the threshold properties and pulse generators. Therefore for these cells we will use the simplified model presented in Fig. 8. It must be stressed however that equivalent circuit parameters such as the time constants of these cells are quite different. The transmittance $g_o(t)$ in formula (11) represents transients and delays in the output signals (so called presynaptic properties). The input-output relations may be formally described by the following relations.

$$X(t) = \left[\left(\sum_{k=1}^{K_e} e_{e_k}(t)\right) * g_e(t) + \left(\sum_{k=1}^{K_i} e_{i_k}(t)\right) * g_e(t)\right] * g_o(t) \tag{11}$$

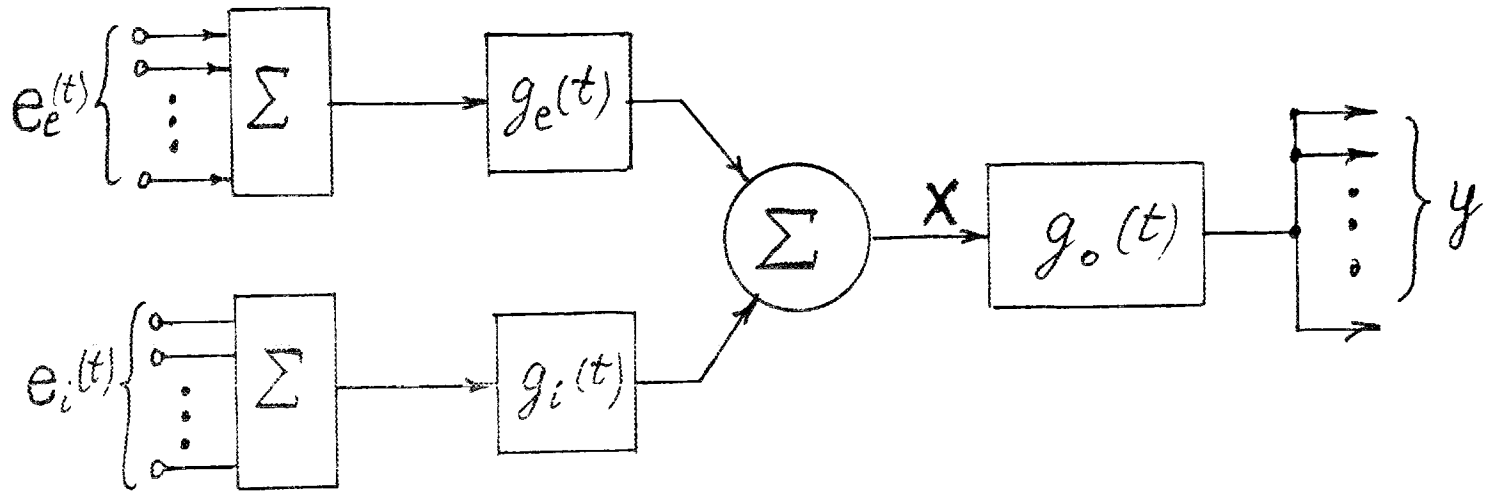

Fig. 8 . Simplified Model of Analog Properties of the Neuron.

where "*" means convolution and

K_e - number of exciting inputs,

K_i - number of inhibiting inputs,

$e_{e_k}(t)$ - exciting signals at the input "k",

$e_{i_k}(t)$ - inhibiting signals at the input "k",

$g_e(t)$ - equivalent transmittance of exciting channels,

$g_o(t)$ - equivalent transmittance of inhibiting channels.

It is possible to write differential equations for these models, but it is much easier and faster to calculate integrals on the computer than to solve differential equations. Moreover an analog model of such a system is easier to construct using the form of Eq. (11).

The transmittance (g_e) of an inertial element may be obtained using operational calculus. (See Fig. 6).

$$g_e(s) = \frac{R_2(1 + s\tau_1)}{R_1+R_2 + s(\tau_1+\tau_2)} \tag{12}$$

where $\tau_1 = R_1 C_1$; $\tau_2 = R_2 C_2$.

An analog implementation of a net composed of such elements is not difficult.

The stability for slow frequency variation of parameters and reference values can be considerably improved using the additional feedback of horizontal retinal cells.

For ganglion cells we have to add threshold elements and a pulse generator. The model of a ganglion neuron is presented in Fig. 9. It is again simplified but sufficient to represent the existing dynamic and nonlinear properties of operator $g_{II}(\cdot)$ in Eq. (1).

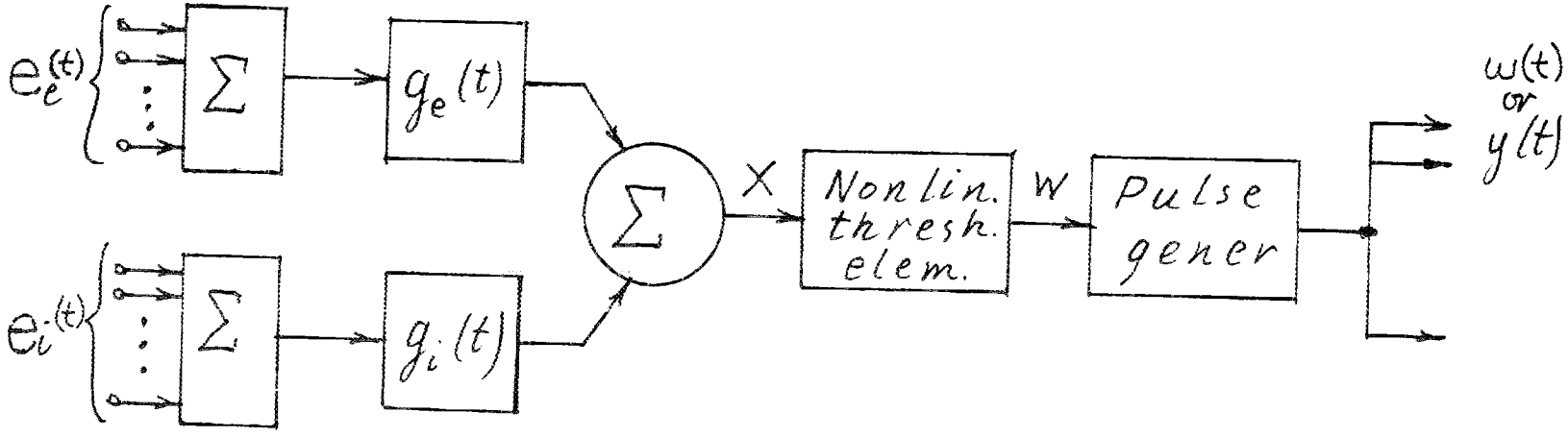

Fig. 9. Simplified Model of a Non-adaptive Ganglion Neuron.

The input-output relations for Fig. 9 may be summarized as

$$Y(t) = \left(\sum_{k=1}^{k_e} e_{e_k}(t)\right) * g_e(t) + \left(\sum_{k=1}^{k_i} e_{k_i}(t)\right) * g_i(t) \tag{13}$$

$$W(t) = \begin{cases} 0 & \text{for:} \quad X \leqslant \theta \\ k(u(t)-\theta) & \text{for:} \quad \theta < X \leqslant \theta_t \\ \omega_{max} & \text{for:} \quad X > \theta_t \end{cases}$$

There are two general theories concerning such pulse coding. The first one assumes that signals are transmitted through nerve fibers by pulse frequency modulation. It means that the amplitude of the signal is represented by an instantaneous frequency ω_y of generated pulses:

where $\omega_y(t) = k\ W(t)$ (14)

and $\omega_y(t_i) = \dfrac{1}{\Delta t(t_i)}$

(defined only for $t = t_i$ where: $\Delta t(t_i)$ is the distance between the pulses i-1 and i.) The integrating circuits of the next stages smooth these discontinuities and usually we assume $\omega_y\ (t_i) \approx \omega_y(t)$.

The second theory is much more complicated and assumes that we must consider pulse-position coding. A signal is coded by the exact position of every pulse in a sequence of pulses transmitted through nerve fibers. There is little evidence that this method of coding really exists in the visual system especially for "black-gray-white" vision.

Equations 7 to 14 may be presented in a simpler form, convenient for visual data processing. For horizontal, bipolar and amacrine cells we present the output-input relation in the form of a linear operator L (•):

$$y(t) = L\ (\underline{X}_e(t),\ \underline{X}_i(t)) \tag{15}$$

where $\underline{X}_e(t)$ is a vector representing all input excitation signals:

$$\underline{e}_e(t) = \left[e_{e_1}, e_{e_2}, \dots e_{e_{k_e}} \right]^T$$

and:

$$\underline{e}_i(t) = \left[e_{i_1}, e_{i_2}, \dots, e_{i_{k_e}} \right]^T$$

(is the same for inhibition signals).

For the ganglion cells we have a series connection of:

1. a linear part
2. a nonlinear part, and
3. some delay τ_d.

$$\omega_y(t+\tau) = N(L \ \underline{e}_e(t), \underline{e}_i(t)) \tag{16}$$

where N $\{\cdot\}$ is a nonlinear threshold operator described by Eq. (13).

3.2. Neuron Interconnections in the Retina

Despite intensive neurophysiological investigations of interregional connections in the retina [see, S. L. Polyak 1957 or R. W. Rodieck (1973)], the existence of several types of connections and their character is still uncertain. Therefore several models of the retina published previously (M. N. Oguztöreli 1983, R. Simonoff 1983, J. C. Curlander et al. 1983, R. E. Kronzauer and Y. Zeevi 1985) differ from each other. Most probably, the authors used different neurophysiological sources and chose different simplifications. It is thus necessary to consider their opinions and select only connections which seem to be important for the current effort.

In Fig. 10 we present a summary of the most convincing information about retinal connections. This figure presents a one-dimensional cross-section of the retina. We assume that a cross-section in any direction gives the same image. That means we have circular or oblong symmetry in structural organization. Notice there is no direct mutual influence between receptors, but there is important indirect influence through a second layer of horizontal cells. Horizontal cells have long connections and permit dynamic processes to be represented by delays and large time constants exceeding 100 msec. Horizontal cells are also excited by photoreceptors, and they exert inhibition on other photoreceptors. As we mentioned previously these influences cause a negative feedback loop controlling local sensitivity when a strong signal is applied to a smaller group of photoreceptors.

Notice that each bipolar cell is connected with a group of photoreceptors. A group of photoreceptors which influences a given cell we call a "receptive field". In the retina receptive fields have circular symmetry (see Fig. 11). A bipolar cell may be excited by a group of photoreceptors placed just opposite (above) the cell and inhibited by receptors placed more peripherally; that is, in a ring around the center. This is an "ON-center" receptive field causing lateral inhibition. Reversed organization or inhibition from the center and excitation from the periphery, is called an "OFF-center" receptive field causing lateral excitation.

There are at least two kinds of bipolar cells:

1. Excitatory (we assume a positive output signal).
2. Inhibitory (we assume a negative output signal).

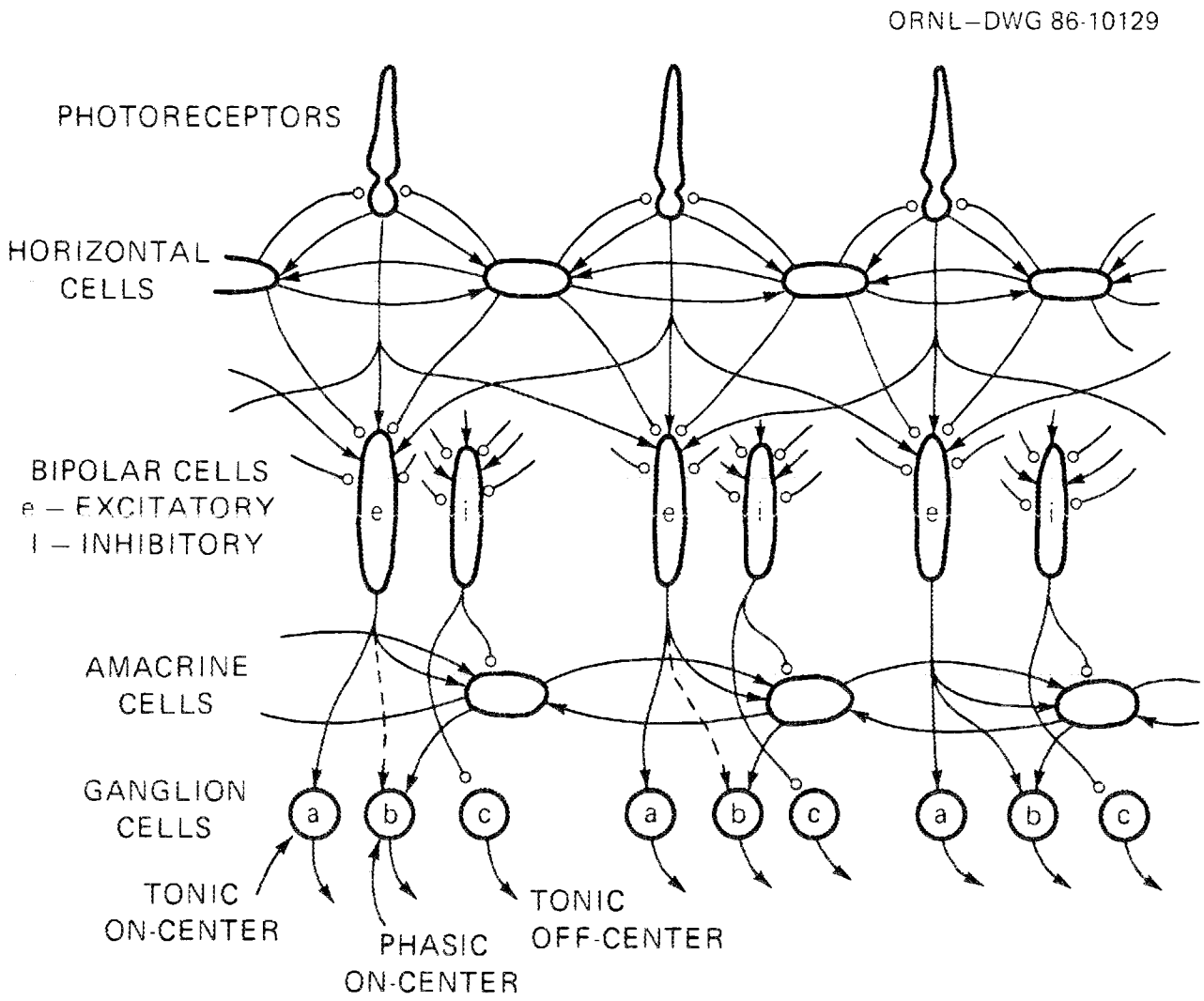

Fig. 10. Simplified Diagram of Most Important Connection in the Retina (Foveal Part).

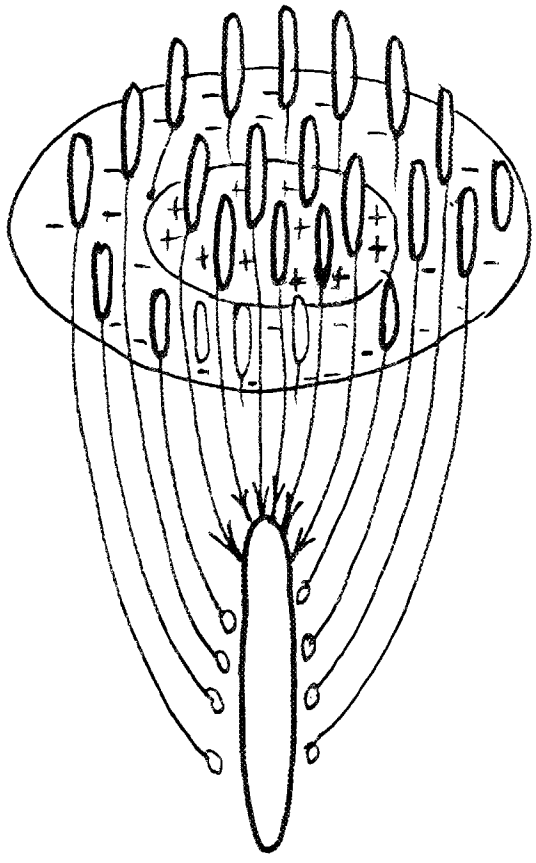

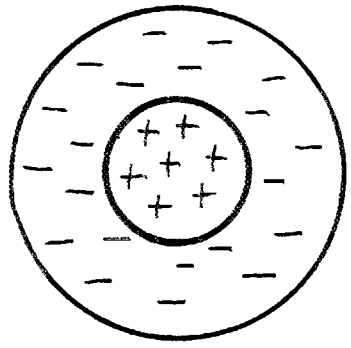

ON-center receptive field.

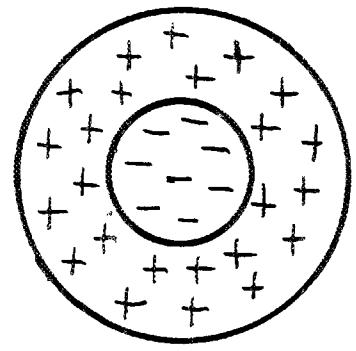

OFF-center receptive field.

Fig. 11. Organization of receptive fields with circular symmetry.

In neuroanatomy there are a minimum of five different kinds of bipolar cells but their functional difference is not clear. In our first year's "black-gray-white" models we do not have sufficient justification to introduce any more bipolar cell types. The next layer containing amacrine cells is organized in a similar way, but transient signals play a more important role. In some animals both ON-center and OFF-center amcrine cell organizations were found, but the ON-center organization is better confirmed. The likely role of the ON-center organization is to generate a so called phasic reaction. A phasic reaction means that the transient reaction (see Fig. 4) to a square wave signal is much stronger than the steady state reaction (the DC component). Such cells emphasize data that captures changes in an image and send them to higher levels of the neural system.

If we take into account small eye movements described in the previous section, we see that really all signals coming from photoreceptors vary even with constant images. These variations cause a modulation of input signals to the visual system and are less dependent on slow changes of system parameters.

The last layer is composed of "ganglion cells". They are strongly nonlinear with threshold characteristics. The output signals from ganglion cells have short pulse shapes (1 msec) of constant duration. These pulses are transmitted through the optic nerve to the central part of the brain.

As a first approximation, ganglion cells may be divided into three groups (ignoring phasic off-center cells) although over 13 types have been identified:

1. Tonic ON-center cells reacting positively to signals from the central part of the receptive field and inhibited by signals from the periphery (outer ring).

2. Tonic OFF-center reacting in just the opposite way as the previous group (the cells in the periphery of the receptive field are inhibited by cells in the center of the receptive field),

3. Phasic ON-center ganglion cells which have a similar organization to the receptive field of the tonic ON-center cells.

The main difference is that the phasic cells have a much stronger transient component and the reaction for a constant signal is very weak.

Summary of Interconnections in the Retina

In conclusion the most important features of interconnection are:

1. Partial multilayer symmetry.

2. Mutual connections resulting in receptive fields (mutual inhibition and mutual excitation).

3. Local dynamic processes that react to any sudden changes in visual data.

4. Approximately linear summation of signals in the first four layers (until the ganglion cells), and a strong nonlinear reaction thereafter.

Our problem then is to select the simplest model for connections and parameters which still maintains the properties important for visual data processing. Next we will present two approaches to retinal models.

3.3. The Static Linear Operator Equations

Lateral Inhibition in Retinal Vision

Lateral inhibition as discusssed in the previous section performs certain mechanistic, image sharpening functions. The amount of inhibition which a photoreceptor exerts on its neighbors is determined by the amount of light falling upon it. Therefore, the amount of inhibition sent out by a strongly illuminated photoreceptor is greater than that which is received from its more weakly illuminated neighbors. This process results in an enhancement of edges.

Evenly illuminated photoreceptors likewise inhibit each other so large homogeneous areas of illumination where there is little information content tend to be suppressed. Although lateral inhibition is simple in concept, figuring out an activation level for all the photoreceptors becomes difficult in practice. This is because in real biological systems, even though each photoreceptor directly inhibits only its neighbors. Each of these neighbors, in turn, inhibits their neighbors and so on. For example, in Fig. 12 photoreceptor A influences photoreceptor B, photoreceptor B influences photoreceptor C, photoreceptor C influences photoreceptor D, and so forth. Ultimately, photoreceptor A has indirect influence upon photoreceptor K.

The propogating effects of lateral inhibition can be seen in electrophysiological recordings [for example in the plot of the compound eye of the Limulus (Horseshoe crab)] in Fig. 13. The dashed line represents the impinging light intensity distribution, the open circles the chemical

ORNL–DWG 86-10131

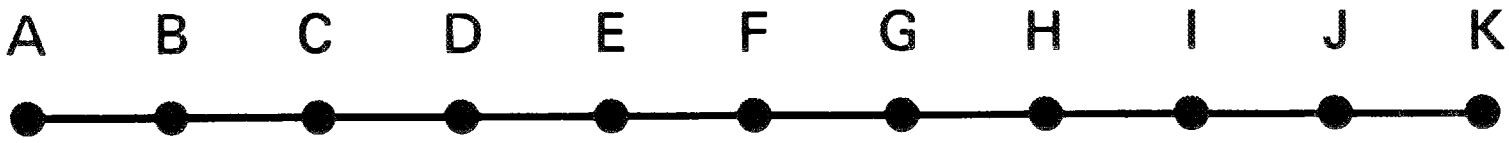

Fig. 12. Photoreceptor Influences.

ORNL-DWG 86-10132

SPATIAL INTERACTION IN THE VISUAL SYSTEM

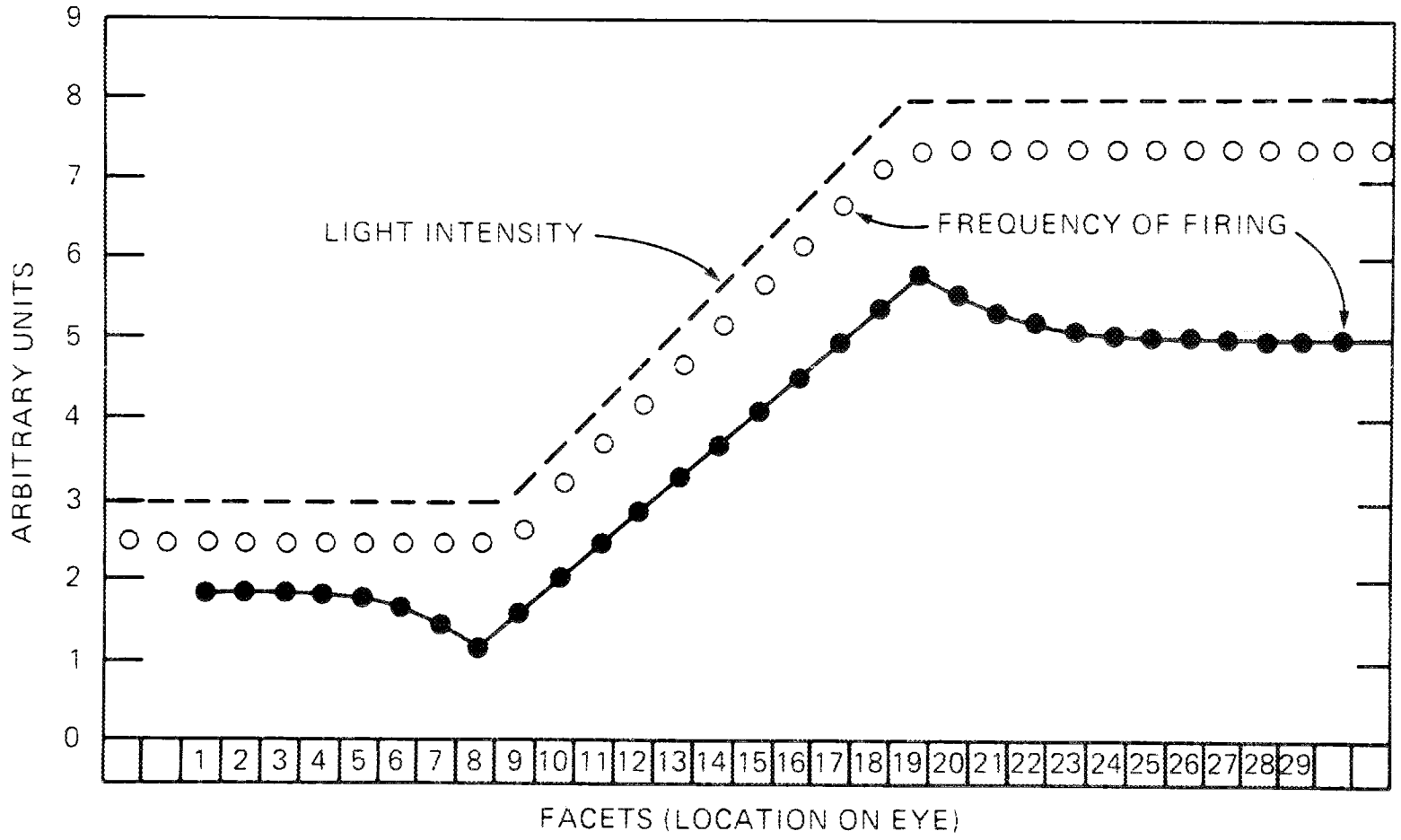

Fig. 13. Lateral Inhibition in the Eye of Limucus.

conversion from light intensity units to neural activation units, and the solid circles the final activation levels.

If for simplicity we assume a totally connected network (i.e., all inhibition is passed directly to the elected neurons) the inhibition process can be described by the following system of simultaneous equations.

Let: a = a constant which converts from light intensity units to neural activation units,

i = the light intensity striking a photoreceptor,

x = the output of a photoreceptor,

j = the column in which a photoreceptor is located,

l = the row in which a photoreceptor is located,

k = (j,l) (j+m,l+n) = inhibitory constant between photoreceptor (j,l) and photoreceptor (j+m,l+n).

Then,

$$
\begin{aligned}
x(j,\ell) = {} & ai(j,\ell) - k(j,\ell)(j+1,\ell)x(j+1,\ell) \\
& - k(j,\ell)(j-1,\ell)x(j-1,\ell) - k(j,\ell)(j,\ell+1)x(j,\ell+1) \\
& - k(j,\ell)(j,\ell-1)x(j,\ell-1) - k(j,\ell)(j+2,\ell)x(j+2,\ell) \\
& - k(j,\ell)(j-2,\ell)x(j-2,\ell) - k(j,\ell)(j,\ell+2)x(j,\ell+2) \\
& - k(j,\ell)(j,\ell-2)x(j,\ell-2) - k(j,\ell)(j+3,\ell)x(j+3,\ell) \\
x(j+1,\ell) = {} & ai(j+1,\ell) - k(j+1,\ell)(j+2,\ell)x(j+2,\ell) - k(j+1,\ell)(j,\ell)x(j,\ell) \\
& - k(j+1,\ell)(j+1,\ell+1)x(j+1,\ell+1) - k(j+1,\ell)(j+1,\ell-1)x(j+1,\ell-1) \\
& - k(j+1,\ell)(j+3,\ell)x(j+3,\ell) - k(j+1,\ell)(j-1,\ell)x(j-1,\ell) \\
& - k(j+1,\ell)(j+1,\ell+2)x(j+1,\ell+2) - k(j+1,\ell)(j+1,\ell-2)x(j+1,\ell-2) \\
& - k(j+1,\ell)(j+4,\ell)x(j+4,\ell) \; . \; . \; .
\end{aligned}
$$

$$\vdots$$

The above equations are simply a modified (threshold factor omitted) form of the lateral inhibition equations first proposed by Hartline and Ratliff.

The solution of such a system of equations, although straightforward in theory, becomes difficult in practice if the system is very large. We would actually like to solve a system of a million (1000 x 1000 array of photoreceptors) equations each having a million terms. However, the present state-of-the-art for a direct solution in a reasonable amount of time is only a few thousand equations each having a few thousand terms. Therefore, as discussed in the next section, it was necessary to modify the above equations by making a simplifying assumption about symmetries and to then attempt a solution using a computationally efficient method.

The Solution of the Lateral Inhibition Equations

To implement these ideas in a solvable form, we assume a square array of receptors located at the lattice points $\vec{x} = (j,k)$, $0 \leq j \leq N-1$, $0 \leq k \leq N-1$. A vector of incident intensities $\vec{P} = [P_{\vec{x}}]$ is related to the vector of intensities after the lateral inhibition process $\vec{Y} = [Y_{\vec{x}}]$ via a linear transformation matrix A:

$$A\ Y = P \quad . \tag{1}$$

Because of the physical process involved, the matrix A is not completely arbitrary, but rather has a very special form. It is physically reasonable that the inhibition between two receptors $\vec{x}_1 = (j_1, k_1)$ and $\vec{x}_2 = (j_2, k_1)$ or $\vec{x}_2 = (j_2, k_2)$ depend only on their relative position vector (j_1-j_2, k_1-k_2). For example, the inhibition relating the sites (0,0) and (1,1) is the same as that for the pair $\{(1,1), (2,2)\}$, while the same is true for the two step pairs $\{(0,0), (0,3)\}$ and $\{(2,2), (2,5)\}$.

This constraint is reflected in the structure of matrix A. If the matrix elements are denoted by $a_{\vec{x},\vec{y}}$ (representing the inhibition connecting the sites $\vec{x}$ and $\vec{y}$), then for any $\vec{z}$ such that $\vec{x} + \vec{z}$ and $\vec{y} + \vec{z}$ are also receptors (i.e. the coordinates satisfy the constraints $0 \leq j \leq N-1$, $0 \leq k \leq N-1$)

$$\text{then} \qquad a_{\vec{x}+\vec{z},\,\vec{y}+\vec{z}} = a_{\vec{x},\vec{y}} \tag{2}$$

(In fact there is further symmetry present, but this will be ignored for the moment).

The provision that $\vec{x} + \vec{z}$ and $\vec{y} + \vec{z}$ also be pixels is needed because of the finite size of the array, and this condition makes the mathematics considerably more difficult. A reasonable approximation, considering the number of pixels present in the retina, is to allow the system to be infinite in extent ($-\infty < j < \infty$, $-\infty < k < \infty$). The matrix A then becomes translationally invariant: Eq. (2) holds for any $\vec{x}$, $\vec{y}$, $\vec{z}$. Because of the translation invariance, the infinite matrix A is mathematically much more tractable.

To solve, we define the Fourier Transform of a vector $[\hat{R}(\vec{q})]$ of a vector $R = [r_{\vec{x}}]$ by:

$$\hat{R}(\vec{q}) = \sum_{\vec{x}} r_{\vec{x}} e^{-i\vec{q}\cdot\vec{x}} \quad ; \tag{3}$$

here $q = (q_1, q_2)$ and $-\pi \leq q_1 \leq \pi$, $-\pi \leq q_2 \leq \pi$. The corresponding transform of the matrix A is given by:

$$\hat{A}(\vec{q}) = \sum_{\vec{x}} A_{\vec{o},\vec{x}} e^{-i\vec{q}\cdot\vec{x}} \quad ; \tag{4}$$

Both $\hat{R}$ and $\hat{A}$ are complex valued functions of the variable $\vec{q}$. The matrix multiplication [Eq. (1)] in "real space" has the form of a convolution (as was discussed in Chapter 2) and under Fourier Transformation,

convolution becomes simple multiplication. In "$\vec{q}$-space". Equation (1) is therefore

$$\hat{A}(\vec{q})\ \hat{Y}(\vec{q}) = \hat{R}(\vec{q}) \tag{5}$$

Since this is just a multiplication of functions,

$$\hat{Y}(\vec{q}) = \frac{\hat{R}(\vec{q})}{\hat{A}(\vec{q})} \quad . \tag{6}$$

and the real space vector $Y = [y_{\vec{x}}]$ can be obtained by an inverse Fourier Transformation. Thus, once the matrix A is known the system of linear equations (1) can be easily solved and the transformation effect of this operation on a pattern can be computed.

Moreover since Eq. (5) can also be written as

$$\hat{A}(\vec{q}) = \frac{\hat{R}(\vec{q})}{\hat{Y}(\vec{q})} \tag{5}$$

if both R and Y were known and $Y \neq 0$, then A can be computed. This is in fact, the procedure that has been followed using a series of subjective illusions (see Chapter 4). In this case the incident illusion intensity $r_{\vec{x}}$ is either 0 (white) or 1 (black); the values for Y were obtained experimentally by asking subjects to gauge the brightness of the illusory effects. The procedure for obtaining the values for Y is discussed in detail in Chapter 4 and the graphic results obtained are presented. First however, we will complete the mathematical discussion of retina modeling by presenting a second approach to simulating the effects of early retinal layers. This approach will consider nonlinear and dynamic characteristics

not captured by a single lateral inhibition matrix. The mathematics are considerably more complex and readers can go directly to Chapters 4 and 5 for summary statements if desired.

3.4. The Gawronski Model

A Mathematical Description of the Multilayer Net Modelling Retinal Processes

As mentioned in the introduction, the retina is a multilayer structure. Such a structure is very useful if one deals with parallel multichannel signals. Multilayer organization means that neuron cells are distributed on parallel surfaces. From a functional point of view, those surfaces may be treated as parallel planes. The most important property of such organization is that the connection rules and parameters between two similar neural elements are the same (excluding some boundary effects). In the retina we noted circular symmetry in the receptive fields reflected in a circular symmetry of neural connections. Some examples of layers, shown in a one-dimensional cross section are presented in Fig. 14. The simplest configuration is shown in Fig. 14a where every element of the first layer sends signals to a group of elements in the second layer. No feedback loop exists in this configuration. Such a net may be described by the relation:

$$X_k = a_0 e_k + a_{-1} e_{k-1} + a_1 e_{k+1} \quad . \tag{17}$$

Here only the influence from the nearest neighbors is assumed as in Section 3.2. If the range of mutual influence is greater than one (for example, it is equal to "h") we have the relation.

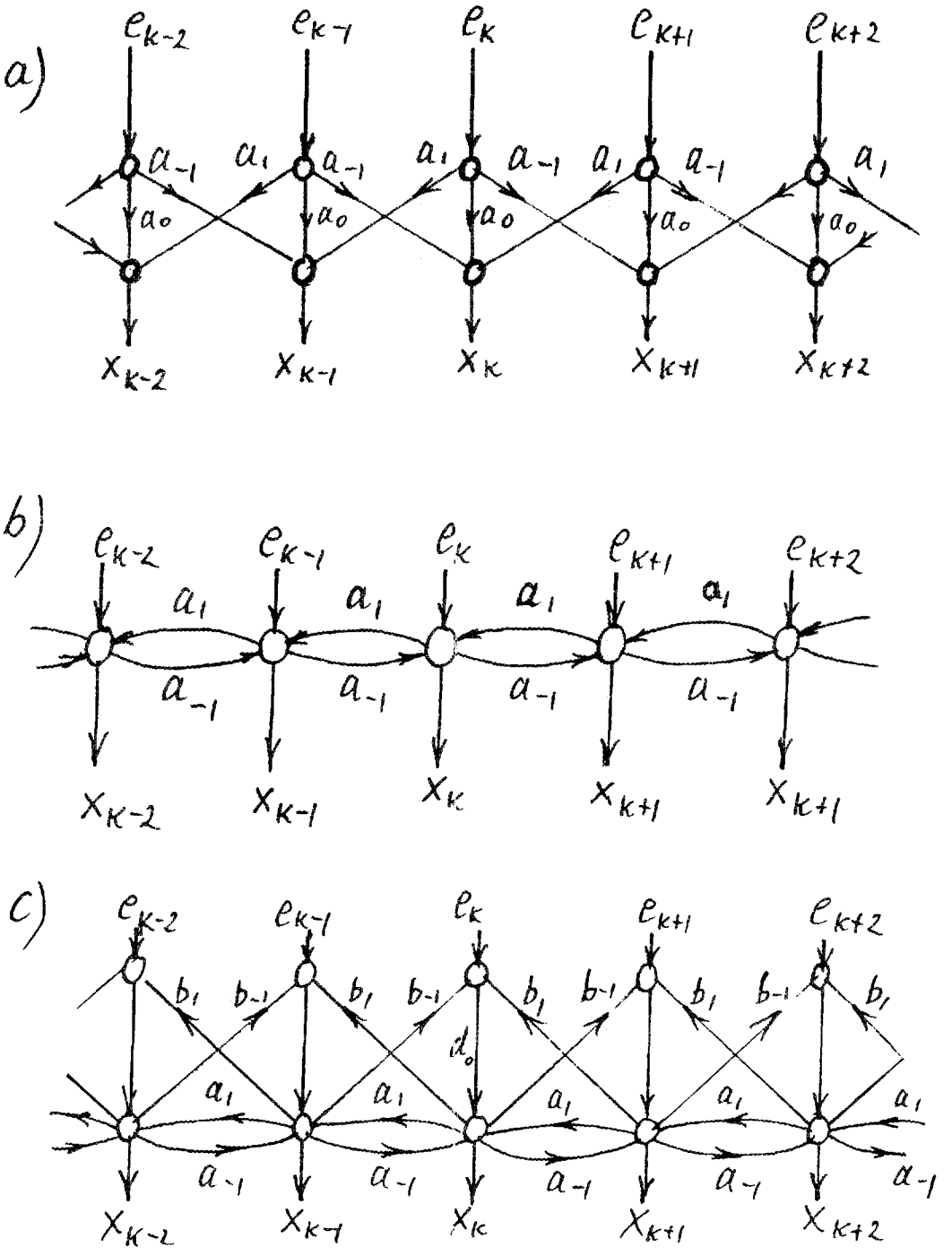

Fig. 14. One-Dimensional Layer Nets.

$$x_k = \sum_{s=-h}^{s=h} a_s \, e_{k+s} \quad , \tag{18}$$

where:

a_s - Coefficient of influence from a cell in the first layer which is shifted from cell k by "s" elements.

e_{k+s} - value of excitation (output from the first layer) of cell number "k+s".

In Fig. 20b we have a one layer net with mutual connections that form many feedback loops. The relation between the input "e" and output "x" is now defined by the equation:

$$x_k = a_0 x_k + a_{-1} x_{k-1} + a_1 x_{k+1} + b e_k \tag{19}$$

or for more connections:

$$x_k = \sum_{s=-h}^{s=h} a_s x_{k+s} + b e_k \quad . \tag{20}$$

Thus we generate a set of "k" equations assuming that "a_s" and "b" are constant and k = the # of elements. These equations may be presented in matrix form as:

$$\underline{x} = A \, \underline{x} + b\underline{e} \tag{21}$$

where: A is a multidiagonal band matrix:

and $\underline{x}$ is a vector of output values x.

$$A = \begin{bmatrix} a_0 & a_1 & a_2 \; \cdots & a_h & 0 \cdots 0 \\ a_{-1} & a_0 & a_1 \; \cdots & a_h & 0 \cdots 0 \\ & & & & \\ 0 \cdots 0 & a_h \cdots & & a_{-2} \; a_{-1} & a_0 \end{bmatrix} \tag{22}$$

if $a_s = a_{-s}$, matrix A is then symmetric which leads to some interesting properties considered later.

In Fig. 14c, feedback from layer II to layer I is introduced. These more complex input-output relations are described by the relations.

$$x_k = b_o\, e_k + b_{-1}\, y_{k-1} + b_1\, y_{k+1} \tag{23}$$
$$y_k = d_o x_k + a_{-1}\, y_{k-1} + a_1\, y_{k+1} + a_o y_k$$

and are equivalent to a single equation:

$$y_k = (a_{-1} + d_o b_{-1})\, y_{k-1} + (a_1 + d_o b_1)\, y_k{+1} \tag{24}$$
$$+ a_o\, y_k + d_o b_o e_k$$

This equation is also equivalent to Eq. (19). We see then that the nets presented on Fig. 14b and 14c are described by equivalent equations and have the same properties. The structure presented in Fig. 14c is similar to the connections between photoreceptors and amacrine cells. Some dynamic properties of this structure will also be considered later.

Notice that two main types of layer connections exist: one without feedback, the other with feedback.

A similar organization exists for two-dimensional nets. In Fig. 15 the connections of a two-layer net without feedback are presented. For mathematical convenience we have introduced a matrix like distribution of elements. Connection coefficients V_{rs} will be called "input weights and they represent the transmittance between elements from the first to the second layer. Indices "r" and "s" denote correspondingly how many columns and rows are shifted from the source cell (layer I) to the destination cell (layer II). The maximum distance for which connections exist is "range h", that is:

$$0 \leq r \leq h \quad \text{and } 0 \leq s \leq h \tag{25}$$

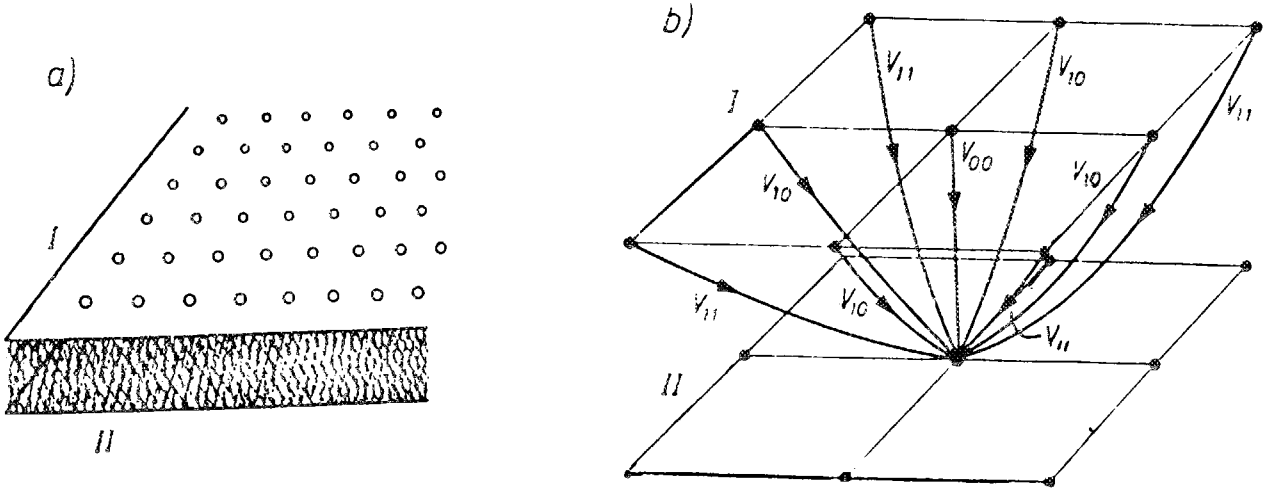

Fig. 15. Two-dimensional, Two Layer-Organization of Parallel Data Processing.

Earlier in the background discussion we noted the circular symmetry of retinal connections, but in higher levels of the visual system, there is a more general rule of symmetry described by the relation:

$$^{\upsilon}|r||s| = {}^{\upsilon}|s||r| \quad \text{where } \upsilon \text{ is a single weight} \tag{26}$$

called radial symmetry. Operationally radial symmetry means that moving along a line away from the center in both directions we arrive at same values of weights υ at equal distances.

The influence of elements of column k in the first layer on the second layer, may be described by an equation similar to (18). For row "i" and column "k" we get:

$$x_{oi,k} = \sum_{l=-h}^{l=h} \upsilon_{l,o}\, e_{i+l,k}\ , \text{ where } x_{oi,k} \text{ is a single output} \tag{27}$$

or in matrix notation:

$$X_o = V_o\, E \tag{28}$$

where: $X_o = [x_{oik}]$ = matrix of outputs

V_o = matrix of weights

E = matrix of inputs

when only influences from the same column are taken into account.

$$V_o = \begin{bmatrix} 00 & 10 & 20 & \cdots & ho & \cdots & \cdots & \cdots & \cdots & 0 \\ 10 & 00 & 10 & 20 & \cdots & ho & 0 & \cdots & \cdots & 0 \\ 20 & 10 & 00 & 10 & 20 & \cdots & \cdots & \cdots & \cdots & 0 \\ \cdots & \cdots & \cdots & \cdots & \cdots & \cdots & \cdots & \cdots & \cdots & \cdot\cdot \\ \cdots & \cdots & \cdots & \cdots & \cdots & \cdots & \cdots & \cdots & \cdots & \cdot\cdot \\ \cdots & \cdots & \cdots & \cdots & \cdots & \cdots & \cdots & \cdots & \cdots & \cdot\cdot \\ \cdots & \cdots & \cdots & \cdots & \cdots & \cdots & \cdots & \cdots & \cdots & \cdot\cdot \\ \cdots & \cdots & \cdots & \cdots & \cdots & \cdots & \cdots & \cdots & \cdots & \cdot\cdot \\ \cdots & \cdots & \cdots & \cdots & \cdots & \cdots & \cdots & \cdots & \cdots & \cdot\cdot \\ ho & h-10 & \cdots & \cdots & 10 & 00 & 10 & \cdots & \cdots & 0 \\ \cdots & \cdots & & \cdots & \cdots & \cdots & \cdots & \cdots & \cdots & \cdot\cdot \\ \cdots & \cdots & \cdots & \cdots & \cdots & \cdots & \cdots & \cdots & \cdots & \cdot\cdot \\ \cdots & \cdots & \cdots & \cdots & \cdots & \cdots & \cdots & \cdots & \cdots & \cdot\cdot \\ \cdots & \cdots & \cdots & \cdots & \cdots & \cdots & \cdots & \cdots & \cdots & \cdot\cdot \\ 0 & \cdots & \cdots & \cdots & 0 & ho & \cdots & 10 & oo & 10 \\ 0 & \cdots & \cdots & \cdots & \cdots & 0 & ho & \cdots & 10 & 00 \end{bmatrix} \qquad (29)$$

V_o - is a multidiagonal matrix with only 2h+1 nonzero diagonals. it represents only influences from column "k" elements just above the column of interest.

The influence from any other column shifted by s right or left may also be represented by a similar matrix of weight V_s.

$$V_s = \begin{bmatrix} 0s & 1s & 2s & \cdots & \cdots & \cdots & hs & 0 & \cdots & 0 \\ 1s & 0s & 1s & \cdots & \cdots & \cdots & h-is & hs & 0 & 0 \\ 2s & 1s & 0s & 1s & & \cdots & \cdots & \cdots & \cdots & 0 \\ \cdots & \cdots & \cdots & \cdots & \cdots & \cdots & \cdots & \cdots & \cdots & \cdot\cdot \\ \cdots & \cdots & \cdots & \cdots & \cdots & \cdots & \cdots & \cdots & \cdots & \cdot\cdot \\ \cdots & \cdots & \cdots & \cdots & \cdots & \cdots & \cdots & \cdots & \cdots & \cdot\cdot \\ \cdots & \cdots & \cdots & \cdots & \cdots & \cdots & \cdots & \cdots & \cdots & \cdot\cdot \\ \cdots & \cdots & \cdots & \cdots & \cdots & \cdots & \cdots & \cdots & \cdots & \cdot\cdot \\ \cdots & \cdots & \cdots & \cdots & \cdots & \cdots & \cdots & \cdots & \cdots & \cdot\cdot \\ hs & h-1s & \cdots & \cdots & 1s & s0 & 1s & \cdots & \cdots & 0 \\ \cdots & \cdots & & \cdots & \cdots & \cdots & \cdots & \cdots & \cdots & \cdot\cdot \\ \cdots & \cdots & \cdots & \cdots & \cdots & \cdots & \cdots & \cdots & \cdots & \cdot\cdot \\ \cdots & \cdots & \cdots & \cdots & \cdots & \cdots & \cdots & \cdots & \cdots & \cdot\cdot \\ \cdots & \cdots & \cdots & \cdots & \cdots & \cdots & \cdots & \cdots & \cdots & \cdot\cdot \\ 0 & \cdots & \cdots & \cdots & 0 & hs & \cdots & 1s & 0s & 1s \\ 0 & \cdots & \cdots & \cdots & \cdots & 0 & \cdots & \cdots & 1s & 0S \end{bmatrix} \quad (30)$$

To calculate the influence of a column shifted by "s" positions, we must multiply corresponding outputs from the first layer $e_{j,k+s}$,

(where $i-h < j < i + h$) by corresponding weights of the shifted matrix V_s. To place this operation in matrix form we introduce a matrix E_s (shifted by "s" columns left or right).

$$E_s = \begin{array}{c} \qquad\qquad\qquad\qquad\qquad\qquad\qquad\qquad\qquad\qquad\qquad\qquad \text{s Column} \\ \begin{bmatrix} e_{1,s+1} & e_{1,s+2} & \cdots\cdots & \cdots\cdots & e_{1,m} & 0 & \cdots\cdots & 0 \\ e_{2,s+1} & e_{2,s+2} & \cdots\cdots & \cdots\cdots & e_{2,m} & 0 & \cdots\cdots & 0 \\ \cdots & \cdots & \cdots & \cdots & \cdots & \cdots & \cdots & \cdots \\ \cdots & \cdots & \cdots & \cdots & \cdots & \cdots & \cdots & \cdots \\ \cdots & \cdots & \cdots & \cdots & \cdots & \cdots & \cdots & \cdots \\ e_{n,s+1} & e_{n,s+2} & \cdots\cdots & \cdots\cdots & e_{n,m} & 0 & \cdots\cdots & 0 \end{bmatrix} \end{array} \tag{31}$$

Shifting a unit diagonal matrix left or right we can obtain post multiplication of E by use of a "shifting matrice" or so called "permutation matrices" H and F:

$$H = \begin{bmatrix} 0 & 1 & 0 & 0 & \cdots & 0 \\ 0 & 0 & 1 & 0 & \cdots & 0 \\ \cdots & \cdots & \cdots & \cdots & \cdots & \cdots \\ \cdots & \cdots & \cdots & \cdots & \cdots & \cdots \\ 0 & \cdots & \cdots & 0 & 1 & 0 \\ 0 & \cdots & \cdots & 0 & 0 & 1 \\ 0 & \cdots & \cdots & \cdots & \cdots & 0 \end{bmatrix} \qquad F = \begin{bmatrix} 0 & 0 & 0 & \cdots & \cdots & 0 & 0 \\ 1 & 0 & 0 & \cdots & \cdots & 0 & 0 \\ 0 & 1 & 0 & \cdots & \cdots & 0 & 0 \\ \cdots & \cdots & \cdots & \cdots & \cdots & \cdots & \cdots \\ \cdots & \cdots & \cdots & \cdots & \cdots & \cdots & \cdots \\ \cdots & \cdots & \cdots & \cdots & \cdots & \cdots & \cdots \\ 0 & \cdots & \cdots & \cdots & 1 & 0 & 0 \\ 0 & \cdots & \cdots & \cdots & 0 & 1 & 0 \end{bmatrix} \tag{32}$$

Further shifts may be obtained by raising matrix H (or F) to a corresponding power e.g., 2,3, ..., k. Therefore we can include the influence from a column right shifted by "s" by introducing the component:

$$X_s = V_s \cdot E \cdot H^s \quad . \tag{33}$$

Correspondingly, the influence from a column shifted left by "s" means the addition of a component:

$$X_{-s} = V_s \cdot E \cdot F^s \quad . \tag{34}$$

Therefore the resulting influence X from all columns may be expressed by a matrix:

$$X = V_k EF^h + V_{h-1}\ EF^{h-1} + \ldots + V_2 EF^2 + V_1 EF + V_o E$$
$$+ V_1 EH + V_2 EH^2 + \ldots\ V_{h-1} EH^{k-1} + V_h EH^h \tag{35}$$

or in shorter form:

$$X = V_o E + V_1\ E[F+H] + V_2 E\ [F^2 + H^2] + \ldots$$
$$\ldots + V_h E\ [F^h + H^h] \quad .$$

To simplify notation again we introduce the operation X defined by formula (36):

$$X = V \otimes E \quad . \tag{36}$$

or written in explicit form as:

$$x_{ij} = \sum_{s=-h}^{s=h} \sum_{r=-h}^{r=h} v_{rs}\ e_{i+r,j+s} \quad . \tag{37}$$

The main advantage of the notation of formulas 25-37 with respect to the simpler notation used in Section 3.2 (and by some other authors also) is a very large decrease in the order of matrices involved.

For n photoreceptors, many authors use square matrices because they use a separate equation for every photoreceptor element. In our notation we will deal with matrices of the order $\sqrt{n} \times \sqrt{n}$. For example if we assume $n = 10^6$ photoreceptors we use matrices of the order $10^3 \times 10^3$. Every element of this type of matrix corresponds to one input or output element. We can reduce relations (35 to 37) to a still simpler form as a matrix product. For this purpose we introduce a new descriptive index for input and output signals, taking the first column, appending the next column and so on to produce a one-dimensional vector from a two-dimensional matrix. We get the vectors:

$$E = \begin{bmatrix} e_1 \\ e_2 \\ \cdot \\ \cdot \\ \cdot \\ \cdot \\ e_{m \cdot n} \end{bmatrix} \quad \text{and} \quad X = \begin{bmatrix} x_1 \\ x_2 \\ \cdot \\ \cdot \\ \cdot \\ \cdot \\ x_{n \cdot m} \end{bmatrix} \tag{38}$$

where: m number of rows and

n number of columns

Next we introduce a multidiagonal matrix V_{II}. Every element of this matrix will now consist of one matrix V_s defined by formula (30).

$$V_{II} \begin{bmatrix} V_0 & V_1 & V_2 & \cdots & V_h & 0 & \cdots & \cdots & \cdots & 0 \\ V_1 & V_0 & V_1 & V_2 & \cdots & V_h & 0 & \cdots & \cdots & 0 \\ V_2 & V_1 & V_0 & V_1 & V_2 & \cdots & V_h & 0 & \cdots & 0 \\ \cdots & \cdots & \cdots & \cdots & \cdots & \cdots & \cdots & \cdots & \cdots & \cdots \\ \cdots & \cdots & \cdots & \cdots & \cdots & \cdots & \cdots & \cdots & \cdots & \cdots \\ \cdots & \cdots & \cdots & \cdots & \cdots & \cdots & \cdots & \cdots & \cdots & \cdots \\ \cdots & \cdots & \cdots & \cdots & \cdots & \cdots & \cdots & \cdots & \cdots & \cdots \\ \cdots & \cdots & \cdots & \cdots & \cdots & \cdots & \cdots & \cdots & \cdots & \cdots \\ \cdots & \cdots & \cdots & \cdots & \cdots & \cdots & \cdots & \cdots & \cdots & \cdots \\ \cdots & \cdots & \cdots & \cdots & \cdots & \cdots & \cdots & \cdots & \cdots & \cdots \\ \cdots & \cdots & \cdots & \cdots & \cdots & \cdots & \cdots & \cdots & \cdots & \cdots \\ \cdots & \cdots & \cdots & \cdots & \cdots & \cdots & \cdots & \cdots & \cdots & \cdots \\ \cdots & \cdots & \cdots & \cdots & \cdots & \cdots & \cdots & \cdots & \cdots & \cdots \\ \cdots & \cdots & \cdots & \cdots & \cdots & \cdots & \cdots & \cdots & \cdots & \cdots \\ 0 & \cdots & \cdots & 0 & V_h & \cdots & \cdots & V_2 & V_1 & V_0 \end{bmatrix} \quad (39)$$

Thus relations (35 to 37) are represented in a still more compact form as:

$$V_{II} \cdot E = X \quad . \qquad (40)$$

However matrix V_{II} still has dimension m•n by m•n which means a terrible increase in the computer time used to calculate the processes, especially if we introduce nonlinearities and dynamic processes. Relation (40) is useful however for formal calculations when we introduce systems with feedback loops.

Recall that our results so far are constrained to static situations. Using the mathematical description of a neuron given in Chapter 3.1 we can extend our results to dynamic processes and then nonlinear outputs.

To introduce dynamic properties in a net we can use Eqs. (9), (10) or (11).

For every signal x(t), in place of the products $v_{r,s} \cdot e_{i+r,j+s}$ we use the convolution operation.

$$e_{i+r,j+s}(t) * g_{r,s}(t) \tag{41}$$

where

$g_{r,s}(t)$ is the pulse response of the transfer function $G_{r,s}$ of the connection which replaces the value of weight v_{rs}.

Therefore we can construct a matrix operator G which replaces matrix V in equations (35) and (36).

Resulting signals $y_{i,j}$ (see Fig. 6 and 8) may be now calculated using the formal relation

$$Y = E \otimes G \tag{42}$$

where:

$$G = \begin{bmatrix} g_{11} & \cdots & g_{1m} \\ \cdot & & \cdot \\ \cdot & & \cdot \\ \cdot & & \cdot \\ g_{n1} & \cdots & g_{nm} \end{bmatrix} , \tag{43}$$

is a symmetric matrix of operators $g_{r,s}$ defined by relation (9), the operation $\otimes$ is analogous to operation (35) but with a transposed order of matrix multiplication:

$$Y = E \cdot G_0 + E(F+H)\ G_1 + \ldots + E(F^h + H^h)G_h \tag{44}$$

and

$$Y = \begin{bmatrix} Y_{11} & \cdots\cdots & Y_{1m} \\ \cdot & & \cdot \\ \cdot & & \cdot \\ \cdot & & \cdot \\ Y_{n1} & & Y_{nm} \end{bmatrix}$$

is a matrix of signals from the output of the linear parts of the neuron defined by position "i,j".

Operations (42) or (44) look complex at first but are still much simpler than a set of $n \cdot m$ (n^2 for a quadratic matrix) differential equations which has been proposed by some authors investigating small portions of the retina e.g., (Oguztoreli 1983, Simonoff 1983).

Here we have avoided the introduction of differential equations by using a convolution integral (9) for local dynamic processes. It is much easier to calculate a simple integral on the computer than use any method for solving differential equations. For future analog modelling, the solution is still easier because we may use RC circuits at the input of each neuron.

In the next steps of retina modelling we take into account nonlinear processes represented by the threshold characteristics of neurons. They

are defined by the second part of Eq. (13). Introducing a matrix of thresholds:

$$T = \begin{bmatrix} \Theta_{11} & \cdots & \Theta_{1m} \\ \vdots & & \vdots \\ \Theta_{n1} & & \Theta_{nm} \end{bmatrix} \tag{45}$$

defined for every neuron of the second layer we, define a <u>nonlinear</u> operator:

$$W_{i,j} = N\,(Y_{i,j} - \Theta_{i,j}) \tag{46}$$

In most cases we may assume $\Theta_{i,j} = \Theta$ constant and is equal for all neurons, but in general the threshold may be variable and represents some adaptive processes in the nervous system.

<u>The Full Model</u>

Using (46) and (42) the final model of a two layer net without feedback may be described by the formula:

$$W = N\,\{E \times G - T\} \tag{47}$$

where the nonlinear operation N acts on every element of the resulting matrix: $E \otimes G - T$.

In most cases it is sufficient to simulate nonlinear properties of a neuron by use of threshold characteristics and saturation.

The situation gets much more complicated if we consider feedback loops formed by mutual connections in one layer. For a one-dimensional case, an analogous situation was considered in Fig. 14 and Eqs. (20-24). A two-dimensional feedback net is presented in Fig. 16 but only the simplest case of connections between neighbors is shown.

For a static case we also introduce two matrices of connection weights:

V_1 - matrix of connections weights existing in the same layer.

V_2 - matrix of connection weights between successive layers.

The matrix of output signals W is now defined by a set of nonlinear algebraic equations:

$$W_s = N \{V_1 \times W + V_2 \times E - T\} \tag{49}$$

This is a set of n•m equations because every element of the matrix W is defined by one equation.

If the solution of this equation exists, then we may define the operation ϕ:

$$W_s = \phi [E] \tag{50}$$

i.e., data processing performed by a two-dimensional net with feedback.*

It is very probable that in living systems we sometimes have situations when there exists more than one solution (i.e., unstable states). In such situations an adaptive mechanism must change the weights V_1 or thresholds T, until a stable situation is achieved.

*For a linear case, W is equivalent to Y. We keep the same notation to emphasize that W is the output matrix for both cases.

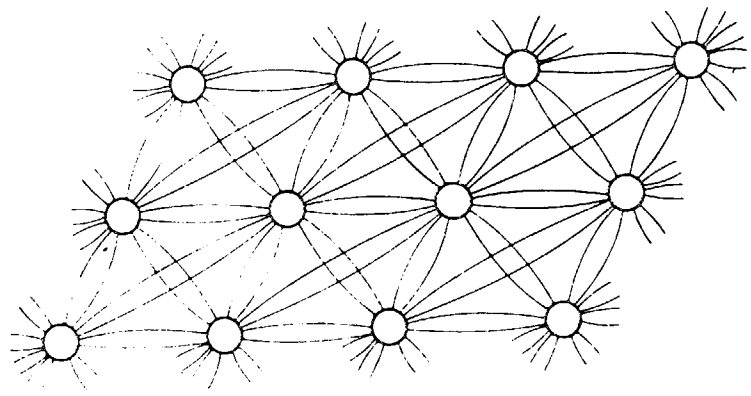

Fig. 16. Two-Dimensional Net with Local Feedbacks.

For dynamic processes, Eq. (49) is replaced by a set of nonlinear differential or integral equations. Using the same matrix notation as in (47) we represent this equation by the formula:

$$W_D = N \{ W \otimes G_1 + E \otimes G_2 - T \} \tag{51}$$

where:

G_1 = matrix of transmittances for signals between elements in the same layer

G_2 = matrix of transmittances for signals coming from the previous layer

N = nonlinear thresholding operation with saturation

Equation (51) also represents $n \cdot m$ equations because every element of matrix W is one variable. Nevertheless, the solution of this equation may be simplified considerably using the fact that the matrices involved in the $\otimes$ operation are symmetric and very sparse.

For large values of $n \cdot m$, calculation of output signals by a digital computer may be impossible and a much more practical solution may be the test construction of a wafer of n x m elements with the necessary connections and transmittances. Every element of such a wafer would have an output at which we could measure the result of parallel data processing.

Fortunately for early retinal processes we may simplify Eq. (51) using the results of our analysis of the retina structure presented previously. The most important assumption was the linearity of processes existing in the first four layers of retina. A large amount of neurophysiological data (see Rodieck 1973) supports this assumption, and most researchers modelling segments of the retina make similar assumptions (e.g., Simonoff 1983). We therefore neglect the nonlinear operator N in

Eq. (49) and for simplicity use standard matrix notation introduced in Eqs. (38-40). We thus obtain a linear set of equations in matrix form:

$$W_S = V_1 \cdot W + V_2 E \tag{52}$$

except now W and E are column vectors defined by (38) and V_1 or V_2 by (39). Assuming that appropriate inverted matrices V_1^{-1} and $(I - V_1)^{-1}$ exist, and solving with respect to W we get:

$$W_S = (I-V_1)^{-1} \cdot V_2 E \tag{53}$$

If we construct a net with connection weights:

$$V_E = (I-V_1)^{-1} \cdot V_2 \tag{54}$$

we obtain a two layer net equivalent to the above net with local feedback.

For modelling it is much more convenient to use a two layer net without feedback. We can then experimentally find values of matrix V_E in place of defining the elements of matrix V_1. As a result we must calculate operator (40) which is much simpler than solving m x n equations (52).

For dynamic processes we apply similar considerations but now must use a matrix of linear integral equations:

$$W_D = W * G_1 + E*G_2 \tag{55}$$

Here also W, E, G_1 and G_2 are defined in an analogous way to (38), (39), and (43). Every element of G is an integral operator acting on variable $W_{i,j}$.

We are interested in a unique solution of Eq. (55), therefore if we assume that the resolution kernel for Eq. (55) exists we get:

$$W_D = E * G_E \tag{56}$$

When two successive layers are applied linearly we obtain a superposition of operator (56)

$$Z = (E*G_{E1}) * G_{E2} = W*G_{E2} \tag{57}$$

where G_{E2} and G_{E1} are the outputs from image E on layers 1 and 2 respectively.

From this result we infer that in place of modelling a very complex multilayer network with feedback we can model an equivalent <u>two</u> layer net performing an operation:

$$Y = E*G_{\gamma} \tag{58}$$

Where Y is a vector of signals output from the linear part of the retinal network. This operation captures data processing performed on the primary image representation E and results in a transformed representation Y. Operation G_{γ} is equivalent to operation (1) described in Chapter 2.

Our ultimate goal is to find an operator G_{γ} which performs "optimal" transformation of the image E. "Optimal" in this case means the "best" from the point of view of a higher level recognition layer. If G_{γ} is "optimal", the structure of a higher level recognition system will be simpler for a given recognition goal. This is a very complex problem of optimal structure synthesis. The best known method of solution is to use an iterative procedure of successive improvements of operator G_{γ} (or its equivalent G_E). It is necessary to remember that G_{γ} is defined by only a small number of parameters. They may actually be evaluated if a proper set of experiments can be designed. These experiments can be based on psychophysical and neurophysiological results obtained for human vision. A first step in this direction is the method described in the next

chapter used to parameterize the equations of Section 3.3. Chapter 4 considers our first experiment in detail.

A Short Description of an Algorithm Simulating the Gawronski Equations

For digital and also analog modelling it is easier to use the matrix notation introduced for Eqs. (35-36) and (47-51). The algorithm for the simulation of retinal processes uses two kinds of data:

1. Structural Data (the model of weight matrices V and G), and
2. Data from processed images.

Structural data must be selected first and stored in memory for constant parameters. Image data may be introduced from any video system. Figure 17 presents an algorithm for the calculation of the data processing of static images. After the introduction of all data the algorithm starts with $S = 0$.

The values of $V_S\ E\ (F^S + H^S)$ are successively calculated and the sum of these components then simulates the output of the linear part of the system "u".

Then next step starts the calculation of the nonlinear portion corresponding to processes in the ganglion cells. Remember that the resultant transfer functions $g_{i,j}$ of matrix G represent a superposition of the dynamic properties of all four linear layers in the retina.

For dynamic processes two different solutions are possible. As in the previous case, parameters representing the structure and time constants of the linear layer and parameters of the nonlinear layer are introduced. Then we use a set of input signals in the form of a set

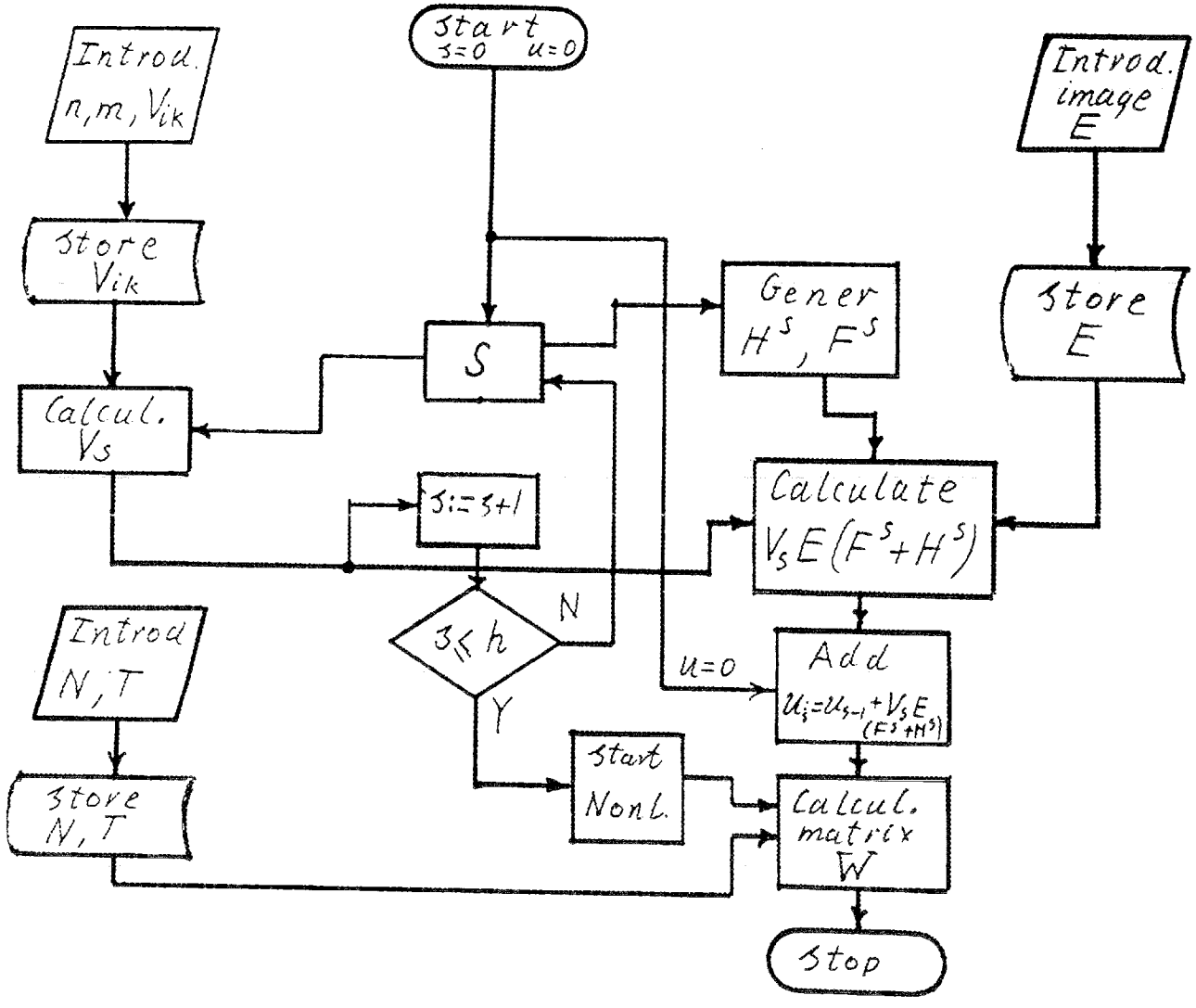

Fig. 17. Algorithm for Modelling Static Data Processing in the Retina.

of matrices $E(k \cdot \Delta t)$, where $0 \leq k \leq k_{max}$. $E(k\Delta t)$ represents successive frames of an image. Next a loop is started for the calculation of integrals representing the convolution $[e_{i,j}(k\Delta t)*g_{i,j}(k\Delta t)]$. The result is a set of matrices $E(k\Delta t)(F^S + H^S)\ G_S\ (k\Delta t)$ for every $0 \leq k \leq k_{max}$. The set of matrices corresponding to values $U(k\Delta t)$ is then calculated and the modelling of the last nonlinear layer is the same as in the previous case.

It is also possible to reverse the sequence of loop calculation. If we have a very fast computer we could first calculate all components $E(k\Delta t)(F^S + H^S)\ G_S\ (k\Delta t)$ for a given k and for all "i", "j", and "s". Then we obtain output matrices $U(k\Delta t)$ and $W\ (k \cdot \Delta t)$ for given k. In this case we obtain an on-line simulation of dynamic processes but it is still only possible for small values of $n \cdot m$. This is one more reason to apply parallel computation which will allow us to increase the number of pixels in the image. Depending on the computer and available software, we may use special procedures to simplify calculations of the convolution integrals and summations defined by Eq. (44).

Computer Simulation of the Gawronski Equations

A preliminary simulation of these equations has been programmed in Turbo Pascal on an IBM PC. Designed as an interactive research tool, the simulation has four parts:

1. An input signal specification section.
2. A net segment of 40 neuron elements with adjustable connection weights whose effects can be followed over 3 layers.
3. A menu for changing dynamic properties of retinal neurons.
4. And a result plotting section for each layer.

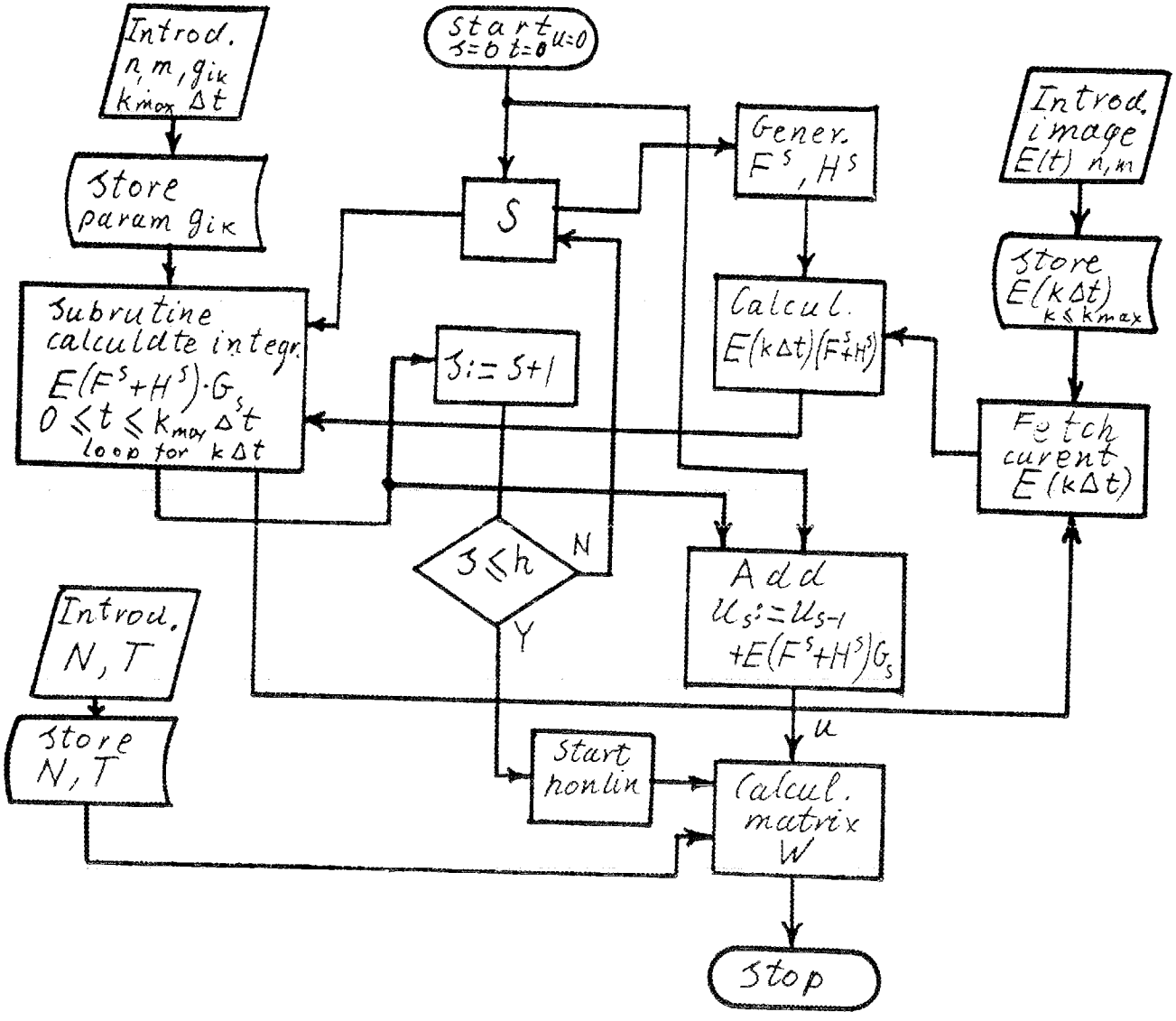

Fig. 18. Algorithm for Modelling Dynamic Data Processing in the Retina.

This preliminary simulation uses a one-dimensional input signal and a one-dimensional line of receptors to investigate the influence of different input signal slopes and the effects of different image shifting speeds across the retina surface. Versions now being programmed will consider two-dimensional effects. Complete details of this model will be presented in 1986, but the present form of the simulation has the following options.

Waveform Characteristics

The user may manipulate:

1. The width of rise for an input visual pulse.
2. The width of the plateau for an input pulse.
3. The width of the fall for the pulse.
4. The distance between pulses if more than one is examined.
5. The width of rise for a secondary pulse (optional).
6. The width of a plateau for a second pulse.
7. The width of fall for a second pulse.
8. The general wave form of the input signals.
9. The weight distribution between neuron interconnections.
10. The velocity of image shifting across the retina.
11. The gamma value for an excitatory channel.
12. The time constant tau for excitatory signals.
13. The gamma value for inhibitory channels.
14. The second tau value.
15. The duration of the period to be examined.

The results of these operations are plotted graphically as in Fig. (19) so that both intra- and inter-layer effects and parametric assumptions can be examined. Because of the speed and graphic limitations of a PC, the simulation has also been recoded for use on an IBM-AT. Later versions will use more powerful machines as appropriate. Such a simulation is necessary because psychophysical experiments may only be able to obtain information for early layers. Thereafter, a graphic simulation

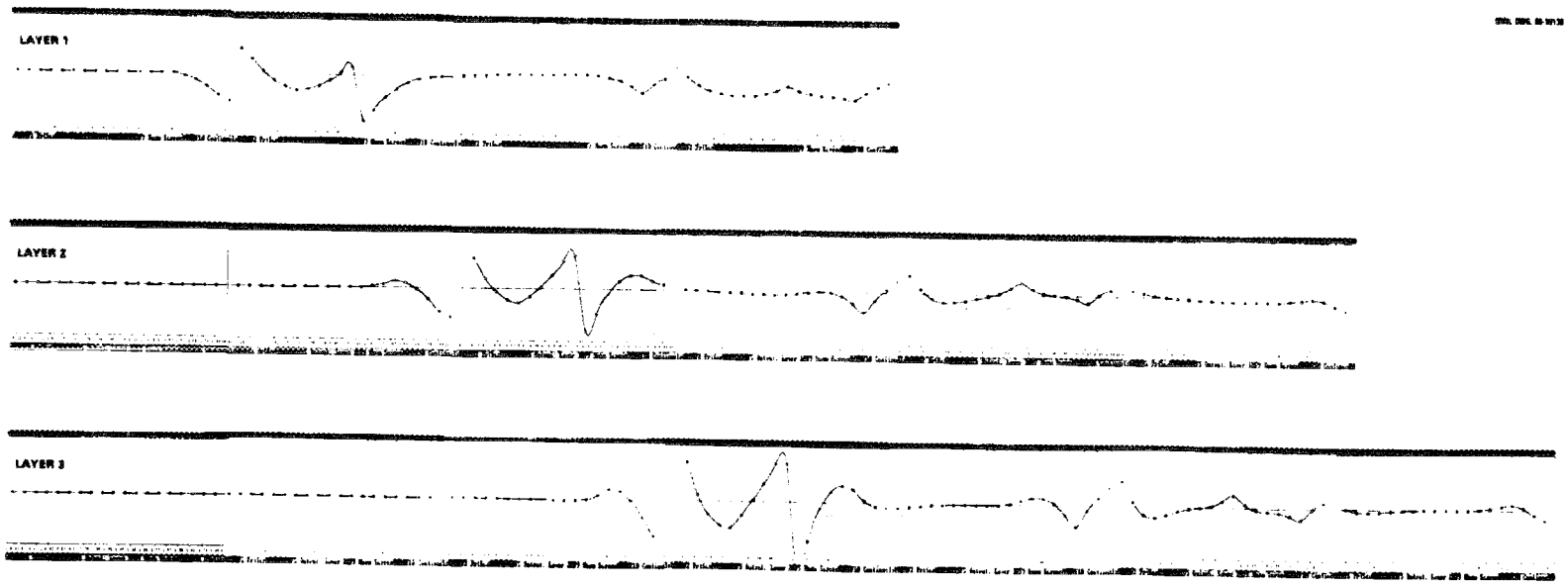

Fig. 19. Two Wave Fronts Passing Through Three Retinal Layers.

tool must be used to observe the compound effects of many transformations on an input image. Also such a tool is of considerable use in experimentally solving for G_Y in Eq. (58).

Figure 19 is a photo reduced plot of two pulses passing through three retinal layers. The X axis is time, the Y axis is signal intensity relative to a resting state. Notice how the magnitude of the spike grows and is enlarged as the output signal is fed from layer to layer and how homogeneous signal areas wash out.

What Lateral Inhibition Effects Result After Applying the Equations

In 1957 Hartline and Ratliff described the properties of mutual inhibition. They showed that the two layers of neurons presented in Fig. 20 may detect sharp changes in excitation of the first layer. Cells of the second layer which are excited from both sides get approximately the same amount of excitation and inhibition. Only the cells close to the edge of the excitation receive more excitation than inhibition. The output signals from these cells are much stronger than from other cells. This principle was later confirmed in many investigations concerning both the retina and also higher levels of the visual system.

To consider the resulting properties of two-dimensional neuron nets with lateral inhibition, let us consider a two layer net described by the equation resulting from (37).

We assume a continuous distribution of excitation $I(x,y)$ over the surface of the first layer where x and y now denote independent spatial variables. The values of function $I(x,y)$ in the eight points surrounding a given point x,y are:

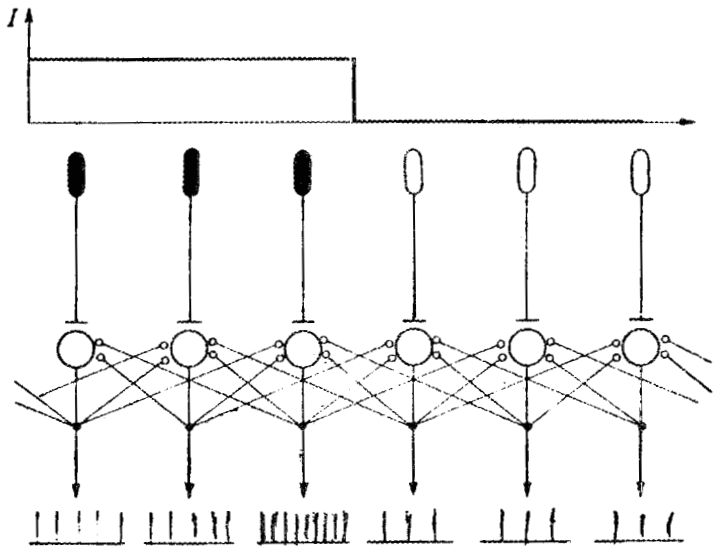

Fig. 20. Edge Detection by a Net with Lateral Inhibition.

$$e(\pm\delta,0) = e(0,0) \pm e'_x\delta + 1/2\, e''_{xx}\delta^2 + \ldots$$

$$e(0,\pm\delta) = e(0,0) \pm e'_y\delta + 1/2\, e''_{yy}\delta^2 + \ldots \tag{59}$$

$$e(\pm\delta,\delta) = e(0,0) + (\pm e_x + e'_y)\delta +$$

$$+ 1/2(e''_{xx} = 2e''_{xy} + e''_{yy})\delta^2 + \ldots$$

$$e(\delta,\pm\delta) = e(0,0)(e'_x \pm e'_y)\delta +$$

$$+ 1/2(e''_x \pm 2e''_{xy} + e''_{yy})\delta^2 + \ldots$$

Using the discrete approximation of (37) and replacing x by i and y by j we get:

$$x(i,j) = \sum_{s=-h}^{s=h} \sum_{r=-h}^{r=h} v_{rs} \cdot e(i+r, j+s\delta) \ ,$$

where

$$r\delta = \pm 1$$
$$s\delta = \pm 1 \ .$$

In the same way we may define excitations in cells at distance 2s, that is $e(\pm 2s,0)$, $e(0,\pm 2s)$, $e(\pm 2s \pm s)$ and so on. If we assume that the distance between neurons is also s and substitute the values of $e(x,y)$ into Eq. (37) we get:

$$X(e_{i,j}) = \sum_{s=-h}^{s=h} \sum_{r=-h}^{r=h} v_{r,s}\ e(r\delta, s\delta) \tag{60}$$

Substituting now the values of (59) into (60) we get:

$$X(E_{ij}) = e(0,0) \sum_{r,s=-h}^{r,s=h} v_{rs} + e'_x \sum_{r,s=-h}^{r,s=h} v_{rs} +$$

$$e'_y \sum_{r,s=-h}^{r,s=h} v_{rs} S + \tfrac{1}{2} e''_{xx} \sum_{r,s=-h}^{r,s=h} v_{rs} r^2 + \tag{61}$$

$$e'_{xy} \sum_{r,s=-h}^{r,s=h} v_{rs} rs + \tfrac{1}{2} e''_{yy} \sum_{r,s=-h}^{r,s=h} v_{rs} S^2 + \ldots$$

A short analysis of this relationship reveals some very interesting properties of lateral ihibition:

1. If the sum of weight operators V_{rs} is equal 0 that is:

$$A = \sum_{r,s=-h}^{r,s=h} v_{rs} = 0 \quad , \tag{62}$$

then operator (60) gives no (zero) output for a constant distribution of input signals. It is clear that constant excitation transfers no information.

For balanced lateral inhibition (or excitation) we have the relation:

$$v_{00} = - \left(\sum_{r,s=-h}^{r,s=-1} v_{rs} + \sum_{r,s=1}^{r,s=h} v_{rs} \right) \tag{63}$$

For lateral excitation we have $v_{00} < 0$ and for lateral inhibition we have $v_{00} > 0$.

Relation (63) may sometimes be satisfied only approximately. In that case it is possible to detect the average excitation of the first layer.

2. If we deal with radial symmetry as described previously then:

$$v_{|r||s|} = v_{|s||r|} \tag{64}$$

and we get:

$$\sum_{r,s=-h}^{r,s=h} v_{r,s}\, r = \sum_{r=1}^{r=h} \sum_{s=-h}^{s=h} v_{r,s}\, r - \sum_{r=-h}^{r=-1} \sum_{s=-h}^{s=h} v_{r,s} \cdot |r| = 0 \tag{65}$$

and in an analogous way we get

$$\sum_{r,s=-h}^{r,s=h} v_{rs} \cdot s = 0 \tag{66}$$

We see now that the symmetric operator does not detect first derivatives. That means that linear changes of an input signal distribution (uniform illumination decreases or increases) do not provide any output signals. It is easy to see that condition (64) also causes:

$$\sum_{r,s=-h}^{r,s=h} v_{rs}\, r \cdot s = 0 \tag{67}$$

We infer from (67) that this result therefore does not depend on mixed derivatives. So, saddle shaped distributions are also not detected.

Taking into account (63) to (67) for the symmetric operator we obtain:

$$X(e_{ij}) = B \left(\frac{\partial^2 e}{\partial x^2} + \frac{\partial^2 e}{\partial y^2}\right) + C \left(\frac{\partial}{\partial x} + \frac{\partial}{\partial y}\right)^4 e(x,y) + \ldots \tag{68}$$

where:

$$B = 2 \sum_{r,s=-h}^{r,s=h} v_{rs}\, r^2 = 2 \sum_{r,s=-h}^{r,s=h} v_{rs}\, s^2 \tag{69}$$

and C is an analogous sum which will appear the at the fourth derivative.

Notice that the symmetric operator (63) detects second and higher order even derivatives of the input distribution.

We have shown (63) detects contours because second and higher order derivatives always appear when edges, corners, and other sharp changes appear in the picture. Some visual examples of the detection of local features and the results of data processing by some symmetric operators are presented in Fig. 21.

If the picture is static, after a transient time period we obtain results similar to those just presented. But if the pictures are changing rapidly, we get interesting effects enabling detection of dynamic properties in a picture. The simplest situation appears when a light spot moves with respect to a background. A signal generated by a single spot expands with time taking more and more space (it is washed away). But a moving spot excites adjoining elements. For a linear system we can add resulting excitations for every element. Continuing this process we see that the signal may be strongly increased by the summation of dynamic processes.

Final Remarks and Conclusions about the Dynamic Retinal Equations

1. The first step of visual data processing was shown to correspond to layers I and II presented in Fig. 3 and may be modelled by a sequence

ORNL–DWG 86-10126

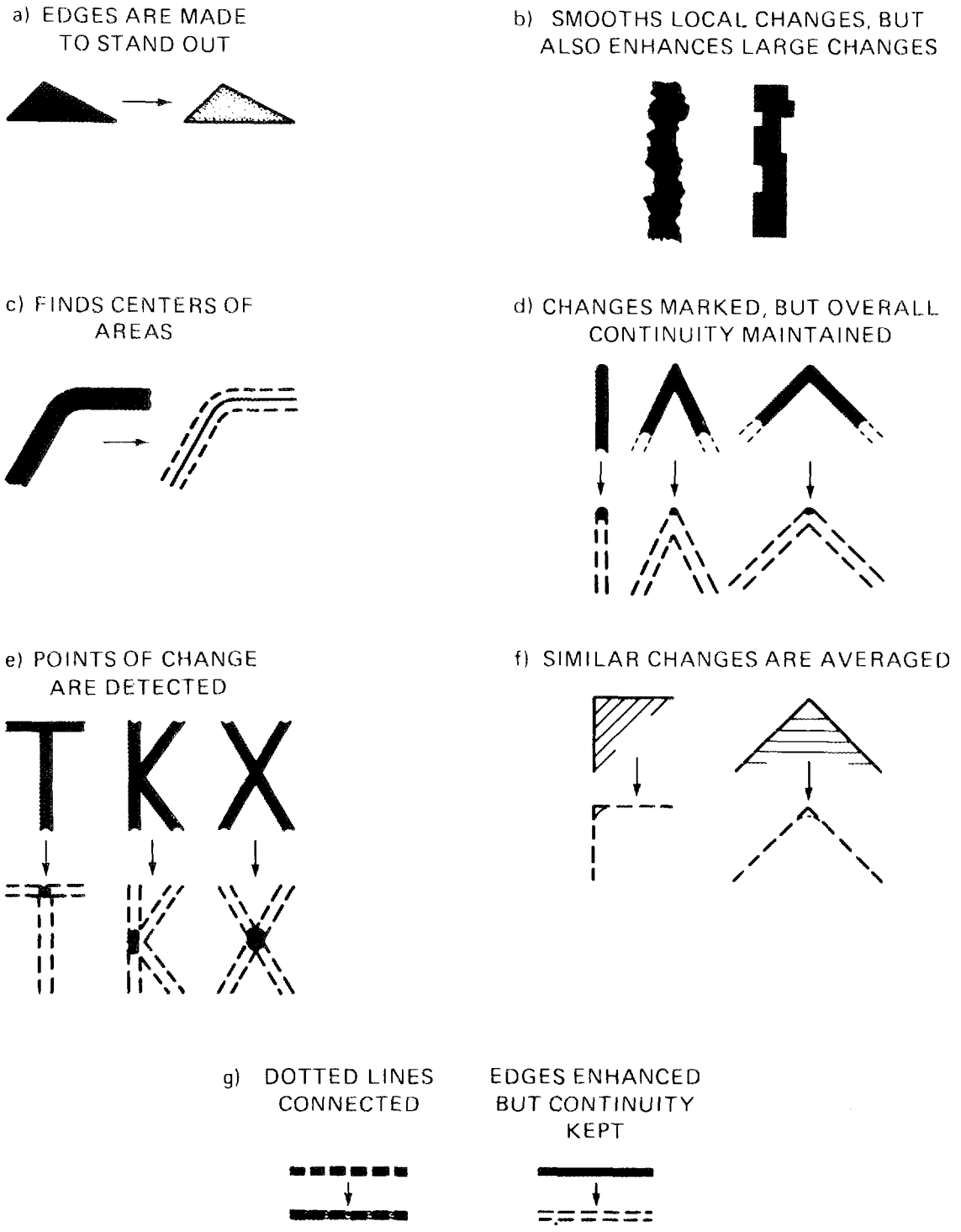

Fig. 21. Some Examples of the Detection of Local Features by a Symmetrical Operator Detecting Even Derivatives with Respect to x and y. (Taken from R. Gawronski: Doctoral Thesis)

of linear operators and one nonlinear operator. The nonlinear operator acts on the result of the linear part and includes threshold properties.

2. Using a computationally effective notation we can model static images by applying a relatively simple computer algorithm. Our final goal is to select a set of r•s values of weights V_{ij} which perform the desired operations for subsequent steps. For a large number of pixels, the amount of calculations increases considerably, but still may be performed on an appropriately powerful computer.

3. For a very large number of pixels it may be useful to construct special chips with a multilayer structure and appropriate local connections. Such chips may perform all operations in parallel. They may use digital or analog technology. Nevertheless, careful preliminary investigation to select connection weights is necessary. The results may then be compared with the results of psychological and neurological investigation like in the next chapter or via the simulation developed in this paper.

4. ON-center and OFF-center organization of the retina, results on picture contrasting, and equations (63) to (69), show that mutual inhibition is the best starting point for the future optimization of retinal data processing. It is also necessary to verify other symmetric operations which may be useful to select local picture properties.

5. For pictures varying in time, it is necessary and probably very useful to take into account the dynamic properties in each element. Modelling of dynamic processes needs a very fast computer with a very large memory. The results of such modelling should reveal new possibilities for the detection of movement and recognition of objects moving with respect to a background.

4.0. PSYCHOPHYSICAL EXPERIMENTS

4.1. Background

It is possible to propose many different mathematical descriptions for neuron functions, but the selection of specific mechanisms, assessment of physiological research, and parameterization of equations present formidable obstacles. For some cases such as lower primates or primitive organisms, direct physical measurements are possible. However, once information is needed that goes beyond neuroanatomical properties problems arise. First, direct measurement of visual processing is rapidly overwhelmed by the sheer number and complexity of neural interconnections. Second, tissue samples sever feedback connections that may be vital for understanding dynamic interactions. And finally, neural pathways ultimately connect to complex associative regions in the occipital lobe of the brain that incorporate other sources of sensory and physiological information. Thus it is unclear at exactly what point higher order cognitive processes are introduced into visual perception.

Fortunately, in the earliest parts of the retina, the processes tend to be sequential, i.e. have less inter-layer feedback than at higher stages. This simpler structure has made possible reasonable conjectures that lead to the equations in this report. One problem that remains, however, in that when equations have been generated, they must still be parameterized to determine their processing behavior compared to human performance. Parameterization in turn requires that at least approximate be obtained. Because direct measurement across several layers of over 6 million neurons seems impossible, another method had to be used to obtain values which could be used. An idea by one of us (Holly) proposed that

parameterizing the vision system may be possible by examining cases where the human vision system breaks down i.e., is fooled. Such situations might provide new clues to bound the parametric values of retinal equations.

He suggested that psychologically quantified perceptions of appropriately chosen visual illusions might provide the necessary post processing data. After consideration of several possibilities, three illusions believed to result from early activity in the retinal layers were selected. These illusions are presented in Figs. 22, 23 and 24.

The first illusion, called the Herman Grid, produces a series of flickering black dots at the junctions between the bright horizontal and vertical lines and weaker, diagonal dark lines across the pattern. The second illusion, called Mach bands after Ernst Mach, consists of apparent regions of increased brightness and darkness occurring at junctions between uniformly increasing or decreasing intensities. The ORNL experiments actually used a modified form of the Mach Band illusion which will be described in more detail later, but is more of an optic "wedge". The final illusion resembles a radiating star in that alternate beams of light and dark rays eminate from a central point becoming wider as a function of their distance from the origin. When contrast display is adequate, the effect of this illusion is to create a shimmer or unstable perceptual area at a set distance from the center point. The logic of using the illusions was that the false appearance of visual information as gray dots or bogus lines are situations where neural processes add false information. Thus the nature of information added and its magnitude provide clues to choose between alternative equation parameters. Further,

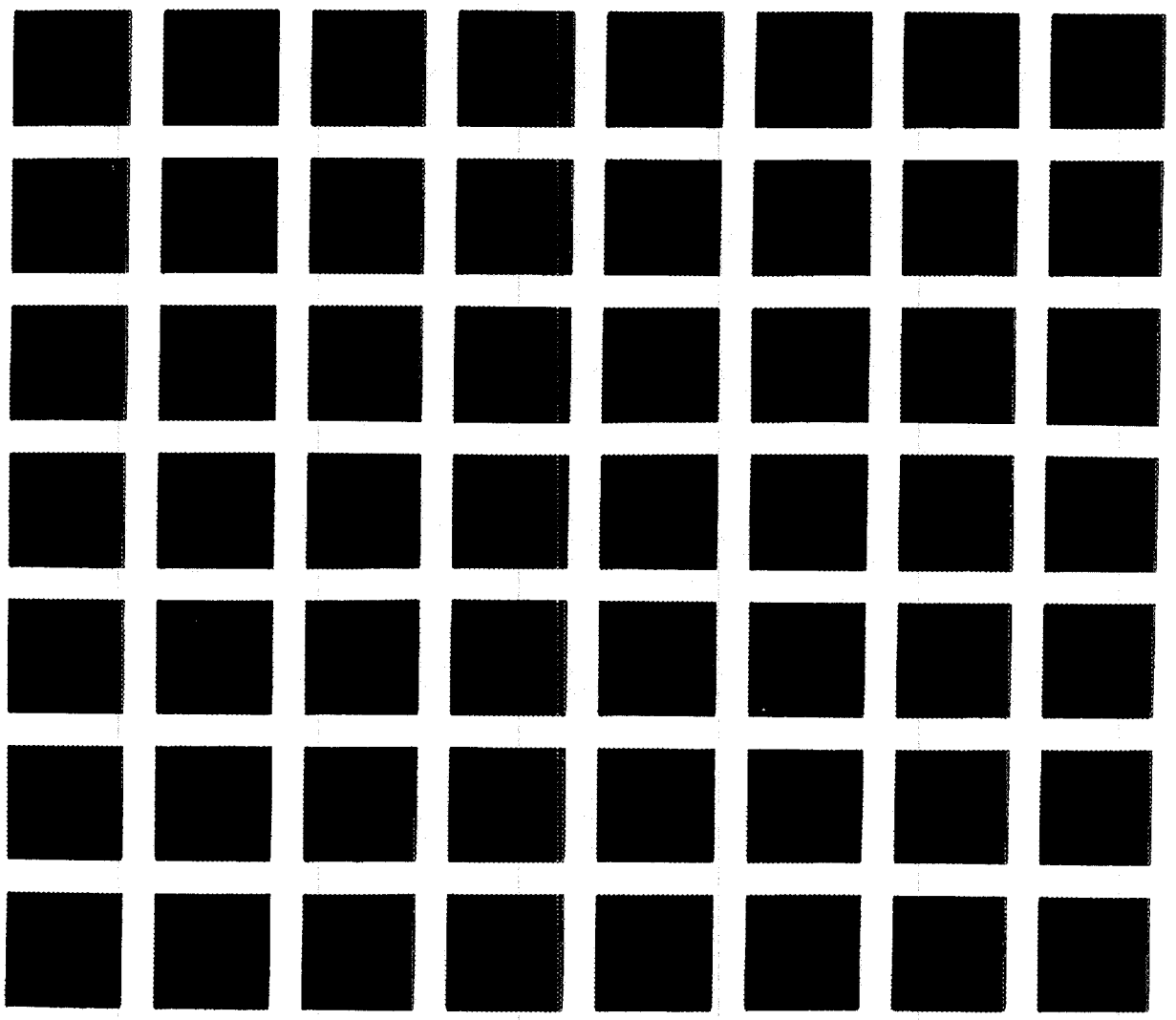

Fig. 22. Herman Grid Illusion.

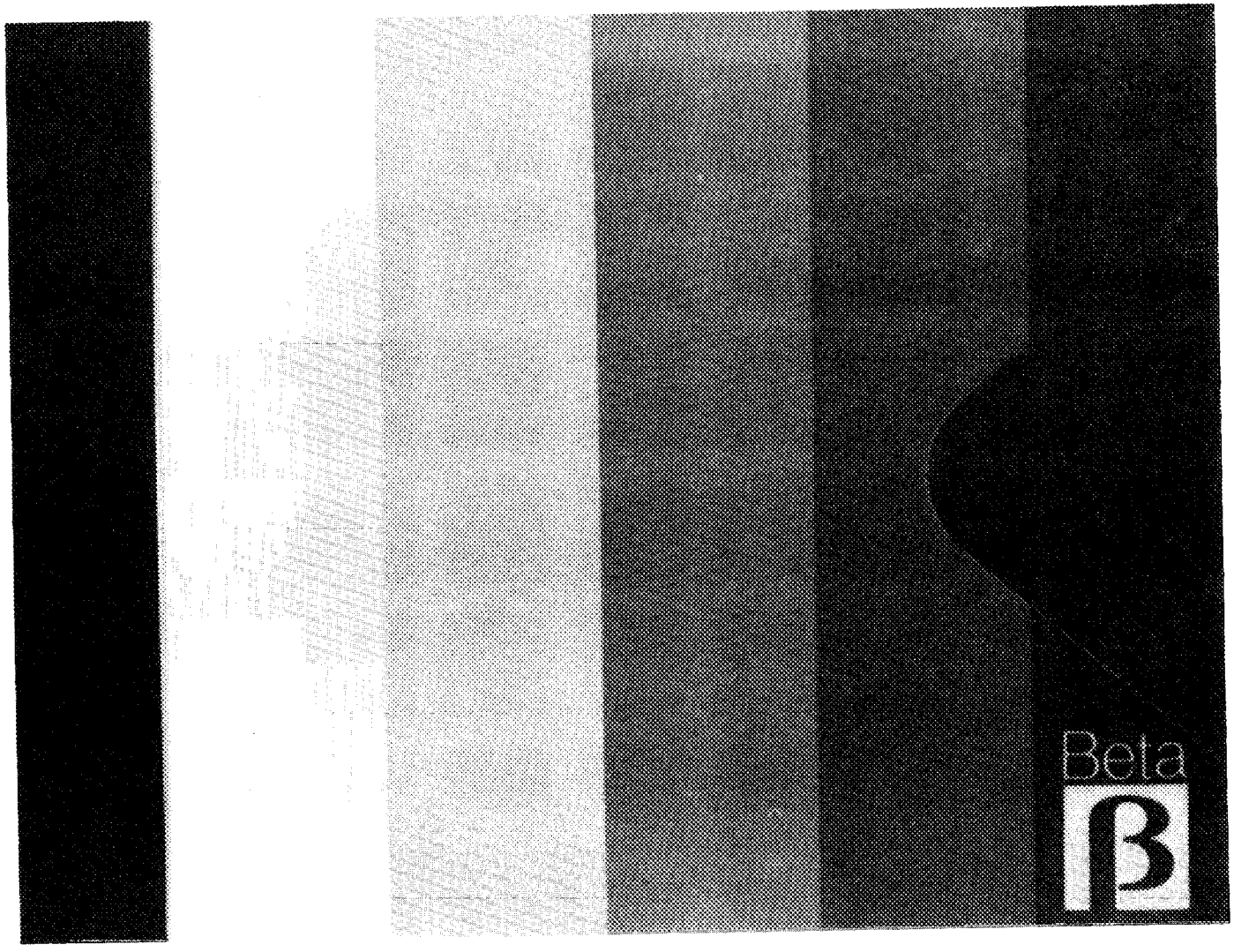

Fig. 23. Mach Bands Illusion.

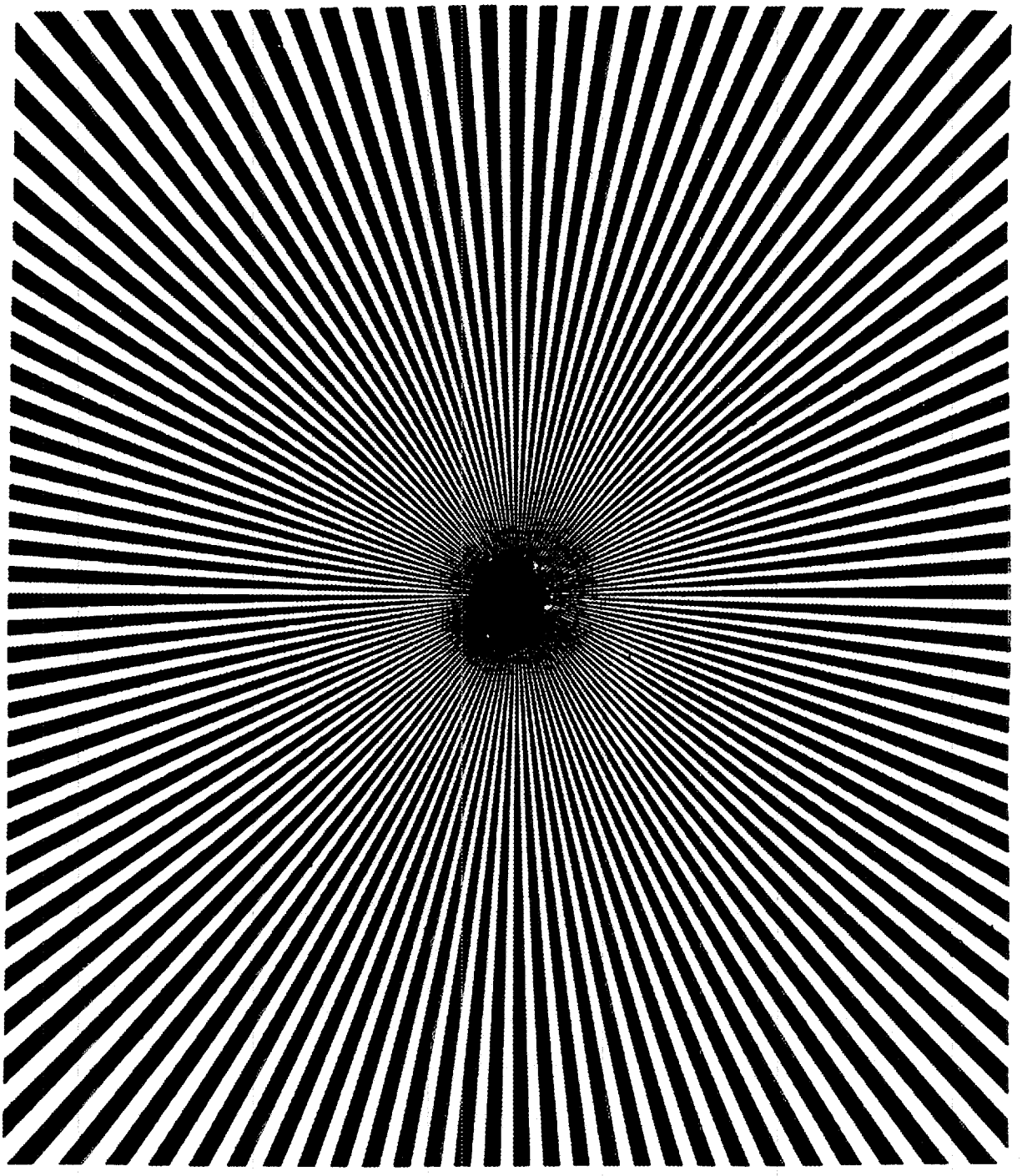

Fig. 24. Star Grid Illusion.

the specific magnitude of the effects, though subjective, may permit an approximate solution to be obtained.

4.2. Approach

Fourteen subjects were presented with randomized sets of three illusions in a mixed within/between subjects design. Each illusion was displayed on a high resolution CRT monitor contained in a light shaded box with a subject face rest 1.3 meters from the screen surface subtending a 17° degree field of vision from the retinal surface to the screen surface. Intensity was standardized by digitizing high contrast black and white drawings and capturing the images with an IRI p300 vision system (Picture 1). Each subject was presented with a regenerated copy of the original image called up interactively at the time of the experiment. Subjective quantification of perceived brightness effects was accomplished by means of a series of FORTH language computer programs which overlayed graphic information on the illusion. This graphic overlay was different for each illusion depending on the data measured. Subjects then provided subjective values about different effects and the locations at which those effects occurred. The numeric information was later reformatted for plotting in a three-dimensional graphic display. A three-dimensional plot of the subjective impression was produced for each illusion. Only one of the illusions was used to parameterize the retinal equations. (These were solved using the Fourier solution technique described in Chapter Three Section Three.) Once solved, the matrix of operator values was used to reproduce the effect of human retinal processing. The two unused illusions were multiplied by the matrix operator

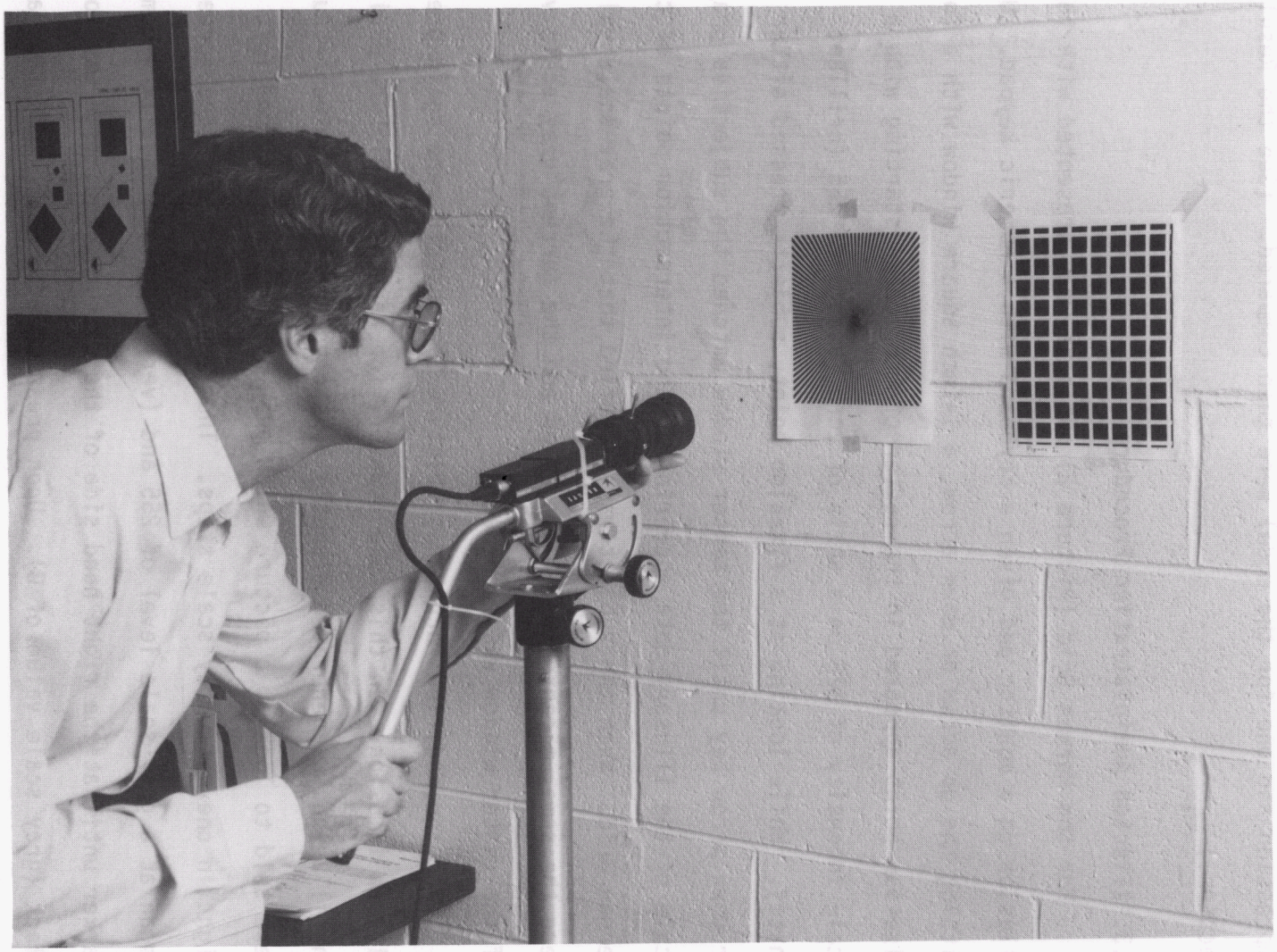

Picture 1. Capturing Illusions.

and the results were plotted. Two outputs, one for the human subjective impression and one for the model were then compared. (See the Results section.)

4.3. Illusion Administration Procedure

For the Herman Grid (Picture 2) subjects were presented with the illusion on a monitor and given a keyboard with a numeric keypad. Upon hitting the up arrow or down arrow, a 1-inch square window with a foveal fixation point appeared in the center of the screen starting with a gray scale intensity of 128 on a scale of zero (black) to 255 (brillant white). While looking at a fixation point, subjects pressed either an up or down arrow key until the center window matched the subjective gray scale of the illusory dots appearing at the intersection points of the Herman Grid. When the subject was satisfied that the gray scale values were the same, a center key was pressed and the current gray scale value of the center window was recorded.

For the Modified Mach bands (Picture 3) subjects were again presented with an illusion. In this case however, for reasons of picture purity, the illusion was generated directly by stored graphics routines. Subjects were told to look at a picture which grew darker linearly from left to right in one unit gray scale steps. Thus the left half of the screen began at a gray scale level of 255 and (very bright) gradually becoming darker until at the right hand side of the picture, the image was totally black (gray scale value of 0). Upon pressing a left or right hand arrow key, a vertical index bar would alternately appear and disappear. The subject could move this bar to align with the first or later appearances

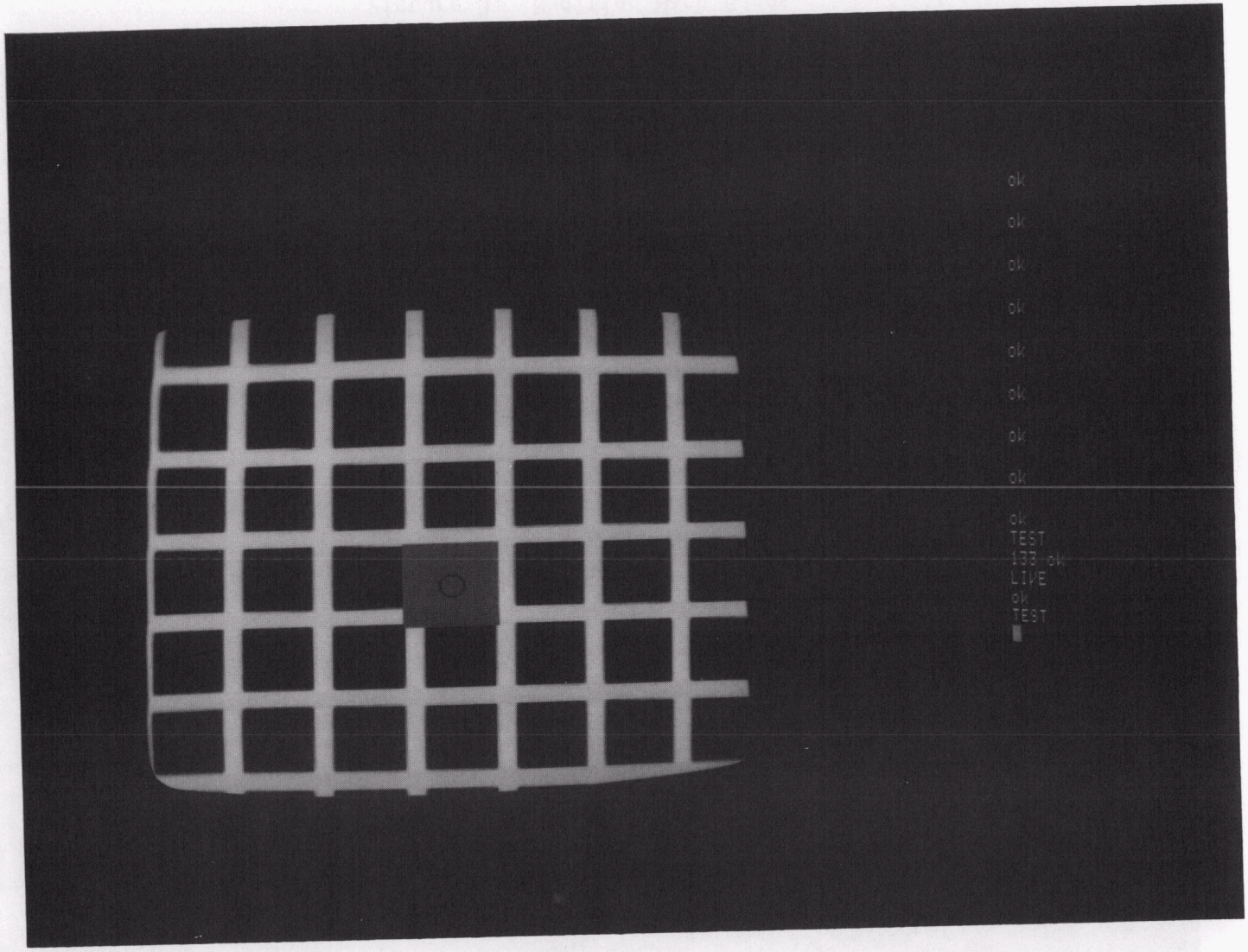

Picture 2. The Herman Grid with a Gray Scale Window.

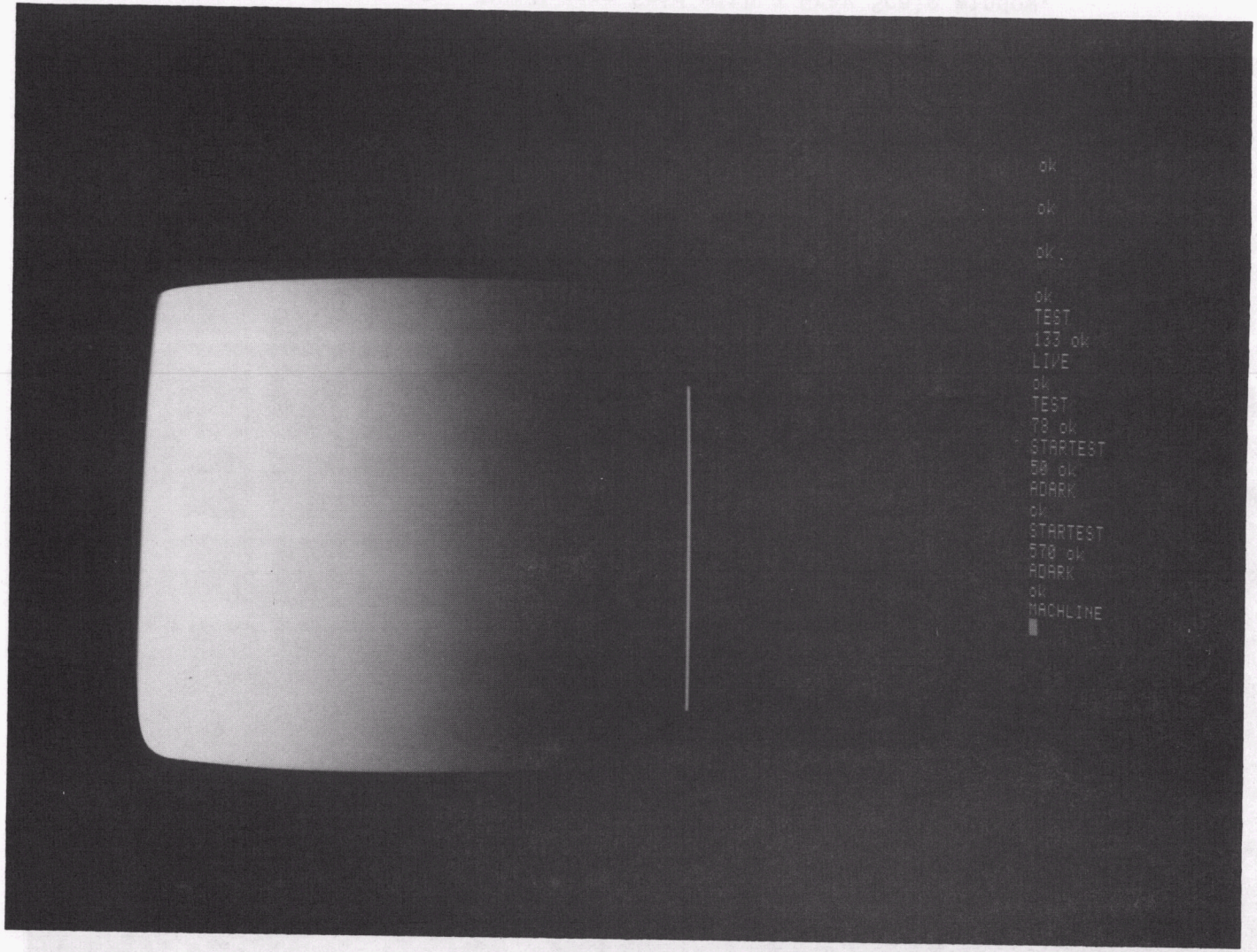

Picture 3. Modified Mach Bands.

of illusory Mach lines. An alternate appearance and disappearance of the bar was required because the bar itself interacted with the effect and caused the Mach line to shift or fade out if left on the screen continually. When satisfied about the correct location, the subjects pressed the center key which recorded the bar location.

The star illusion was presented in a similar fashion except instead of a index bar, an expanding or contracting circular ring appeared which surrounded the center of the radiating star (Picture 4). When the subjects had surrounded an area of maximum distortion, the center key was pressed and the value of the circle radius was recorded.

4.4. Subjects

The subjects were 14 ORNL staff members 7 males and 7 females between the ages of 20 and 42. Male staff members were Ph.D physicists or senior graduate students in electrical engineering. Females were staff members of the Radiation Shielding Information Center (RSIC).

4.5. Apparatus

The apparatus consisted of an experimental box composed of a reinforced tunnel with a viewing slot, chin brace, and eye shades on one end and an open monitor housing on the other. The box was attached to a Hitachi Model VM-129 high resolution monitor. Images on the monitor were controlled by an International Robomation Intelligence P256 vision system consisting of a MC68000 host computer, video digitizer, image buffer memory, and dedicated iconic array processor for point gray scale transformations. Connected to the P256 system was a Sony charged couple device video camera used with the digitizer to capture pictures. Stored pictorial

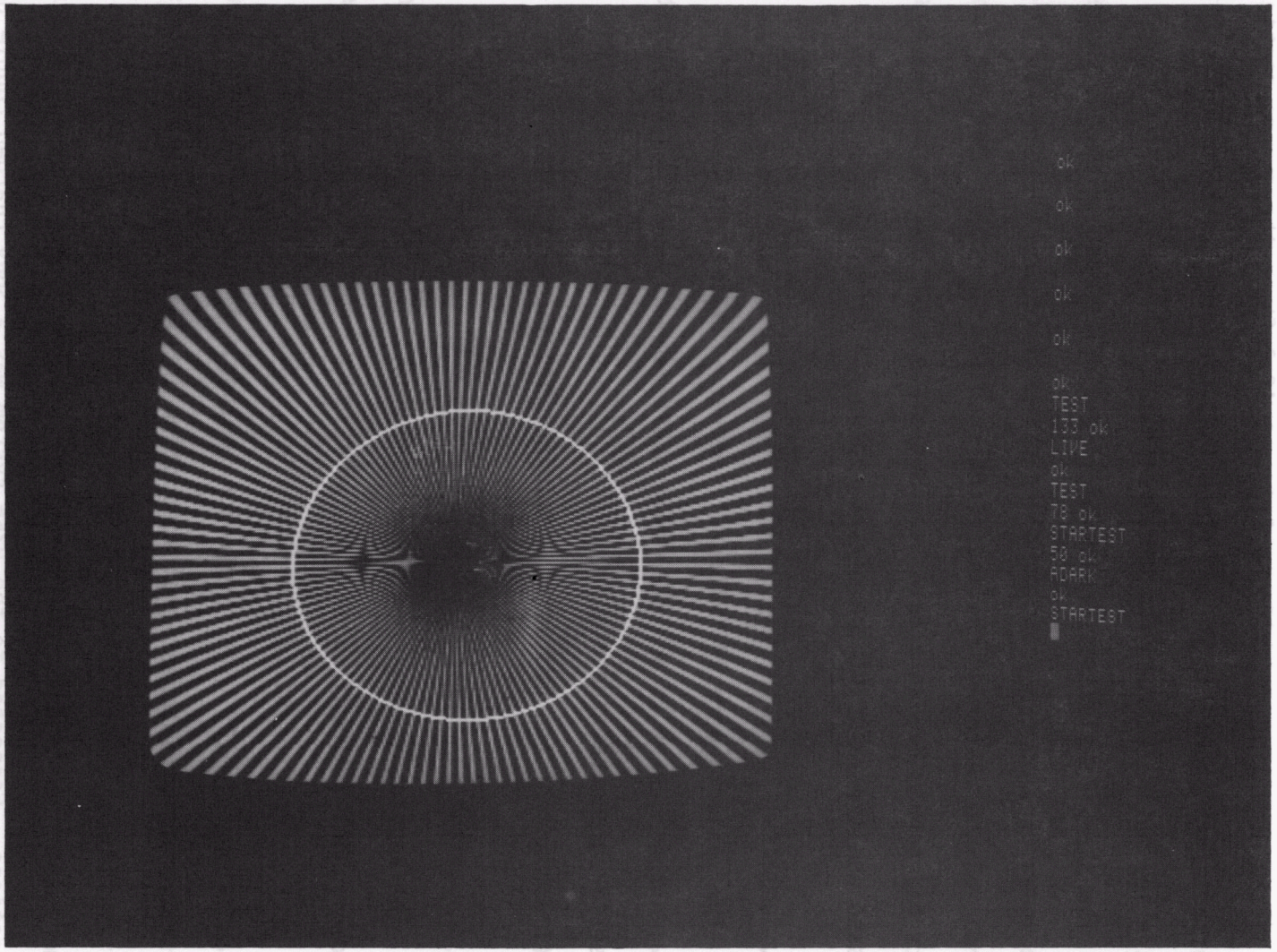

Picture 4. "Star" Illusion.

information was manipulated via a series of FORTH computer language primitives generated by a specialized vision command language and superFORTH interpreter. Subroutines were written in FORTH for the generation of the Mach lines, screen graphics, and data storage routines (Appendix 3).

4.6. Experimental Results

Results for the Herman Grid Test

Tables 1 and 2 present summary statistics and an analysis of variance for the Herman Grid illusion. Table 1 shows that the perceived intensity of the illusion had a mean gray scale value of 154 with a standard deviation of 16.4. As represented in the frequency plot in Table 1, data had an approximately normal distribution. Variation across trials showed no systematic bias. A lack of bias was confirmed by both a three-dimensional surface plot at the bottom of Table 1 and an analysis of variance in Table 2. The analysis of variance compared subjects by subject number, sex and trials. A slight trend (alpha of .08) was observed for sex with males tending to score the perceived dots as slightly brighter (mu equal to 150) versus the females (mu equal to 158). This trend is most clearly seen in Table 2 in a plot of 95 percent confidence intervals for the factor means.

Overall, the effect of sex was judged not statistically significant and a median value of 155 was chosen for the perceived gray scale level for illusory dots in the Herman Grid.

Results for the Machband Illusion

Tables 3 and 4 present the results for the Machband illusion. Only one machline was visible on the monitor due to limited contrast capability

Table 1. Summary Statistics and Surface Plot for the Herman Grid Illusion

Frequency Histogram and
3-D Surface Plot for Herman Grid

		Onesample Analysis
		grid
Sample Statistics:	Number of Obs.	42
	Average	154.24
	Variance	270.72
	Std. Deviation	16.454
	Median	155

Frequency Histogram

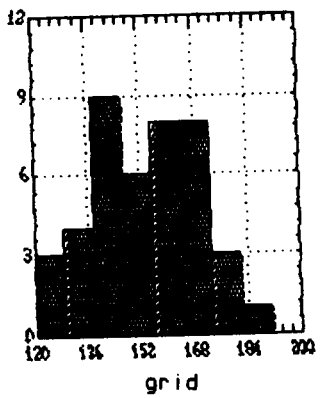

Plot of grid

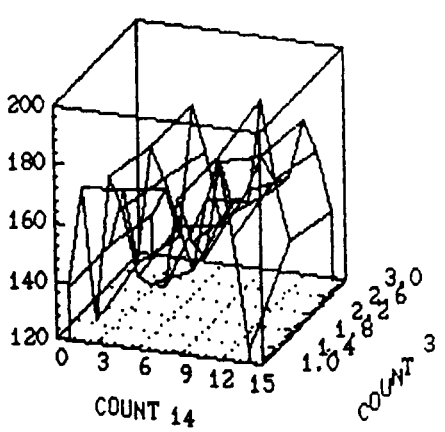

Table 2. Analysis of Variance and 95% Confidence Intervals for the Herman Grid Illusion

ANALYSIS OF VARIANCE FOR GRID ILLUSION WITH FACTORS ON SEX AND TRIALS

ANALYSIS OF VARIANCE - BALANCED DESIGNS

RESPONSE VARIABLE: grid

SOURCE OF VARIATION	SUM OF SQUARES	D.F.	MEAN SQUARE	F-RATIO	PROB(>F)
TOTAL (CORR.)	11099.619	41			
sex	737.5238	1	737.52381	3.090	.08728
trials	394.9048	2	197.45238	.827	.44540
trials*sex	1374.3333	2	687.16667	2.879	.06321
ERROR	8592.8571	36	238.69048		

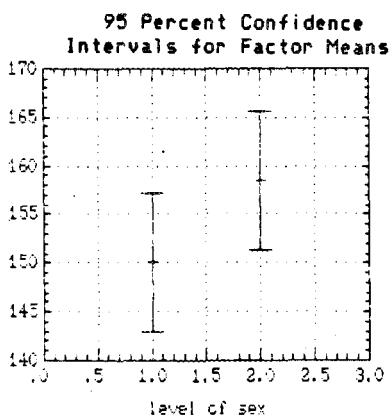

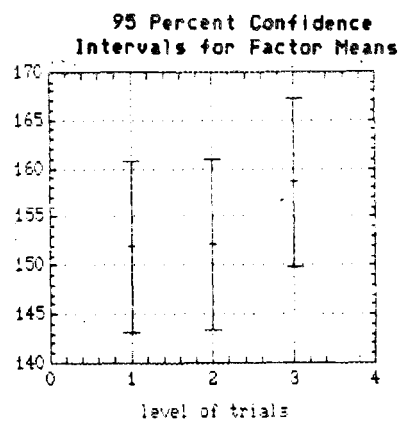

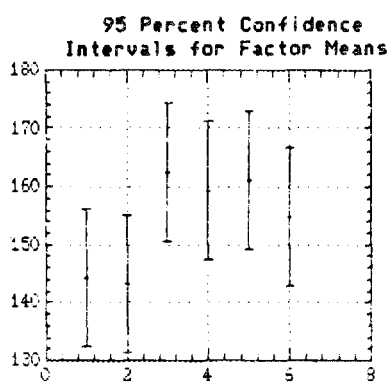

LEVEL	SAMPLE SIZE	EFFECT ESTIMATE	LEVEL AVERAGE	STANDARD ERROR
1	7	-3.309524	144.4286	5.839404
2	7	-4.738095	143.2857	5.839404
3	7	8.047619	162.4286	5.839404
4	7	3.309524	159.4286	5.839404
5	7	4.738095	161.1429	5.839404
6	7	-8.047619	154.7143	5.839404

Table 3. Summary Statistics and Surface Plot for the Mach Band Illusion

Frequency Histogram and
3-D Surface Plot for Machband Illusion

		Onesample Analysis
		mach
Sample Statistics:	Number of Obs.	42
	Average	71.214
	Variance	758.32
	Std. Deviation	27.538
	Median	68

Frequency Histogram

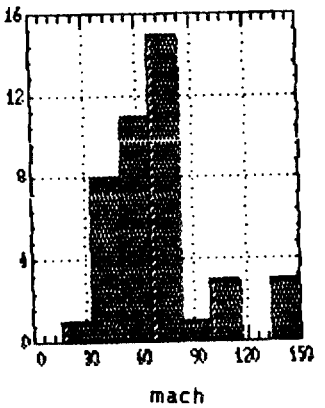

Plot of mach

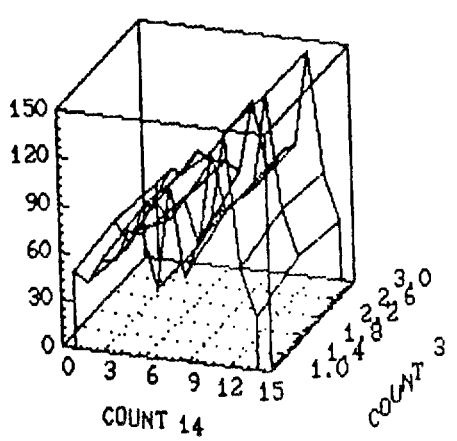

Table 4. Analysis of Variance and 95% Confidence Intervals for the Mach Band Illusion

ANALYSIS OF VARIANCE FOR MACHBAND ILLUSION
WITH FACTORS ON SEX AND TRIALS

ANALYSIS OF VARIANCE - BALANCED DESIGNS

RESPONSE VARIABLE: mach

SOURCE OF VARIATION	SUM OF SQUARES	D.F.	MEAN SQUARE	F-RATIO	PROB. (F)
TOTAL (CORR.)	31091.071	41			
trials	4825.000	2	2412.5000	4.452	.01872
sex	5.357	1	5.3571	.010	.92340
sex*trials	6753.571	2	3376.7857	6.232	.00474
ERROR	19507.143	36	541.3651		

95 Percent Confidence Intervals for Factor Means

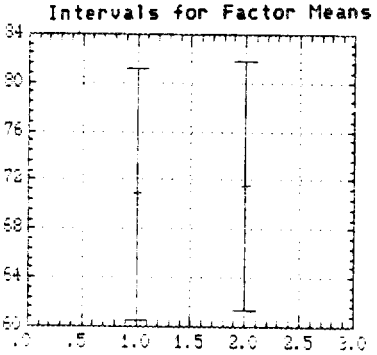

level of sex

STANDARD ERROR
5.079675
5.079675

LEVEL	SAMPLE SIZE	EFFECT ESTIMATE	LEVEL AVERAGE
1	21	-.357143	70.85714
2	21	.357143	71.57143

95 Percent Confidence Intervals for Factor Means

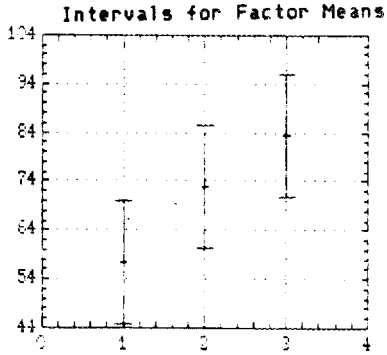

level of trials

STANDARD ERROR
6.221306
6.221306
6.221306

LEVEL	SAMPLE SIZE	EFFECT ESTIMATE	LEVEL AVERAGE
1	14	-13.92857	57.28571
2	14	1.78571	73.00000
3	14	12.14286	83.35714

95 Percent Confidence Intervals for Factor Means

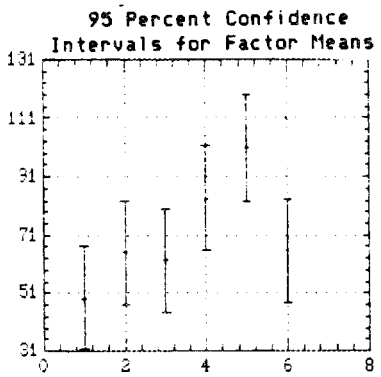

level of sex*trials

LEVEL	SAMPLE SIZE	EFFECT ESTIMATE	LEVEL AVERAGE	STANDARD ERROR
1	7	-7.50000	49.4286	8.798255
2	7	7.50000	65.1429	8.798255
3	7	-10.35714	62.2857	8.798255
4	7	10.35714	83.7143	8.798255
5	7	17.85714	100.8571	8.798255
6	7	-17.85714	65.8571	8.798255

This line was perceived at an average position 71 steps from the left-hand margin of the illusion border or approximately 28 percent of the total possible range into the figure. The standard deviation was unusually high at 27.5. The surface plot at the bottom of the Table 3 gives a clue as to why. The average perceived location of the bar increased directly with the number of the experimental subject and also increased with trials for each subject. The result was a wedge shaped surface plot with a roughness indicative of normal inter-subject variations. Thus, subjects definitely perceived a machline, but its location changed over the two day time period of the experiment. The change of machline location was apparently due to a drift in the contrast level of the monitor. The longer the monitor was running the weaker the contrast became. The slight drop in contrast level shifted the perceived location of the machline to the right resulting in a ramp-like surface plot and a gradually increasing value for the machine locations.

Future experimentors should be aware of the extreme sensitivity of this illusion to slight changes in screen conditions. The analysis of variance confirmed the existence of the effect within subjects by a significant value for both trials (alpha less than .02) and sex by trials (alpha less than .004) in Table 4.

Results for the Star Illusion

Table 5 presents the results for the star illusion. One concern early in the experiments was the adequacy of ORNL monitor screen resolution. Although the monitor used was the best available on site, the data illustrate it was not able to generate the subjective illusion properly. That fact is illustrated in a very interesting manner by the

Table 5. Summary Statistics and Surface Plot for the Star Illusion

Frequency Histogram and
3-D Surface Plot for Star Illusion

		Onesample Analysis
		star
Sample Statistics:	Number of Obs.	39
	Average	68.846
	Variance	212.45
	Std. Deviation	14.576
	Median	65

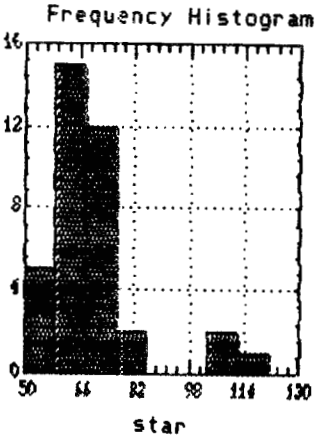

Plot of star

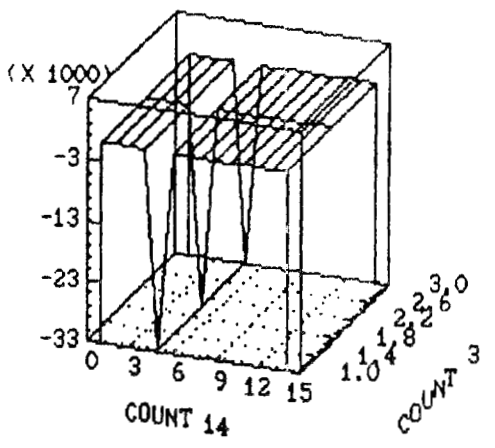

3-D surface plot at the bottom of Table 5. Notice the flat surface of the plot and the one sharp dip for subject number 4. The flat surface is the clue that what subjects reported seeing was actually in the screen image and not the subjectively perceived effect. If it were, the surface would be ragged like that of the Herman Grid. Subject 4 provided a example of the Shepard effect i.e., the response of experimental subjects to social pressure. Prior to the test, subjects had been presented with a printed copy of the star illusion having very clear black and white definition. The effect from this drawing was very strong, much more so than can be reproduced on the monitor and was used to insure that the subjects understood the effect they were to note in the experiment. Unfortunately, it also convinced the subjects they would see an effect. When the effect did not occur, they apparently looked for any unusual area on the image that looked similar.

Such an image did exist but was caused by a harmonic distortion by the IRI camera. Finding no other distortion, the subjects circled the harmonic and reported its value, all but one strong-willed subject who did not see the effect and refused to report any value. That subject's data is the sudden dip in the planer surface. An interesting result of this test was how obvious the bogus effect was when the data was plotted as a three-dimensional surface rather than analyzed by standard statistical methods. The use of only the latter could have resulted in a false parameter having been chosen for the retinal equations.

Conclusions

Only the Herman Grid had stable enough results to safely use in comparing the output of the MATRIX of linear operators and human perception. As it turned out, Machline values provided enough parametric data for an approximate solution of the operator matrix. The Machline data was used because of periodicity problems in the Herman Grid data matrix when the Fourier method was attempted, so the Herman Grid data was used instead as a comparison standard with human perception. The Star illusion could not be used with the current equipment. Further research with better experimental devices may remedy the situation but extreme care should be taken regarding adequate screen resolution, contrast control stability, and the sensitivity of experimental subjects to expectations and social pressures. Graphic plots of data and experimental results may also be important in the proper selection of parameters as well as the identification of flaws in experimental designs or equipment.

The gray scale values from the Herman Grid illusion were used to create a graphic 3-D plot where pixel location was defined on the x-y axis, and gray scale intensity was plotted along the Z axis. Picture 5 shows a small portion of a Herman Grid. The higher the value, the darker the area on the original illusion. Subjective "dots" are treated as having normal distributions around a midpoint. Similarly, the subjective effect of the machband (the 3-D Ramp in Picture 6) and segments of the star (Picture 7) were generated.

The gray scale data matrices of the Herman Grid was then multiplied by the matrix of operators and the output was input into the plotting routine. (For a discussion of this routine see Appendix 2).

ORNL DWG 86-10125

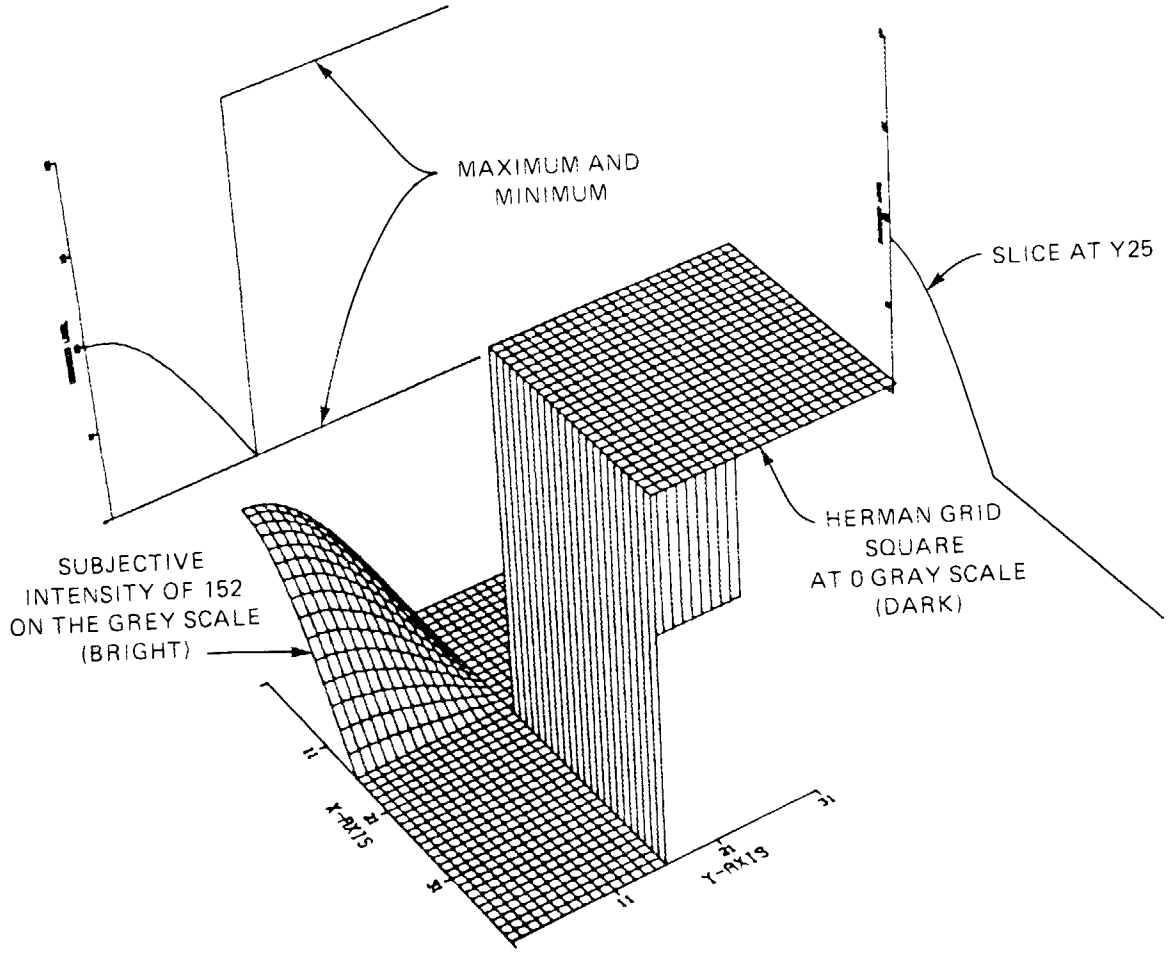

Picture 5. Plotting a Two-Dimensional Subjective Effect in 3-D.

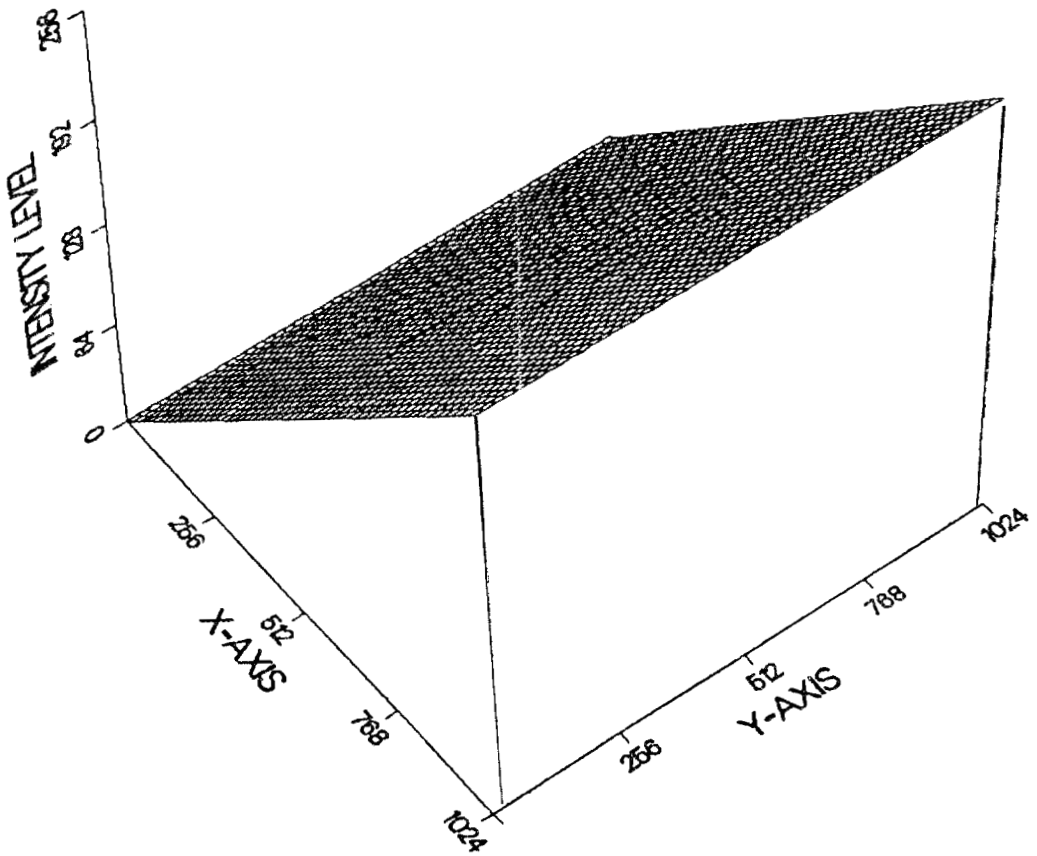

Picture 6. The Mach Band Illusion in 3-D.

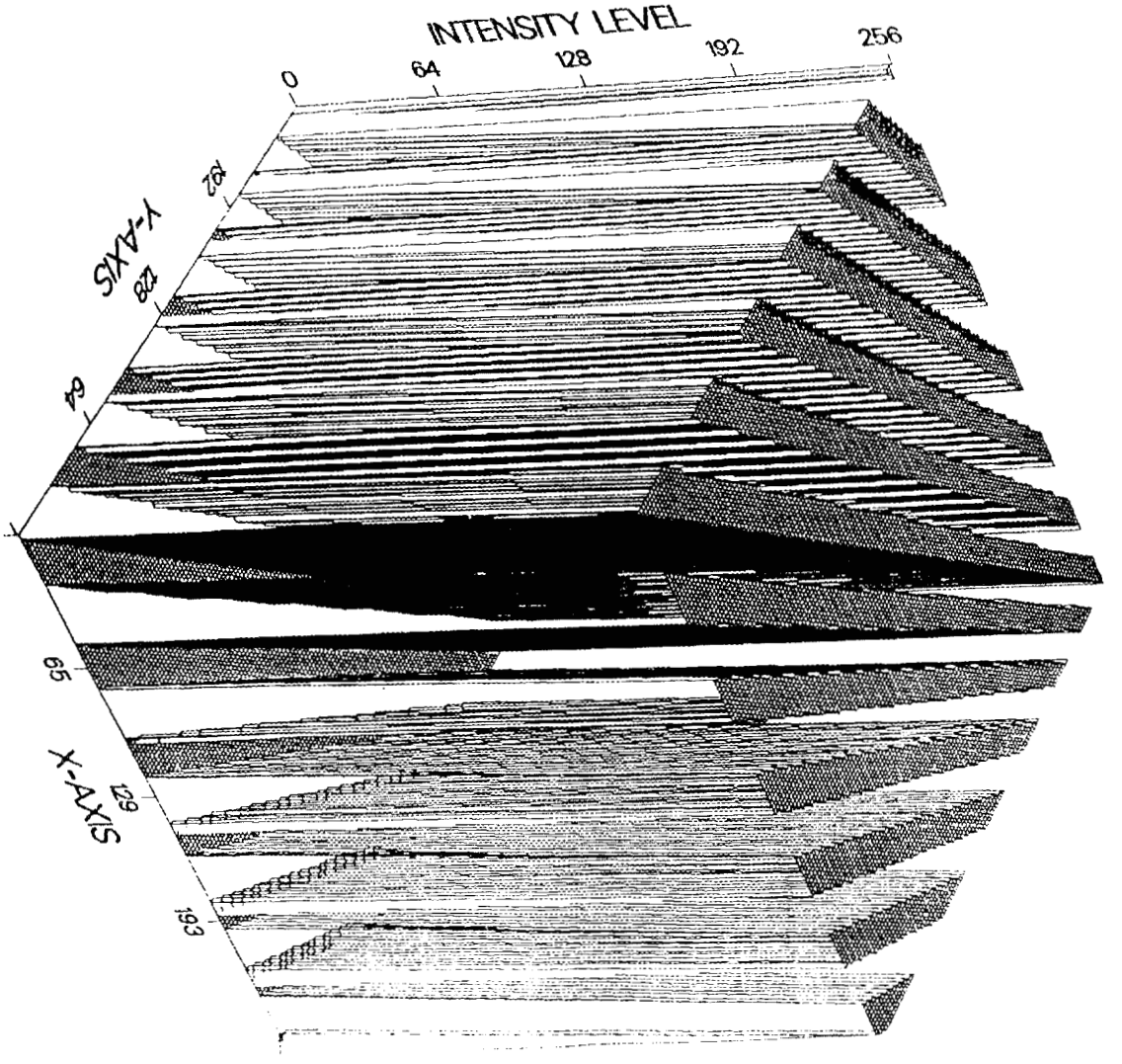

Picture 7. One-Quarter of the Star Illusion in 3-D.

Pictures 8-11 present the results of applying the linear matrix operator of Chapter 3.3 to two sets of data. The first represents a three dimensional plot of two areas of the Herman grid before and after the operator was applied. In the first picture a three-dimensional plot of four of the dark squares of the Herman grid is shown. Below it is the effect on the front part of two of these squares after the matrix operator is applied. Notice that the homogeneous region in the center of the square is suppressed (because there is no change of brightness across the homogeneous field) but the outer edges are outlined. (Actually they are enhanced but the sharpening effect is truncated by the plotting routine.) Notice also that at the bottom of the plot, the flat surface area begins to rise. The plot of this area is shown in Picture 9 and corresponds to the region where human subjects subjectively see a dot appearing between four of the Herman grid squares. Notice that the region is also raised up by the matrix operator which means it is now darker than the original illusion before the operator was applied. Thus, the subjective dot illusion of the Herman Grid was reproduced. The result is of interest because the matrix operator was actually using only information from the modified Machband illusion, not the Herman Grid.

In this case at least, the retinal effects producing one illusion was captured by the matrix operators and accurately produced effects experienced by humans in another illusion. An attempt was made to apply the operator to the Star illusion but the results were inconclusive because the plotting resolution in three dimensions produced too much noise to detect any unique effects.

ORNL--DWG 86-10121

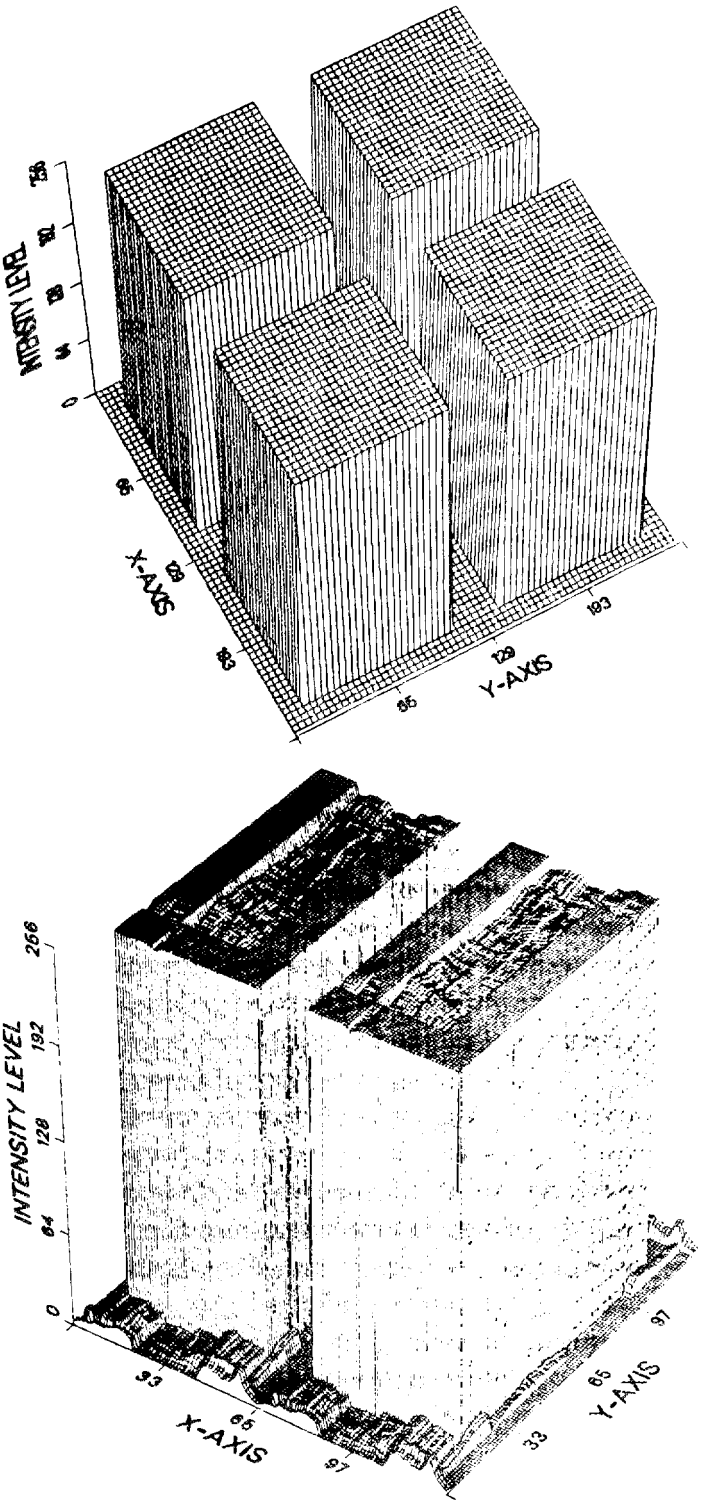

Picture 8. Herman Grid Before.
Herman Grid After Visual Operator Application.

ORNL–DWG 86-10127

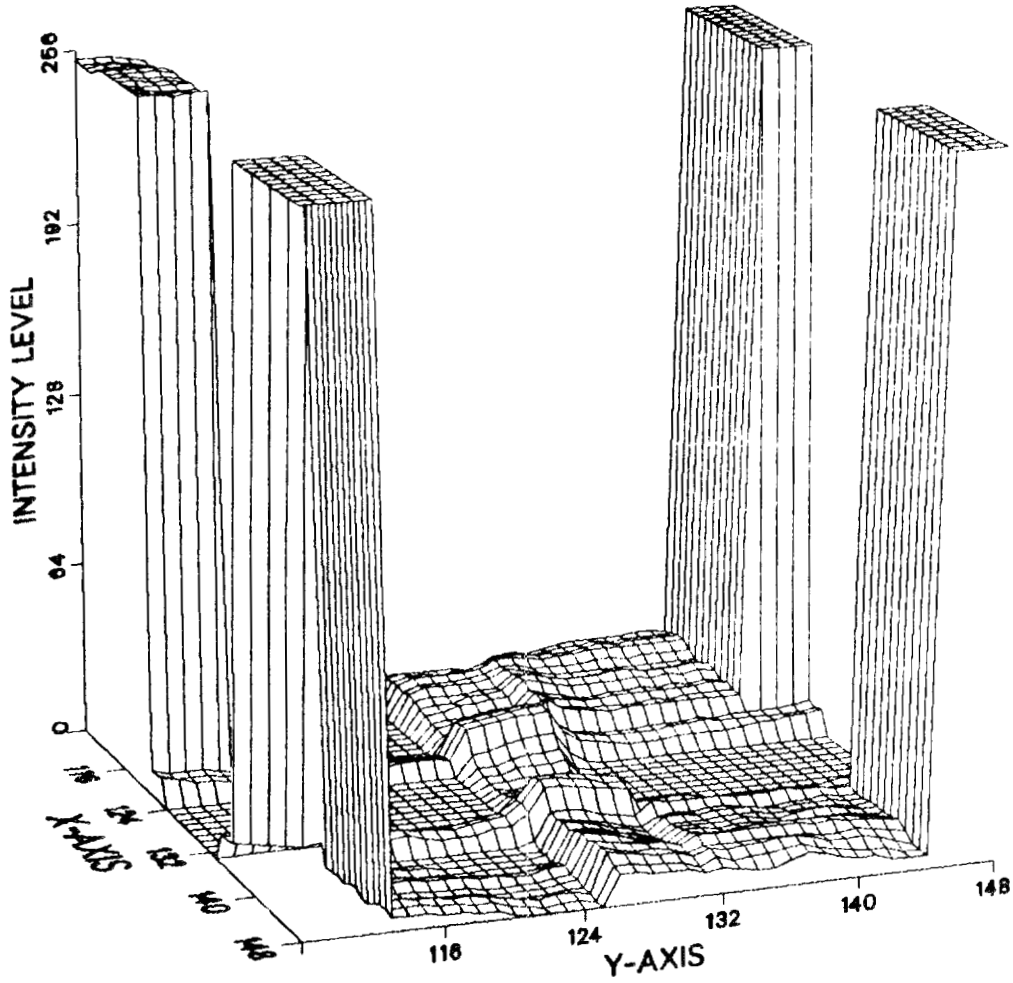

Picture 9. 3-D Plot of an Estimated Illusory Dot in the Herman Grid.

ORNL–DWG 86-10124

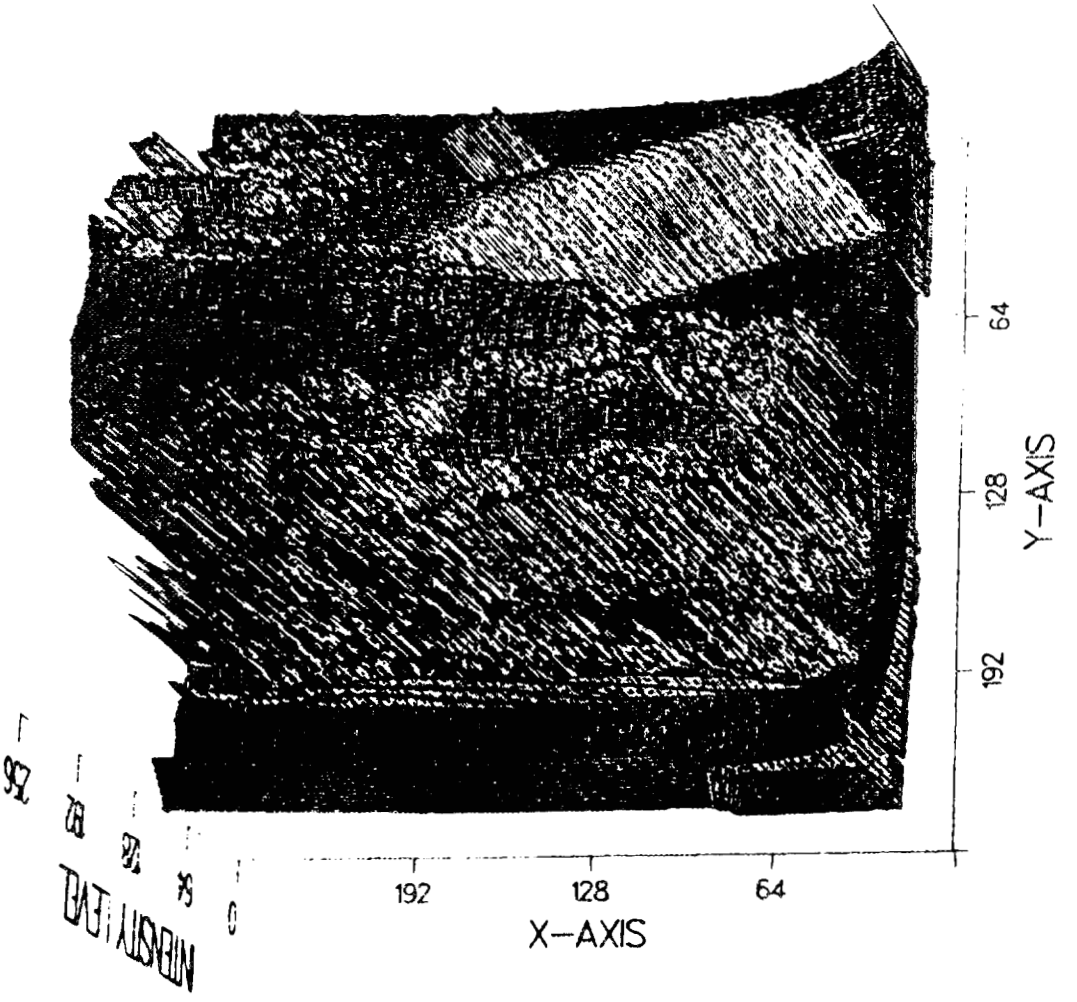

Picture 10. Original Tank Picture and its 3-D Plot.

ORNL–DWG 86-10123

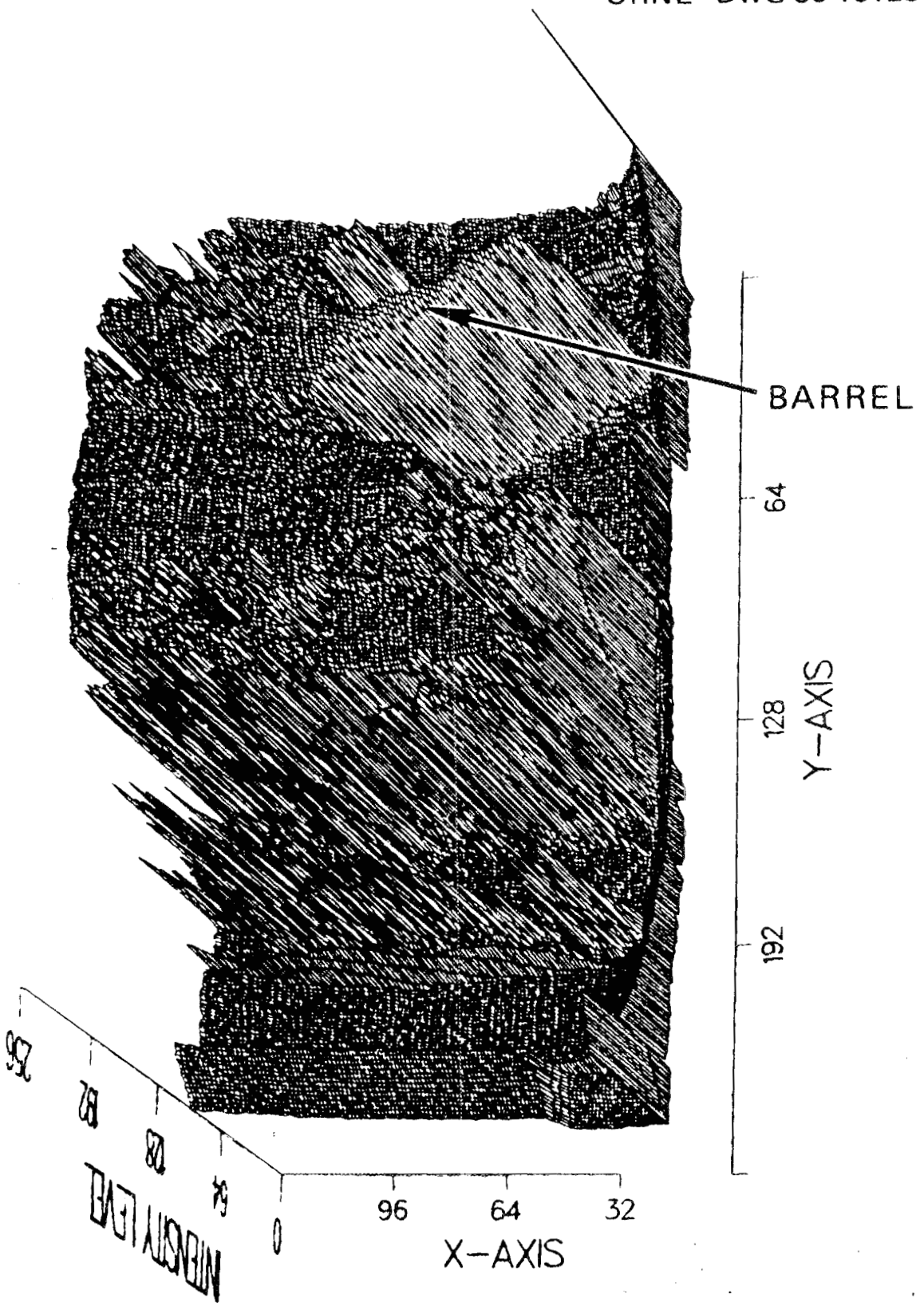

Picture 11. Plot of 3-D Tank Picture After Application of the Matrix Operator.

Because one goal of the project is to capture the information processing characteristics of the human for application to real world scenes, an attempt was also made to apply the matrix operator to a black and white picture of a tank about to be struck by a copperhead antitank artillery shell. Picture 10 shows the original image. Below this picture is the result of plotting the same picture intensity levels in three dimensions. The three-dimensional plots are required because the optical effects are subtle and occur as brightness levels of various parts of the image. These differences do not show up well in standard photos and would not reproduce in two-dimensional images. Consequently, the last Picture (11) is part of the three-dimensional tank plot after the operator has been applied. Some gray scale effects can be noted, but in general, information is lost in the complexity of the plot. If the information was used in a higher order image interpretation system, this image would first be filtered to band pass only the extremes. The effect, which is a common one with such transformations as the Sobel operators, would be to leave only a skeleton of the image with certain areas enhanced.

The second year of this effort is, in fact, doing exactly that. Other images were also processed but have not been included in the present report. The primary intent in applying the linear matrix operator was to determine whether or not the equations were reproducing subjective effects and to provide values to test the Fourier solution method. Although adequate for these purposes, the matrix operator so obtained should be treated with caution. Several factors lead to this conclusion. First, the illusions were not tested under a wide range of contrast and

lighting conditions. It is not known whether these subjective judgements would vary in a nonlinear or highly irregular way. Second, the monitors showed a minor but significant tendency to automatically correct for wide changes in screen luminance. This "averaging" effect tended to wash out extremely sharp edges and thus reduce the magnitude of an illusory effect. Finally, some acuity loss also occurred between the original image and the stored image because of degradations in the digitizer.

It is anticipated that in 1986 two events should improve our confidence in the psychophysical data. First, both HEL and ORNL will have available improved graphic displays resulting in sharper more stable images. Second, HEL may perform more controlled experiments with larger numbers of subjects. If additional illusions can be found for the early retinal layers, the logical intersection of multiple subjective confidence rating intervals may have the effect of narrowing the variance in the data used to solve for the matrix operator.

5.0. CONCLUSIONS AND FUTURE DIRECTIONS

As stated earlier, the long-term goal of this research program is to develop a robotic vision system based on principles of human vision. Within the context of the more limited goals of the first year, considerable progress has been made. It has become apparent from actually applying the neural models both in simulations and with human experiments that a variety of interesting effects occur. That is not surprising, but what is valuable are insights from observing the cumulative effects of retinal mechanisms on the original pictorial information. With large systems of equations it becomes very difficult to anticipate or even visualize compounded results of neural processing. By breaking down the models into a simulatable form, this effort has permitted a step-by-step examination of what may be going on during human information extraction and early pattern analysis.

The use of illusions to parameterize equations provided a method for computational measurement of processing in early retinal layers. Although it now appears that simple linear systems of equations will not be flexible enough to capture retinal dynamics, the conjecture has been empirically explored in the present research.

At the other extreme of complexity, the Gawronski equations appear to be able to capture retinal dynamics with a cost of considerable increases in computational requirements and complexity. So far, the most interesting results of this work has been that neural process dynamics and retinal symmetries can result in interactions that dramatically simplify the representational problem. Also, a powerful simulation tool

has been produced. The extension of this approach to faster hardware architectures such as the ORNL NCUBE machine appears to hold real promise for future real world implementations. It is anticipated that this work will be accelerated more in the coming year due to the promising initial results. The greatest limitation is the probable inability to determine more equation values from psychophysical experiments. Instead, simulations and parameter selection based on observation of processing layers will be required. Such an approach poses new difficulties.

Technical Issues

The direction which this research will take in the future depends on the resolution of several issues which will become more important the closer the effort comes to hardware implementation. In the immediate future, the processing of neural information needs to be linked to higher levels of cognitive processes included in pattern recognition and learning. Most existing methods do not utilize concepts of parallelism and dynamic feedback. If a future robot vision system will emulate human processing characteristics at higher cortical levels, research should also begin on pattern recognition procedures capable of accepting neural types of input. It is not at all clear what the supporting hardware mechanisms will look like except there is a high probability they will have to exhibit adaptability and feature selection that corresponds to plasticity and associative processes in the neural column.

A second issue concerns the inclusion of dynamic processes. It is evident that dynamics occur both within nerve layers and between nerve layers as feedback. In fact such processes are critical to handle the

space-time relationships inherent in real time vision. The present effort considered some feedback, but the range of influence within layers was limited and the amount of inter-layer feedback minimal. In addition to dynamics within the neural system, the effort will eventually have to address dynamics in the external image environment. Up to this time, only static, digitized pictures have been processed. How much dynamics can be handled, where dynamics should be utilized, and what the effects might be remain stubborn problems.

Closely related to dynamics is the philosophy for incorporating the results in hardware. Computationally it seems clear that some parallel computing logic will be utilized. What is not clear is which type of architecture is best and whether the research results should be embedded in an advanced existing system such as a hypercube, butterfly, or Non Von machine. Perhaps the majority of computation should best take place on a custom chip. The decisions about the global approach should be made relatively early in this effort because of the potential lead times inherent in the fabrication of new chips and the generation of computer code on advanced computer architectures.

Specific choices for each of these issues should become more obvious as experience in the behavior of the neural models is gained. It is clear that a great deal of research interest exists in the use of human sensory analogs evidenced by the variety and magnitude of R & D programs now beginning to appear. It is premature to select one of these approaches over the other. The present effort looks promising yet considerable obstacles remain before the goal of a retinal based vision system can become reality. The payoff of a successful system is so great, however, that the obstacles are more than overshadowed by the potential.

6.0. REFERENCES

1. Baylor, D. A. and M.G.F. Fuortes, "Electrical Responses of Single Cones in the Retina of the Turtle, J. of Physiol., Vol. 207, pp. 77-92 (1970).

2. Curlander, J. C. and V. Z. Marmarelis, "Processing of Visual Information in the Distal Neurons of the Vertebrate Retina," IEEE Trans. Syst. Man Cyb., Vol. SMC-13, pp. 934-943, (September-October, 1983).

3. Ebenholz, S. M., "Perceptual Coding and Adaptations of the Oculomotor Systems," Sensory Experience Adaptation, and Perception, Spillman, L. and Wooten, B. R. (Eds.), Lawrence Erlbaum Assoc., Hillsdale, N.J. (Pub.) pp.335-363 (1984).

4. Fu, K. S., "Sequential Methods in Pattern Recognition and Machine Learning," Academic Press, New York (1968).

5. Fu, K. S., "Syntactic Methods in Pattern Recognition," Academic Press, New York (1974).

6. Fu, K. S., "Recent Developments in Pattern Recognition," IEEE Trans. Comp., Vol. C-29, pp. 845-854 (Oct. 1980).

7. Gawronski, R. R., "Bionics - the Nervous System as a Control System," Elsevier Pub. Co. PWN (1971).

8. Gawronski, R. R., "Problems of Bionics in Large Scale Systems," (in Polish), MON.Pub. Warsaw (1975).

9. Granit, R., "Receptors and Sensory Perception," Yale Univ. Press, New Haven and London (1955).

10. Hagins, W. A., R. D. Penn and S. Yoshikami, "Dark Current and Photocurrent in Retinal Rods," Biophys. J., Vol. 10, pp. 380-412 (1970).

11. Hartline, H. K. "The Response of Single Optic Nerve of the Vertebrate Eye to Illumination of the Retina," Amer. J. of Physiol., Vol. 121, pp. 400-415 (1938).

12. Hebb, D. C., "The Organizaton of Behavior: A Neurophysiological Theory," J. Wiley and Sons (1957).

13. Nilsson, N. J., "Learning Machines," McGraw-Hill Book Co. (1965).

14. Konorski, J., "Integrative Activity of the Brain," The University of Chicago Press (1967).

References (cont'd)

15. Kronzauer, R. E. and Y. Y. Zeevi, "Reorganization and Diversification of Signals in Vision," IEEE Trans. Syst. Man Cyb., Vol. SMC-15, pp. 91-101 (January-February 1985).

16. Kupfmuller, K. and F. Jenik, "Uber die Nachrichtenverarbeitung in der Nervenzelle," Kybernetik (now Biological Cybernetics), Vol. 1, pp. 1-6 (1961).

17. Lerner, E. J., "Robotics - The Birth of Vision," Science Digest, pp. 29-35 and 76-77 (July 1985).

18. Lettvin, J. Y., R. R. Maturana, W. S. McCulloch and W. H. Pitts, "What the Frog's Eye Tells the Frog's Brain," Proc. Inst. Rad. Eng., Vol. 47, pp. 1940-1951 (1959).

19. Maar, D., "Vision," W. H. Freeman and Co., New York (1982).

20. McCulloch, W. S. and W. Pitts, "A Logical Calculus of the Ideas Imminent in Nervous Activity," Bull. Math. Bioph., Vol. 5, pp. 115-133 (1943).

21. Oguztoreli, M. N., "Modeling and Simulation of Vertebrate Primary Visual System: Basic Network," IEEE Trans. Syst. Man Cyb., Vol. SMC-13, pp. 766-781 (September-October 1983).

22. Polyak, S. L., "The Vertebrate Visual System," Univ. of Chicago Press, Chicago (1957).

23. Rodieck, R. W., "The Vertebrate Retina - Principles of Structure and Function," W. H. Freeman and Co., San Francisco (1973).

24. Sebastyen, G., "Decision-Making Processes in Pattern Recognition," MacMillan Co., New York (1962).

25. Siminoff, R., "System Analysis of an Analog Model of the Vertebrate Cone Retina," IEEE Trans. Syst. Man Cyb., Vol. SMC-13, pp. 1021-1028 (September-October 1983).

26. Stone, J., "Parallel Processing in the Visual System," Plenum Press (1983).

27. Tulanay-Keesey, U., "Effects of Fixational Eye Movements on Contrast Sensitivity," Visual Psychophysics and Physiology, J. C. Armington, J. Krauskopf and B. R. Wooten (Eds.), Academic Press, pp. 341-352 (1978).

APPENDIX A

FORTRAN Code for the Fourier Solution of the Linear Matrix Equations

```
      IMPLICIT REAL*8 (A-H,O-Z)
      REAL*4 XINT
      COMMON NPOINT
      DIMENSION WORK(384),XR(128,128),XI(128,128),BR(128,128)
      DIMENSION BI(128,128),AR(128,128),AI(128,128)
      DIMENSION XINT(1024)
      NPOINT = 128
      LWORK = 3*NPOINT
      DO 1000 I=1,NPOINT
      DO 1000 J=1,NPOINT
      XI(I,J) = 0.D0
 1000 BI(I,J) = 0.D0
      DO 600 NN=1,NPOINT
      READ(1) XINT
      DO 650 J=1,NPOINT
  650 BR(NN,J) = 1.D0 - XINT(J)
      READ(2) XINT
      DO 750 J=1,NPOINT
  750 XR(NN,J) = 1.D0 - XINT(J)
  600 CONTINUE
      CALL FFT(XR,XI,WORK,LWORK)
      CALL FFT(BR,BI,WORK,LWORK)
      WRITE(6,4000)
 4000 FORMAT(' BR')
      WRITE(6,3000) ((BR(I,J), J=1,NPOINT), I=1,20)
      WRITE(6,4001)
 4001 FORMAT(' XR')
      WRITE(6,3000) ((XR(I,J), J=1,NPOINT), I=1,20)
      DO 2001 I=1,NPOINT
      DO 2000 J=1,NPOINT
      D = XR(I,J)*XR(I,J) + XI(I,J)*XI(I,J)
      IF(D.LE.1.D-30) GO TO 50
      AR(I,J) = (BR(I,J)*XR(I,J)+BI(I,J)*XI(I,J))/D
      AI(I,J) = -(BI(I,J)*XR(I,J)-BR(I,J)*XI(I,J))/D
      GO TO 2000
   50 WRITE(6,51) I,J,XR(I,J),XI(I,J),BR(I,J),BI(I,J)
   51 FORMAT(' ZERO DENOMINATOR'/2I4,4E16.8)
      AR(I,J) = 1234.5678D0
      AI(I,J) = 0.D0
C*********************************************************
C*(AR,AI) IS THE COMPLEX CONJUGATE OF A(Q)-B(Q)/X(Q)
C*CONJUGATE IS CALCULATED IN ORDER TO TAKE INVERSE TRANSFORM
C*********************************************************
 2000 CONTINUE
      WRITE(6,2002) I
 2002 FORMAT(1X,'ROW ',I3,'COMPLETED')
 2001 CONTINUE
      DO 5000 I=1,NPOINT
      DO 5000 J=1,NPOINT
      IF(AR(I,J).NE.1234.5678D0) GO TO 5000
      N1=I-1
      N2=J
      N3=I
      N4=J+1
      N5=I+1
      N6=J-1
      IF(N1.EQ.0) N1=NPOINT
      IF(N6.EQ.0) N6=NPOINT
      IF(N4.EQ.NPOINT+1) N4=1
      IF(N5.EQ.NPOINT+1) N5=1
 5000 AR(I,J) = (AR(N1,N2)+AR(N3,N4)+AR(N5,N2)+AR(N3,N6))/4.D0
      WRITE(6,4002)
 4002 FORMAT(' AR RIGHT SIGN')
      CALL FFT(AR,AI,WORK,LWORK)
      WRITE(6,3000) ((AR(I,J), J=1,NPOINT), I=1,30)
      WRITE(6,4003)
 4003 FORMAT(' AI')
      WRITE(6,3000) ((AI(I,J), J=1,NPOINT), I=1,20)
 3000 FORMAT(1X, 16F6.2)
      STOP
      END
      SUBROUTINE FFT(X,Y,WORK,LWORK)
      IMPLICIT REAL*8 (A-H,O-Z)
      COMMON NPOINT
      DIMENSION ND(2), X(NPOINT,1), Y(NPOINT,1)
      DIMENSION WORK(1)
      NDIM = 2
      ND(1) = NPOINT
      ND(2) = NPOINT
      N = ND(1)*ND(2)
      IFAIL = 0
*     CALL C06FJF(NDIM,ND,N,X,Y,WORK,LWORK,IFAIL)
      RETURN
      END
```

*C06FJF is a standard numeric algorithm routine for FFT transforms.

APPENDIX B

Graphics Program Description

A FORTRAN program was written to create three- and two-dimensional plots of the scene intensity data used in the machine vision project. The three-dimensional plots show the intensity level at every grid point in the digitized scene. These plots allow a rapid comparison of the mathematical model's output for the illusion scenes with that obtained from studies with human subjects. The two-dimensional plots can be used to show the mathematical model's output for more complex scenes which are more easily verified by looking at the two-dimensional views.

This program uses the DISSPLA graphics software. For the simple type of graphics produced in this program, the use of this program has several advantages. First, the output from the program can be a graphics metafile which can later be plotted on any of the devices available at Martin Marietta Energy Systems. Quick, but high-quality, plots can be obtained on the Versatec or CalComp plotters, while 35mm slides and glossy prints can be obtained from the FR80 film recorder. Secondly, since the DISSPLA package is used on many of the available computer systems, it could easily be transported to another system. This might become necessary if, for example, the processing speed of the Cray X/MP was deemed to be necessary for production of plots.

This development of this program is to the point at which the initial production of plots for the illusion data can begin. Additional features may be added as the need for them arises.

Program Overview

The basic function of the program, hereafter referred to as PLOTINT, is to read a data file of scene intensity values and create a three-dimensional plot on one of two devices - a Tektronix 4027 graphics terminal, or a graphics metafile. Working interactively on the Tektronix terminal, the user can manipulate the plot until it suits his needs. Once the final plot has been designed, the commands to PLOTINT necesary to construct the final plot can be saved in a file. This file is then run through PLOTINT again, this time with the graphics metafile as the output device. The metafile can then be plotted on any of the available devices through existing methods.

The production of two-dimensional plots is a secondary function of PLOTINT. The output is a file containing raster data for the Versatec raster plotter, and is thus not in a form that can be plotted on other devices. Since the Versatec plotter can not produce pixels of arbitrary intensity level, but only on or off, varying intensity levels are produced by representing each grid point in the scene by a matrix of pixels on the plotter. Various combinations of dots are used to create the appropriate shades. This process is fairly crude and makes the two-dimensional output of PLOTINT appropriate only for rough visualization of the output of the mathematical model.

In what follows, the basic capabilities of the program are listed, along with planned extensions where appropriate.

Input Data

The input data can be in one of two forms - real numbered data or character data. If it is real-numbered data, each datum is an intensity

level, in the range 0.0 - 1.0, for a single grid point. If it is character data, each character again represents a single grid point, but the intensity value is represented as a discrete level in the range 0-255. The level is given by the ordinal value of the character in the EBCDIC collating sequence. The advantage of storing character data is that it only requires 1/4 the storage space of the real-numbered data file. Also, the program stores the input data internally as character data in order to keep it's region requirements at a minimum. Thus, the only reason for allowing real-numbered data as input is that it is an easier format for the mathematical model to output.

Plotting Region

The input data consists of a 1024 x 1024 grid. Any rectangular portion of this grid may be used for the plots.

Mesh Spacing

The user can adjust the mesh spacing for three-dimensional plots. A value of one means that every grid line in the plotting region will be used, while a value of five means that only every fifth grid line will be used. This feature is useful for speeding up the production of the plot in the interactive plot phase.

Viewpoint

Every three-dimensional plot must have a viewpoint defined, which includes the viewing direction relative to the center of the plot, and the distance from the plot. This allows the user to rotate the plot until it best illustrates the scene being plotted. Changing the distance

from the plot allows the user to shrink or expand the plot to make room for titles or other necessary messages.

Annotation

Currently, a title of up to three lines, with each line possibly a different height, can be added to a three-dimensional plot. The DISSPLA package is now deciding where to put the title, but this will be changed to give the user control over placement. Also, the ability to add messages anywhere on the plot will soon be added.

Multiple Views

One can automatically produce multiple views of the plot by designing the starting and ending plots, and then specifying the number of plots to be interpolated between these two extremes. If there is sufficient interest, this feature can be expanded to allow the production of movie clips on the FR80 film recorder.

Projections

At times a three-dimensional plot, no matter how well manipulated, cannot adequately display an important feature. For these cases, the ability to add two-dimensional projections of the three-dimensional data has been added. This can take one of two forms. In the first form, a vertical slice along a grid line is projected on a plane parallel to that slice and displaced far enough from the three-dimensional plot to be clearly visible. The curve in that projection is the intensity level along that grid line. The user has control of the position of the projection. In the second form, the projection consists of two curves, which are the minimum and maximum intensity levels along the appropriate grid lines.

Two-Dimensional Plots

Two-dimensional plots can be produced on the Versatec raster plotter. Each grid point in the plotting region is represented as either a 1 x 1, 2 x 2, or 4 x 4 matrix of pixels on the plotter. This gives several levels of approximation to the actual two-dimensional image.

ORNL/TM-10031
CESAR-86/05

DISTRIBUTION LIST

INTERNAL DISTRIBUTION

1- 5. Barhen, J.
6. de Saussure, G.
7. Eads, B. G.
8. Hamel, W. R.
9-13. Howe, E. S.
14. Ingersoll, J. K.
15-19. Jones, J.
20. Jorgensen, C. C.
21. Lucius, J. L.
22-26. Maienschein, F. C.
27. Mynatt, F. R.
28. Oblow, E. M.
29-33. Weisbin, C. R.
34. Zucker, A.
35. Dickson, P. W. (Consultant)
36. Golub, G. H. (Consultant)
37. Haralick, R. M. (Consultant)
38. Steiner, D. (Consultant)
39-40. Central Research Library
41. ORNL Y-12 Technical Library Document Reference Section
42-43. Laboratory Records
44. ORNL Patent Office
45. Laboratory Records - RC
46-50. EPMD Reports Office

EXTERNAL DISTRIBUTION

51. Dr. Stanley Deutsch, National Research Council, 2101 Constitution Ave., Washington, DC 20418.

52. Major John Evers, AFATL/DLCM, Elgin Air Force Base, Florida 32542.

53-57. Dr. Richard R. Gawronski, University of West Florida, Systems Sciences Department, Pensacola, FL 32514-003.

58. Dr. Ralph Gonzalez, Department of Electrical Engineering, University of Tennessee, Knoxville, TN 37916.

59-63. Major Frank Holly, Director USA LABCOM, USAHEL, Attn: SLCHE-CS (Holly) Aberdeen Proving Ground, Maryland 21005-5001.

64. Dr. Edward Johnson, Director, U.S. Army Research Institute, 5001 Eisenhower Blvd. Alexandria, VA 22015.

65. Dr. Donald Malkoff, Naval Personnel Research and Development Center, Code 71, San Diego, CA 92152-6800.

66. Dr. Fredrick Muckler, Chief Scientist, Essex Corporation, 741 Lakefield Road, Westlake Village, CA 91361.

67. Dr. Dave Nagel, NASA Ames Research Center, Life Sciences Bldg., MS-239-21, Moffett Field, CA 94035.

68. Dr. John O'Hare, Office of Naval Research, 800 North Quincy St., Code 422, Arlington, VA 22217.

69. Dr. Mariana Rudisill, NASA Johnson Space Center, SP-22, Houston, TX 77058.

EXTERNAL DISTRIBUTION (cont'd)

70. Dr. Michael H. Strub, Chief, ARI Field Unix, P.O. Box 6057, Ft. Bliss, TX 79916.

71. Office of Assistant Manager for Energy Research and Development, DOE-ORO, Oak Ridge, TN 37830.

72-98. Technical Information Center, P.O. Box 62, Oak Ridge, TN 37830.